Structure-Based Monomerization of Human Serine Protease HTRA1 towards Evolutive Engineering of Activity Modulators

TECHNISCHE
UNIVERSITÄT
DARMSTADT

Vom Fachbereich Chemie
der Technischen Universität Darmstadt

zur Erlangung des akademischen Grades eines
Doctor rerum naturalium (Dr. rer. nat)

Genehmigte Dissertation vorgelegt von
Dipl. Biol. Niklas Weber
aus Bad Hersfeld

Referent:	Prof. Dr. Harald Kolmar
Korreferent:	Prof. Dr. Heribert Warzecha
Tag der Einreichung:	04.09.2017
Tag der mündlichen Prüfung:	17.10.2017

Darmstadt 2017
D17

"Human beings are the only creatures on earth that claim a God and the only living thing that behaves like it hasn't got one."

Paul Kemp in the novel "Rum Diary",

by Hunter S. Thompson

Publications, Patents and Presentations

Publications Resulting from this Work

Zielonka, S., Weber, N. *et al.* Shark Attack: high affinity binding proteins derived from shark vNAR domains by stepwise in vitro affinity maturation. J Biotechnol 191, 236-45 (2014).

Weber, N. & Kolmar, H. DegP Protease. Handbook of Proteolytic Enzymes (ed. Barrett, R., Woessner) 2567-2571 (Elsevier, 2013).

Publications during this Work

Glotzbach, B., Reinwarth, M., Weber, N. *et al.* Combinatorial optimization of cystine-knot peptides towards high-affinity inhibitors of human matriptase-1. PLoS One 8, e76956 (2013).

Patent applications during this Work

Glotzbach, B., Weber, N., Tomaszowski, M., Hock, B., Kolmar, H. (2013) Potente Inhibitoren der humanen Matriptase-I auf Basis von MCoTI-II abgeleiteten Varianten, EP-Nr.: 13001869.0

Presentations

Weber, N. Breaking the Cage: Towards Protease HTRA1 Inhibition. Invited talk at PEGS Summit Europe 2012, Vienna

Table of Contents

1. Abstract

1.1. Zusammenfassung

Die humane Serinprotease HTRA1 spielt eine wichtige Rolle bei vielen verschiedenen physiologischen Prozessen. Sie ist dabei an der Erkennung und Prozessierung einer Vielzahl verschiedener Substrate beteiligt. Eine wachsende Zahl an Studien deutet darauf hin, dass HTRA1 bei der Entstehung oder Progression unterschiedlicher Krankheiten wie beispielsweise Arthrose, Krebs, altersbedingter Makulardegeneration oder Alzheimer eine Rolle spielt.

Ziel dieser Arbeit war die Entwicklung von Modulatoren, welche die Aktivität von HTRA1 beeinflussen, um dadurch Werkzeuge zur Validierung von HTRA1 als mögliches Zielmolekül für neue Therapieansätze zu generieren.

Der ursprüngliche Ansatz war die Herstellung von Monomeren der multimeren Protease HTRA1, welche sich sowohl als Trimer, oder als höheres Oligomer von unbekannter Zusammensetzung, assembliert. Der erste Schritt zur Monomerisierung des Zielmoleküls sollte zu einem leicht handhabbaren und beherrschbaren Zielmolekül für das evolutive Proteindesign führen. Daher wurden Strukturdaten des Trimers genutzt um Aminosäureaustausche vorzunehmen, die als hauptsächlich für die Trimerisierung beschrieben wurden. Diese führten zu stabilen, monomeren Fraktionen der katalytischen Domäne von HTRA1.

Proteinbibliotheken drei verschiedener Grundgerüste wurden für die Durchmusterung nach Bindern für monomeres HTRA1 eingesetzt. Die auf dem Miniprotein McoTI-II basierende Bibliothek, welches ein Trypsin Inhibitor aus Kürbisgewächsen ist, lieferte ein einzelnes Molekül, welches zwar mit nanomolarer Affinität monomeres HTRA1, aber nicht natives trimeres, erkannte. Ähnlich verhielten sich die beiden Moleküle, die aus einer immunisierten cameliden VHH Bibliothek, wobei es sich um die variable Domäne eines Einzelketten-Immunglobulins eines Lamas handelt, isoliert wurden. Hier erkannten ebenfalls beide Moleküle zwar das monomere HTRA1 mit nanomolaren Affinitäten, aber nicht das native, trimere.

Bei der dritten Bibliothek handelte es sich um ein vNAR Grundgerüst, welches die variable Domäne eines Einzelketten-Immunglobulins von Haien darstellt, bei der CDR3 synthetisch randomisiert wurde. Bei der Durchmusterung wurden sechs Moleküle isoliert, die mikromolare Affinitäten gegenüber monomerem HTRA1 aufwiesen und von denen fünf auch natives, trimeres HTRA1 erkannten. Durch schrittweise Affinitätsmaturierung von CDR1 und HV2 konnten Affinitäten im zweistellig nanomolaren Bereich erzielt werden.

Zuletzt wurden die erfolgversprechenden vNAR Varianten löslich exprimiert und in Aktivitätstests wurde überprüft, ob sie einen Einfluss auf die Aktivität von HTRA1 haben. Drei Moleküle erhöhten die Aktivität in einem Bereich von 150 % bis 400 %. Diese Modulatoren können für *in vitro* und *in vivo* Analysen eingesetzt werden und dazu beitragen die Frage zu beantworten, ob HTRA1 ein sinnvolles therapeutisches Ziel darstellt.

1.2. Abstract

Human serine protease HTRA1 plays an important role in a plethora of physiological processes by recognition and conversion of numerous different substrates. Various studies suggested that HTRA1 is involved in several diseases, such as osteoarthritis, cancer, age-related macular degeneration or Alzheimer disease. The aim of this work was the generation of molecules that modulate HTRA1 activity, which could act as tools for validation of HTRA1 as a potential therapeutic target.

An initial approach was the monomerization of multimeric HTRA1 that is composed of trimers as well as higher oligomers of unknown composition to get an easier to handle and more controllable target for evolutionary design of interacting molecules. Accordingly, structural data of the trimer was applied for the design of amino acid replacements that are supposedly important for trimerization, resulting in stable monomeric fractions of HTRA1 catalytic domain.

Three different scaffold libraries were screened by yeast surface display towards binding of monomeric HTRA1. The miniprotein McoTI-II-based library, which is a trypsin inhibitor from squash plant, delivered a single molecule that bound monomeric HTRA1 with nanomolar affinity, but not native trimeric HTRA1. Similarly, the two molecules isolated from an immunized VHH library, which is the variable domain of a single domain camelid immunoglobulin, also bind only monomeric HTRA1 with nanomolar affinities, but not native trimeric HTRA1.

The third library was a vNAR library, which is the variable domain of a single domain shark immunoglobulin that was synthetically randomized in CDR3. Six independent molecules were isolated against monomeric HTRA1 and five of them were shown to bind native trimeric HTRA1 with micromolar affinities. By stepwise affinity maturation of CDR1 and HV2, affinities were improved to double digit nanomolar affinities.

Finally, promising vNAR molecules were soluble expressed and evaluated for modulation of HTRA1 activity by activity assays, resulting in three molecules that enhance HTRA1 activity in a range from 150 % to 400 %. Therefore, we successfully generated activators that enhance HTRA1 activity with different strengths that can be used in *in vitro* and *in vivo* assays for validation of human HTRA1 as novel therapeutic target.

2. Introduction

Degradation of molecules is an extremely important feature found in all living organisms with respect to nutrition uptake, tissue remodeling, recycling of biomolecules or degradation of toxic substances. Moreover, it is also an important tool for regulation of homeostasis to keep control of a plethora of effector functions. Many degradative proteins are themselves regulated by degradative processes, since they exist in an inactive pre-form that has to be partially degraded to become an active compound[1, 2]. In the last decade, systems biology tried to quantify these events occurring on many different pathways in multi-cellular organisms for a better understanding of these events[3]. Nevertheless, many degradative events as well as their interplay with regulation of cellular and organismic processes are not fully understood.

One of the most prominent building blocks of life are amino acids, which are assembled during the process of translation to proteins. During protein biosynthesis, information stored in the nucleotide sequence of DNA is translated into proteins via formation of peptide bonds between amino acids in an ordered and defined manner[4].

Under physiological conditions the peptide bond is quite stable[5] but tools for cleaving it have evolved during evolution. Protein cleaving enzymes that are capable of catalyzing the hydrolysis of peptide bonds are called protease and thousands are currently known[6-9]. Proteases have been classified into seven different groups by the intrinsic mechanism for catalytic support of peptide bond cleavage[6, 10]. One of the most prominent mechanisms is based on the nucleophilic attack of the peptide bond carbonyl by an activated serine residue which gives these enzymes the name serine proteases[11]. Two further amino acids are involved in this type of catalysis, a histidine and an aspartate. Together they form the so-called catalytic triad. The specific distances between these residues caused by the tertiary structure of the enzyme causes a proton shuttle, where the aspartate with its negatively charged carboxyl side chain stabilizes a positive charge of the imidazole ring of the histidine side chain during the reaction. The basic reaction mechanism is shown in figure 1.
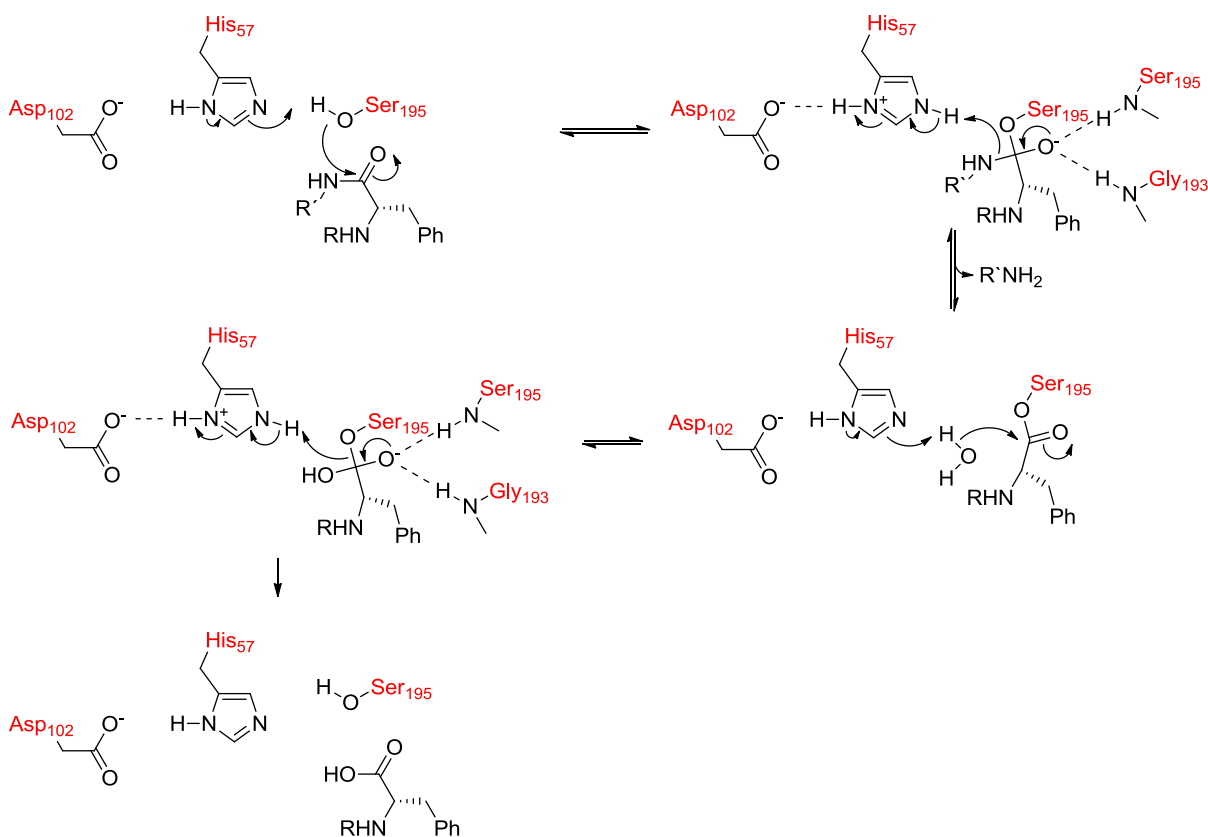
Figure 1 Basic reaction mechanism catalyzed by serine protease chymotrypsin. Amino acid residues of chymotrypsin involved in catalysis are shown in red. Asp102, His57 and Ser195 build up the catalytic triad. The phenylalanine is in P1 position of the **substrate. P2 and P1' position of the substrate are indicated by R (amino**-terminus) a**nd R' (carboxyl**-terminus).

The reaction center of an enzyme is called active-site and is surrounded by amino acid side chains giving each protease its special substrate specificity. This area is called substrate-specificity pocket and selects whether a substrate will be cleaved or not, which is mediated by hydrogen bonds, electrostatic interactions and hydrophobic interactions of the specificity pocket and the substrates amino acid sequence. As a consequence, many proteases cleave adjacent to a specific amino acid or amino acid sequence.

Regulation of serine protease activity is based on various modes of action. One strategy is protease inhibition with molecules binding covalently or non-covalently to the active-site[12, 13]. Most organisms use this strategy to prevent unwanted proteolysis by synthesizing inhibitors to control their own or to escape host proteases. Another strategy relies on the fact that a substrate cleavage site is buried inside a folded substrate or covered by an interacting molecule such that it only undergoes proteolysis if the substrate becomes unfolded or the interacting molecule is dissociated. Furthermore, it is conceivable to modulate the tertiary structure of a protease by ligands, thereby disordering the important distances between the residues of the catalytic triad. But also changes in the environment like pH, temperature or salt shifts could reduce or enlarge the activity[14, 15]. Thus, modulation of proteolytic activity is an essential physiological regulation mechanism, which can also be used for controlling diseases by external intervention strategies.

2.1. Protease HTRA1

HTRA1 is the abbreviation for high temperature requirement protein A1. The first representative of this class of enzymes was discovered in *E. coli* and was designated as DegP or protease Do[23]. Null mutants of DegP showed reduced growth at an elevated temperature, respectively the expression is controlled by the stress signaling pathway σ[E] and the Cpx pathway [24, 25]. One task of a heat shock protein, namely degradation of misfolded proteins, could be predicted by the homology to serine

proteases. Moreover it was demonstrated that DegP combines proteolytic function with chaperone activity[26, 27]. Thus, it was shown that DegP plays an important role to overcome the harmful effect of misfolded proteins during heat stress in *E. coli*[26, 27]. Moreover, expression of human HTRA1 is induced by oxidative stress and it promotes premature cell senescence through p38 MAPK in a protease activity-dependent manner[28].

According to the *MEROPS* database, a classification system which groups all known proteases based on the alignment of their amino acid sequences[7-9],DegP and human HTRA1 belong to the clan PA, family S1 and subfamily S1C. The *MEROPS* identifier is S01.277.

Further bioinformatics analysis revealed strong homology of *E. coli* DegP to proteins found in all empires of life. So it is highly conserved in vertebrates fulfilling a totally different task compared to HTRA1 in microorganisms. In vertebrates HTRA1 is mainly localized in the extracellular matrix and found in all tissues. There it was found to have a broad substrate spectrum focusing on signaling molecules and extracellular matrix components. This task and its altered expression patterns found in patients lead to the idea that HTRA1 plays an important role in disease. The following chapters describe **human HTRA1's structure, function and its role in disease.**

2.1.1. Structure of HTRA1

HTRA1 is a multi-domain protein consisting of a trypsin-like protease domain and at least one carboxyl-terminal so-called PDZ domain[29]. Further domains which are not found in all species are for example a second PDZ domain in *E. coli*, *S. cerevisiae* and *A. thaliana* or an amino-terminal insulin-like growth factor binding protein (IGFBP) and a Kazal-like inhibitor domain (KI) in vertebrates. The carboxyl-terminal PDZ domain shows no influence on proteolytic activity of human HTRA1[30, 31], in contrast to DegP in *E. coli*[27]. Organization of domains of different species is shown in figure 2. Interestingly, the PDZ domain has an influence on length of product peptides after cleavage[27, 31]. The vertebrate-specific amino-terminal domains are also not well characterized. They most likely do not influence HTRA1 activity[30]. Recent findings suggest that IGFP and the Kazal-like domain can act as a redox sensing probe. Reduction of its several disulfides results in an autolytic degradation of the N-terminal domain of HTRA1 while not affecting proteolytic activity of HTRA1[32]. Additionally, there are membrane-bound HTRAs with an amino-terminal transmembrane anchor or signal sequences as localization signals found in several species[29].
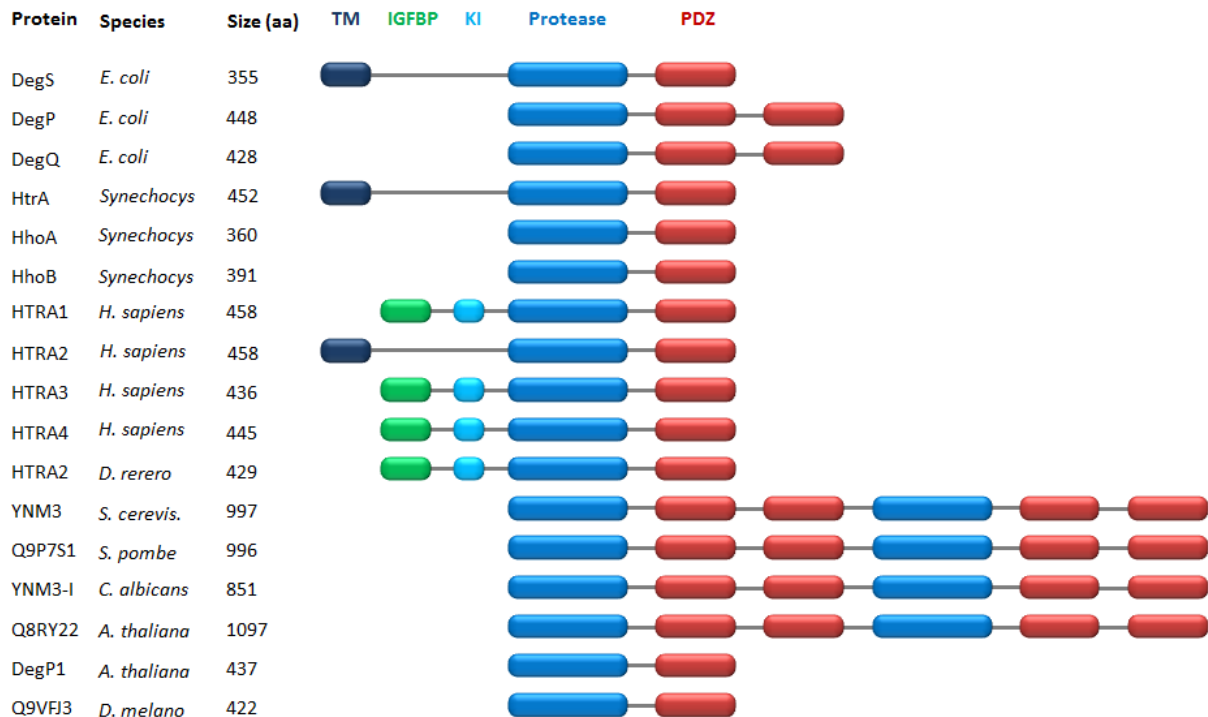
Protein	Species	Size (aa)	TM	IGFBP	KI	Protease	PDZ
DegS	E. coli	355					
DegP	E. coli	448					
DegQ	E. coli	428					
HtrA	Synechocys	452					
HhoA	Synechocys	360					
HhoB	Synechocys	391					
HTRA1	H. sapiens	458					
HTRA2	H. sapiens	458					
HTRA3	H. sapiens	436					
HTRA4	H. sapiens	445					
HTRA2	D. rerero	429					
YNM3	S. cerevis.	997					
Q9P7S1	S. pombe	996					
YNM3-I	C. albicans	851					
Q8RY22	A. thaliana	1097					
DegP1	A. thaliana	437					
Q9VFJ3	D. melano	422					

Figure 2 HTRA domain organization of different organisms (modified from Clausen et al.[29]). Transmembrane domain (TM) in dark blue; insulin-like growth factor binding protein (IGFBP) in green; Kazal-like inhibitor domain (KI) in light blue; catalytic domain (protease) in blue and post synaptic density, discs large, zonula occludentes-1 domain (PDZ) in red.

Most classical serine proteases, especially of the SA clan, are synthesized as inactive zymogenes which are converted into an active form by proteolytic cleavage of an amino-terminal pro-peptide, as found in trypsin for example[33]. In contrast to this irreversible activation mechanism, it was found that there are also proteases like HTRA1 which have a reversible activation mechanism. This activation is thought to be substrate induced but latest crystal structures revealed that there is a substrate independent equilibrium between the active and the inactive state[30, 31]. It is suggested that the switch from competent to incompetent active-site conformers is only separated by a low-energy barrier, causing a conformational selection by substrate[30, 34]. Whether there are further allosteric activation signals involved remains to be investigated.

Crystal structures of DegP, as well as of HTRA1, revealed a homo-trimeric structure mediated by hydrophobic interactions of aromatic amino acids at the amino terminus of the protease domain (figure 4b). The protease domains have a flat disk shape where the active-site is localized at the **opposite direction of the protease's amino and carboxyl**-terminus (figure 3b). A single protease domain consists of two perpendicular β-barrel lobes (β1-β6 and β7-β12) with the catalytic triad residues histidine220, aspartate250 and serine328 located in the cleft between them. The amino and carboxyl-terminus of the protease domain are enclosed by an α-helix each. A low resolution structure of the molecular envelop of trimeric full-length human HTRA1 revealed that the PDZ domains protrude from the protease core and the amino-terminal domains are lying flat on the opposite side of the active-site. Several structures of DegP showed various oligomeric states of trimers, hexamers, 12-mers and 24-mers (figure 3a)[27, 35, 36]. In human HTRA1 only crystal structures of trimers were observed (figure 3b)[31]. However, size-exclusion chromatography revealed complexes about MW 600,000, thereby indicating the formation of higher oligomers in solution. Interestingly, these higher oligomers were formed in presence of an artificial substrate leading also to a 2.8-fold higher activity[31]. However, it is unclear whether these higher oligomers of human HTRA1 resemble the cage-like structure of DegP or if they assemble in a completely different manner. Interestingly, a higher oligomerization state of human HTRA1 was observed in variants lacking all domains except the protease domain, while for DegP crystal structures reveal an involvement of PDZ domains in higher oligomer formation[35].
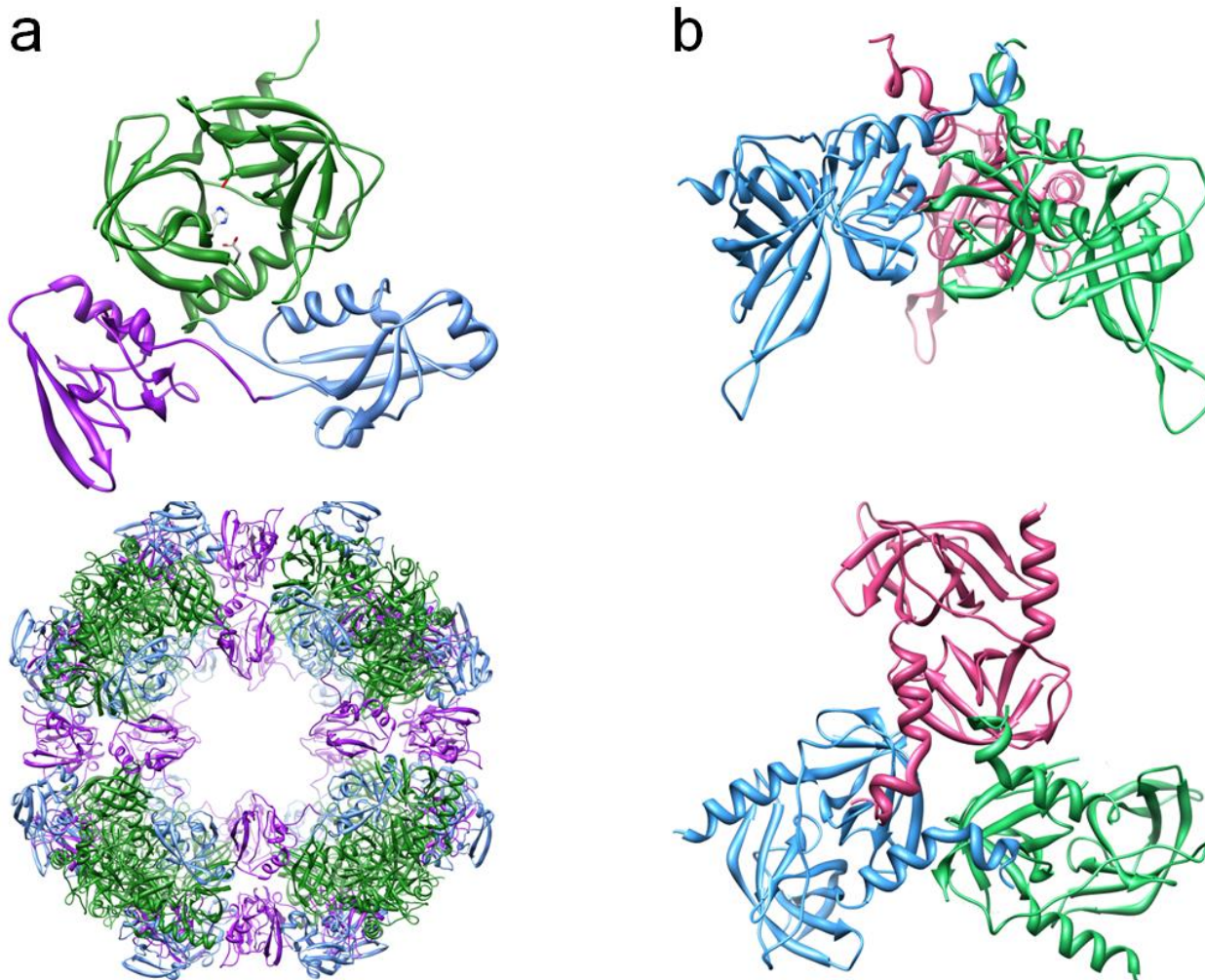
Figure 3 a) X-ray crystal ribbon structure (PDB entry 3CS0) of DegP monomer protease domain (green) with its two carboxyl terminal PDZ domains (blue, purple) is shown at the top. Side chains of catalytic triad are shown in grey. DegP 24-mer is shown at the bottom. b) X-ray crystal ribbon structure (PDB entry 3NUM) of trimeric human HTRA1 protease domains (each in green, blue, and red) in side view at the top and in top view at the bottom.

In the active state the loops L1, L2, L3 and LD rearrange from a disordered to an ordered conformation resulting in catalytic active distances of the active-site residues (figure 4a). The oxyanion hole, which stabilizes negatively charged oxygen of serine328 during catalysis, is formed by the residues 325-327 of loop L1. Loops are described using the chymotrypsin nomenclature. The specificity pocket selecting for P1 residue, which is the substrate's amino acid of which the carbonyl group is attacked and thereby cleavage occurs, is built of the side chains of the residues lysine346 and isoleucine323 suggesting a preference for aliphatic residues such as leucine or valine. Studies about the preferable attacked P1 residue's side chain showed a strong preference of leucine followed by valine, alanine and threonine[30, 31]. Cleavage was also observed after methionine, serine, isoleucine and glutamine[30]. A mixture-based oriented peptide library screen confirms the P1 preference and reveals that in P1' and P3' position polar residues, namely arginine and aspartate, are dominant. Nonpolar residues, namely proline and phenylalanine were preferred at P2' and P4' position[37].
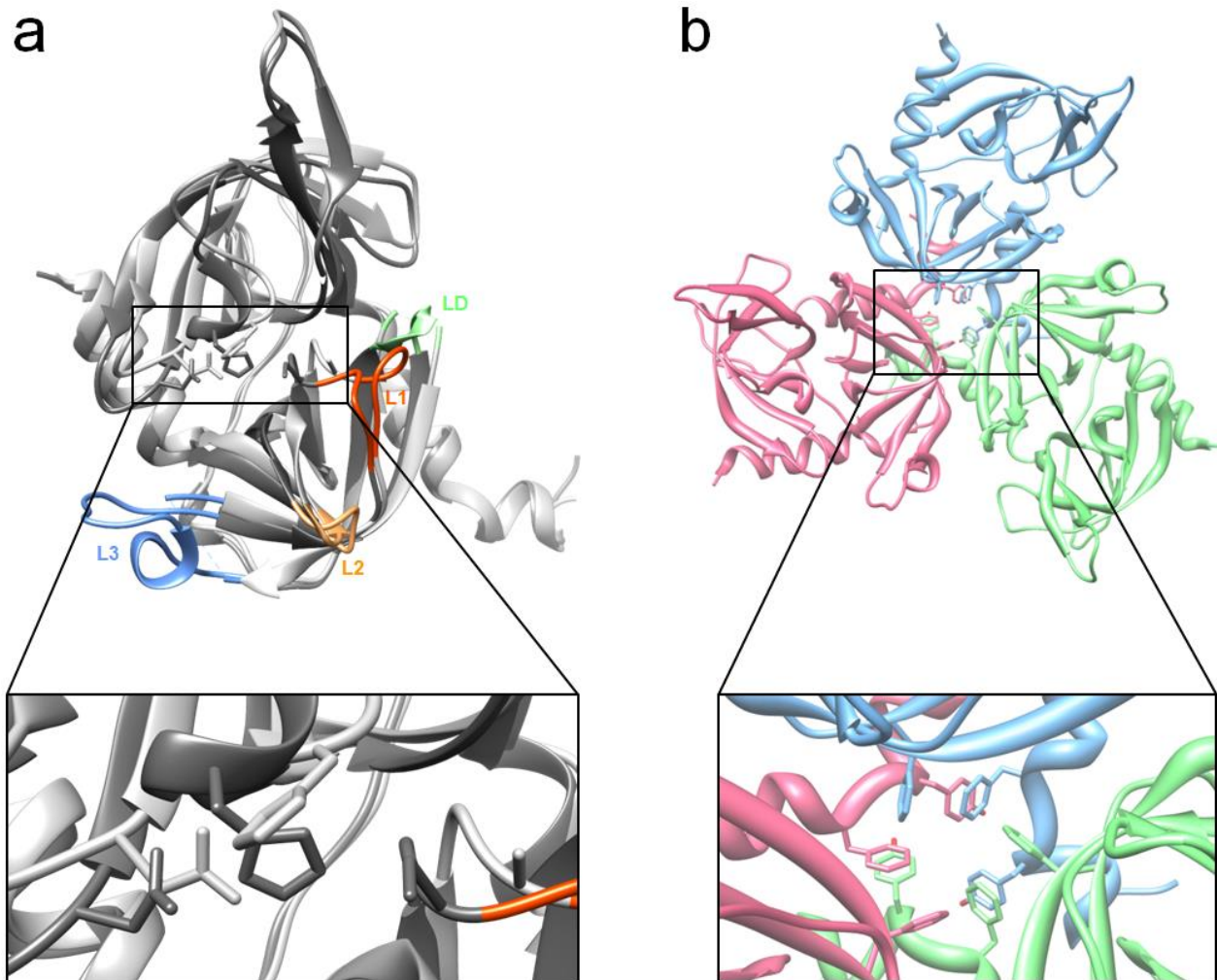
Figure 4 a) X-ray crystal ribbon structures of human HTRA1 protease domain in active (dim grey) and inactive state (grey) superimposed. The loops LD, L1, L2 and L3 involved in reversible activation mechanism are indicated in green, red, gold and blue. Active side residues are shown in detail at the bottom. b) X-ray ribbon structure of human HTRA1 trimer. Aromatic residues mediating trimerization by hydrophobic interactions are shown in detail at the bottom.

2.1.2. Function of HTRA1

Recent studies revealed that mammalian HTRA1 is involved in many physiological processes of cells such as migration, growth, invasion and neoplasticity[38-43]. These multiple tasks are correlated to its broad substrate spectrum. It was shown that HTRA1 is a mediator in signaling pathways. It degrades insulin growth factor binding protein (IGFBP5) which results in the release of insulin growth factor 1 (IGF1) that stimulates cell proliferation[44]. Another target of HTRA1 is transforming growth factor beta (TGFβ). Its inactivation is a control mechanism in neuronal maturation as well as developmental survival[45]. Additionally, further members of the TGFβ family are processed by HTRA1 such as bone morphogenic protein 4 (BMP4), growth differentiation factor 5 (GDF5) and activin which was shown to be associated with defects in chick eye development[46]. Tuberin, a tumor suppressor protein is activated by cleavage of its pre-form. This activates the downstream elements eIFE4E-binding protein (4E-BP1) and S6 kinase (S6K) leading to initiation of translation[47]. Besides cell signaling molecules, numerous proteins of the extracellular matrix have at least one HTRA1 cleavage site, such as fibronectin, decorin, aggrecan, type-II collagen, vitronectin, fibromodulin, biglycan, clusterin, a disintegrin and metalloproteinase domain-containing 9 (ADAM9) and the amyloid precursor protein fragment Aβ [18, 46, 48-50]. DegP as well as HTRA1 were shown to degrade the unstructured protein β-casein into several polypeptide fragments. DegP, as well as human HTRA1 are endoproteases[31, 51, 52].

Although structural studies reveal preference of HTRA1 for cleavage after large aliphatic amino acid side chains[31] there are substrates being cleaved after other residues[30]. Alignment of known substrate

sequence residues before P1 residue does not indicate a clear consensus sequence to be preferred in cleavage by HTRA1, raising questions of the mechanism of substrate recognition and specificity[30, 31, 53]. Besides the natural substrates mentioned above, some artificial chromogenic substrates of HTRA1 especially for DegP were developed such as peptides labeled with para-nitroaniline derived from *E. coli* citrate synthase sequence (DPMFKLV-pNA) and anti-RNA polymerase sigma factor E sequence (VFNTLPMMGKASPV-pNA)[31]. Another fluorescence-quenched peptide substrate (Mca-IRRVSYSF(Dnp)KK) named H2opt derived from a substrate library screened on HTRA2 was also reported[30, 53]. This substrate allowed more sensitive measurements of HTRA1 activity compared to chromogenic substrates. The poor affinity to all known artificial substrates reveals that HTRA1 activity is low *in vitro* possibly due to a lack of physiological allosteric activators[30]. Furthermore, it remains unclear whether HTRA1 recognizes structural motifs or sequence motifs distant from the P1 position[30].

For DegP it was shown that activity raises at temperatures above 30 °C in a non-linear manner, whereas it was almost inactive at temperatures below 20 °C[15, 54]. A similar temperature-dependent gain of activity was observed for human HTRA1[31].

Only few inhibitors of human HTRA1 are known. It is inhibited by diisopropyl fluorophosphate (DFP) like DegP[30]. Interestingly, for DegP it was demonstrated that it was only inhibited by DFP but not by phenylmethylsulfonyl fluoride (PMSF)[51]. Both irreversible small molecule inhibitors are unspecific and highly reactive with the serine protease catalytic active serine. Another boronic acid-based HTRA1 inhibitor NVP-LBG976 was developed by Novartis[55]. Further inhibitors for DegP were developed by introducing chloromethyl ketone or boronic acid functionalities at the carboxyl-terminus of artificial peptide substrates. It was shown that human HTRA1 was inhibited by DPMFKLboroV which also acts on *E. coli* DegP[31, 47]. Additionally, it was shown that HTRA1 activity is inhibited by the serum protease inhibitor alpha-1 anti-trypsin, a finding that points in the direction of alpha-1 antitrypsin being a potential physiologic inhibitor[56].

DegP was found to be attached to cellular membranes due to positively charged residues of first and second PDZ domains[57, 58]. Similar observation was made for human HTRA1 where positive charges on the surface distal from the active-site were assumed for localization on liposomes[31]. This localization could be relevant for cell migration by processing signaling molecules, as well as molecules of the extracellular matrix[59]. Although human HTRA1 possesses a signal sequence that translocates it to the extracellular matrix, about 20 % is located in the cytoplasm[55]. Interestingly, HTRA1 was observed to be co-localized to tubulin[31]. The mechanism for the cellular distribution remains unclear.

2.1.3. Role of HTRA1 in Disease

HTRA1 expression was observed to be altered in various human diseases[40]. Elevated expression levels were detected in osteoarthritis (OA), age-related macular degeneration (AMD), rheumatoid arthritis (RA) and preeclampsia[48, 56, 59, 60]. Additionally a mutation resulting in a loss-of-function variant of HTRA1 causes the inherited neuronal defect cerebral autosomal recessive arteriopathy that is associated with subcortical infarcts and leukoencephalopathy (CARASIL)[19].

Lower expression levels up to total loss of HTRA1 is observed in different cancers and results in reduced sensitivity to chemotherapy, indicating a role as a tumor suppressor[61]. This observation is confirmed by inhibition of proliferation *in vitro* and reduced tumor growth *in vivo* by overexpression of HTRA1[43]. Low expression levels of HTRA1 were reported in ovarian and endometrial cancer compared to healthy tissue[62-64]. Ductal glands usually highly express HTRA1, while its expression is reduced or even totally lost in ductal carcinoma *in situ* as well as in invasive breast carcinoma[65]. Additionally downregulation of HTRA1 is associated with poor survival in cancer. This was shown for mesothelioma and hepatocellular cancer[66, 67]. It is presumed that poor survival is especially caused by the strongly reduced response to chemotherapy by HTRA1 downregulation. This is reported for ovarian and gastric cancer[61, 68]. It is suggested that the reduced response **to chemotherapy is due to HTRA1's ability to** promote apoptosis by degradation of X-linked inhibitor of apoptosis (XIAP). Additionally, migration of cancer cells is enhanced by absence of HTRA1[16, 41]. In non-neoplastic epithelial cells, detachment causes apoptosis. Loss of HTRA1 contributes to survival after dissemination of these cells in metastatic

cancer[69]. The co-localization of HTRA1 and microtubules mentioned before could be correlated with cell motility. Enhanced HTRA1 expression is correlated with reduced cell motility while low HTRA1 expression is correlated with enhanced motility. This finding lead to the assumption that binding of HTRA1 to microtubules affects microtubule stability and dynamics[41]. Moreover, it was shown recently that loss of HTRA1 in breast cancer results in epithelial-to-mesenchymal transition (EMT). This acquisition of mesenchymal features promotes growth and increases migration of cells[65]. Additionally, the EMT process activates DNA damage response pathways resulting in poor response to chemotherapy[65]. These results in summary indicate that HTRA1 acts as a tumor suppressor although the mechanism of downregulation remains unclear. It is conceivable that mechanisms like loss of heterozygosity or epigenetic modulations are responsible for downregulation[62, 65].

In opposite to downregulation in many cancers, HTRA1 levels were found to be elevated in rheumatoid arthritis (RA) and osteoarthritis (OA)[49, 70]. In OA articular cartilage is degraded due to a trauma caused by an accident or obesity for example. The mammalian cartilage consists predominantly of type-II collagen and further pericellular matrix proteoglycans as aggrecan[70, 71]. These pericellular matrix molecules surround the small amount of chondrocytes in the cartilage which are responsible for its homeostasis[72, 73]. It was shown that HTRA1 is the most abundant protease in human arthritic cartilage with substrate specificity to many extracellular matrix molecules such as aggrecan as mentioned above[74]. A model by Polur *et al.* suggests that HTRA1 is involved in the early progression of OA[75]. In this model HTRA1 expression is assumed to be induced through damage of the articular cartilage and leads to degradation of the pericellular matrix. When the pericellular matrix breaks down, DDR2 receptors of chondrocytes bind to type-II collagen fibrils which are separated by the pericellular matrix in the healthy cartilage. This receptor tyrosin kinase (TRK) initiates after ligand binding cell proliferation as well as expression and secretion of matrix metalloproteinase 13 (MMP-13). This metalloproteinase promotes further degradation of the extracellular matrix of the articular cartilage[75]. Although this process is better understood than involvement in cancer, the role of HTRA1 in OA and its consequences have yet to be investigated in more detail.

Interestingly, it was shown that HTRA1 is the first known protease that degrades protein aggregates, since it was shown to degrade aggregates of Tau protein which seems to be involved in neurodegenerative diseases like Alzheimer Disease or Parkinson Disease[76, 77].

2.2. Antibodies and Scaffolds

Recombinant protein therapeutics became first relevant with the FDA approval of recombinant expressed human insulin in 1982[78, 79]. The technological advance in the past thirty years in this area lead to monoclonal antibodies first developed in mice followed by humanization to prevent immunogenicity. Monoclonal antibodies which were developed first by Koehler and Milstein[80] in 1975 through immortalization of a mouse B-Lymphocyte have important advantages compared to small molecules. They show a longer plasma half-life, enhanced efficacy, increased safety and the success rates in the early clinical development phases are higher. Due to this they exhibit better clinical success rates and higher financial turnover[81]. A great advantage of antibodies besides their highly specific binding of therapeutic relevant targets is that they can directly modulate immune responses through interaction of their constant region with receptors of the immune system[82, 83]. At the present day there are multiple molecular biology technologies available for antibody isolation such as phage-, yeast-ribosomal- and RNA-display[84, 85]. Moreover, a plethora of next generation protein therapeutics have been developed which are based on the immunoglobulin backbone or completely unrelated proteins for tailor-made functionalities *in vivo* [86-92]. Figure 5 shows crystal structures of an IgG antibody, its fragments and related molecules of vertebrates, as well as some alternative scaffolds in the same scale in comparison to the HTRA1 homologue of *E. coli*, the DegP 24-mer with its cage-like structure. The main advantage of alternative scaffolds compared with antibodies is a smaller size, which allows a better tissue penetration of solid tumors and binding to grooves and active-sites of receptors and enzymes. A further advantage concerns potentially lower costs in production and purification as well as circumventing complex intellectual property issues[93].
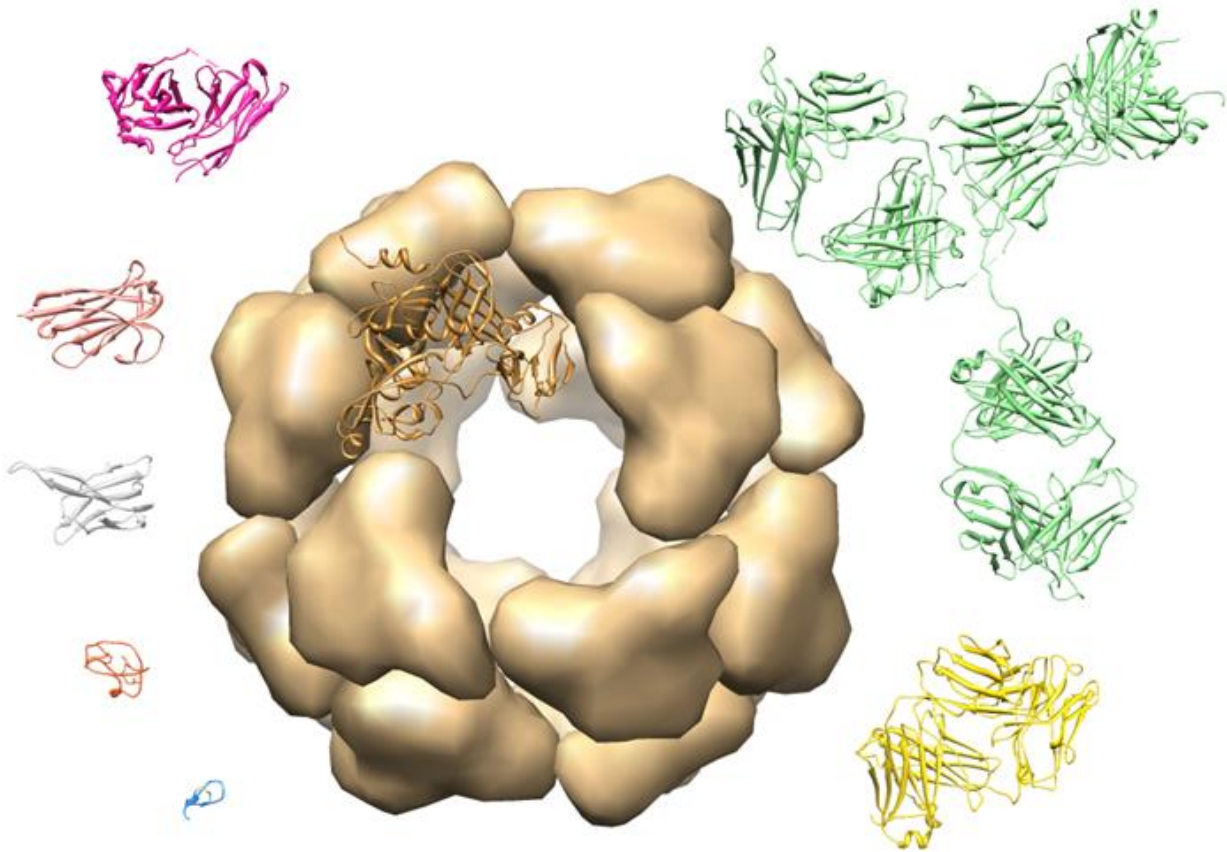
Figure 5 X-ray crystal surface structure of DegP 24-mer (gold). Each monomer consists of 1 protease and 2 PDZ domains. DegP is surrounded by ribbon structures of different molecules used as scaffold for introducing new functionalities. Molecules in clockwise: IgG antibody (green), FAB fragment (yellow), SFTI (blue), ocMcoTI-II (orange), vNAR (silver), VHH (bronze) and scFv (magenta). All molecules are shown in identical scale (PDB entries 3CS0, 1IGT, 3WIF, 1JBL, 1HA9, 1VES, 1I3V, 1X9Q).

While in antibodies target binding is mainly mediated by loop regions that are defined as complementarity derived regions (CDRs)[94], the designer of an alternative scaffold can choose one or multiple regions of the protein scaffold of choice to be used for the generation of a binding site which should be insensitive against sequence variation in view of stable folding. Most abundant are approaches where loops connecting secondary structure elements are randomized[90, 95-98] but there are also concepts randomizing surface-exposed residues of helical structures or β-sheets[90, 95, 96, 98]. For the design of these alternative strategies it is indispensable to study the three-dimensional structure of a scaffold to categorize regions important for a stable fold and for residues which are considered for target binding.

While antibodies are predominantly generated by immunization of an animal with an antigen, there are two completely different ways to engineer a scaffold protein, namely rational design or directed evolution. A typical process of a directed evolution experiment is shown in figure 6a. Additionally a directed evolution approach can be combined with functional optimization based on rational design and/or structural knowledge. For example, random exchange of amino acids can be restricted to regions involved in target binding.

Besides the library design the method for isolating the protein of interest is crucial. The biggest challenge in directed evolution is the isolation of molecules with desired properties from a large set of candidates which is comparable with finding a needle in a haystack. To overcome this problem, it is necessary to establish a screening procedure that allows one to separate the wanted from the unwanted molecules. The fact that it is impossible to sequence one single protein molecule leads to the **problem that if the "needle" is found it is** almost invisible and so impossible to analyze and reconstruct it. The biggest achievement to overcome this problem is the linkage between the molecule of interest

and its encoding genetic information, namely its desoxyribonucleic acid (DNA), named genotype-phenotype linkage. DNA has the benefit compared to proteins that it is easy to amplify *in vivo* and *in vitro* and additionally it is easy to obtain its sequence. Almost thirty years ago Smith *et al.* developed a system, where molecules were presented on the surface of phage particles after they were cloned into a vector and transformed in *E. coli*[99]. Due to the fact that the information-storing DNA for the presented molecule is combined in one phage particle it is possible to re-infect a bacterium and amplify the single DNA copy by divisions of the host followed by DNA-sequencing[100]. In a typical directed evolution experiment, conceptually each phage particle displays a different molecule. The protein of interest can be enriched during repeated selection cycles and finally isolated. In a typical experimental setting for the isolation of binding proteins, the target structure is immobilized on a surface where binding phages are captured and nonbinding phage particles could be washed away[101].

Besides phage display there are also cell-free systems as the RNA and the ribosomal display[102]. Further cell-based systems are the bacterial and the yeast cell surface display (YSD)[103, 104]. The latter was invented in 1997 by Wittrup *et al*[105] and has become, together with phage display, one of the most powerful tools in academic and industrial drug development for biological pharmaceuticals. Particularly the YSD platform emerged as a powerful tool for engineering affinity, specificity and stability of antibodies and other scaffold proteins[103, 106]. The basic idea of YSD is the linkage of a protein of interest on the yeast cell wall where it is exposed for interaction with labeled target molecules in solution. The linkage is mediated by the genetic fusion of the potential binding protein to the mating protein agglutinin alpha 2p (Aga2p) which is anchored in the cell wall via covalent linkage with the Aga1p protein (Aga1p)[107]. The schematic construct presented on the yeast surface is shown in figure 6b. Both mating proteins are expressed under control of the GAL1 promoter, allowing an inducible over-expression. Essential components of the YSD are the shuttle vector pCTCON and its derivates allowing the fusion of Aga2p and the protein of interest by cloning or gap-repair as well as the yeast strain EBY100 and its derivates with the genomic integrated Aga1p under the control of an inducible promoter[105, 108]. Libraries constructed by homologous recombination reach a size of at least 10^{10} transformants which is relatively small compared to other display systems[101, 109, 110], but can be compensated by its general advantages as well as several additional techniques like affinity maturation for example. In addition, there are three basic approaches for library screening through different labeling, namely equilibrium binding, competition for limited antigen and kinetic competition, each addressing different kinetic parameters[103].
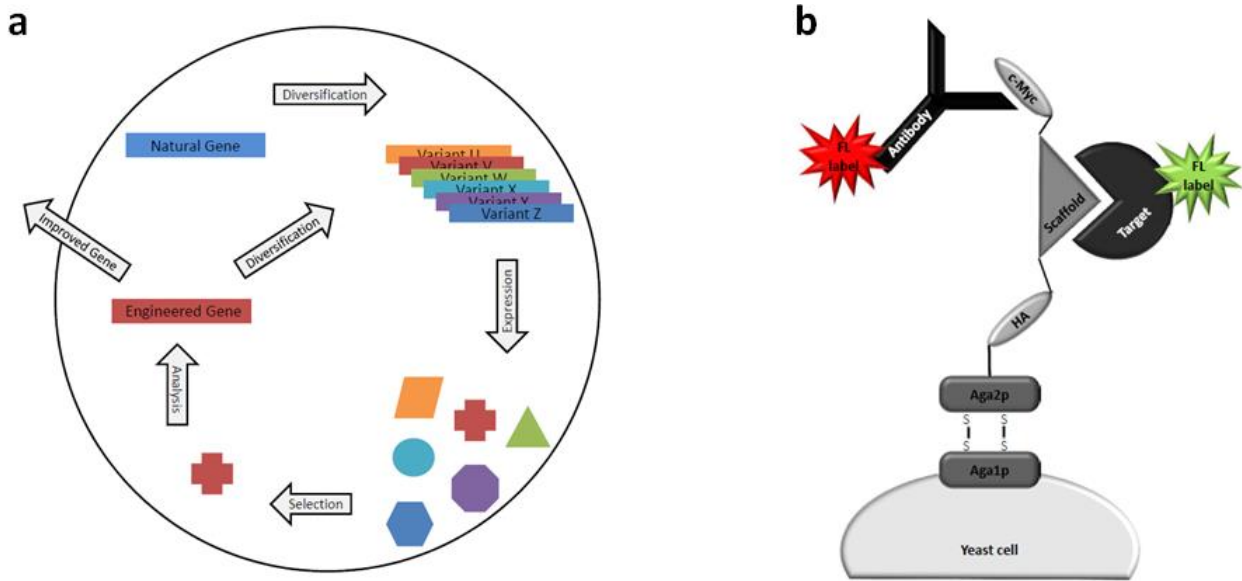
Figure 6 a) Scheme of the workflow of a typical directed evolution experiment. b) Schematic construct presented on the yeast surface in yeast surface display. Aga1p is anchored in the yeast cell wall and is covalently linked to Aga2p by cystines. The displayed scaffold library is flanked by a HA and a myc tag for evaluation of surface presentation via labeling with antibodies. Target molecules and antibodies are typically fluorescently labeled for isolation of molecules by fluorescent-activated cell sorting (FACS).

The main advantage of YSD compared to cell-free systems and phage display is the use of fluorescence-activated cell sorting (FACS) for the isolation of binders of fluorescently labeled target proteins. Furthermore, analysis of isolated single clones is simplified by FACS because the binding properties of their molecules can be easily evaluated on the yeast surface without soluble expression. Acquired data is consistent with measurements using BIAcore or enzyme-linked immunosorbent assay (ELISA)[105, 111-113]. Beyond that the quality control mechanisms of eukaryotic cells residing in the endoplasmatic reticulum ensures removal of misfolded protein variants, a feature that is particularly important for disulfide-containing proteins[114]. A competition of a pre-immune single-chain variable fragment (scFv) gene library in screening of HIV antigen gp120 resulted in 3-fold more specific binding molecules isolated with YSD compared with phage display[115].

Although the most suitable antibody fragment for YSD are scFvs, in the early days of of this technique there are methods and formats reported for successful display of fragment antigen-binding (Fab) fragments[116, 117], single chain Fabs (scFab)[118], fragment crystallizable (Fc) fragments[119], whole immunoglobulin G (IgG)[109] and variable heavy chains of a heavy chain antibody (VHH)[120, 121]. The power of YSD is further documented by the successful generation of scFvs with affinities in the pico- and femtomolar range achieved by error-prone PCR and DNA shuffling[112, 122, 123].

Several antibodies are now in clinical phase III trials and some are already approved and marketed that were developed by phage display such as Belimumab, Briakinumab and Adalimumab, respectively[87]. The fact that approving a drug by the Food and Drug Administration (FDA) or the European Medicines Agency (EMA) takes more than a decade, combined with the twenty years chronological advance of phage display compared with yeast surface display and YSD's general advantages against phage display it is likely that the next generation of therapeutic antibodies will contain a significant fraction of molecules that were developed by YSD.

Moreover, YSD proved its versatility for the development of non-antibody proteins. In detail there are reports on the identification of mutations transmitting activated conformations on cell adhesion molecules or engineering the properties of hormones and cytokines[124-128]. Additionally, alternative binding agents based on non-antibody scaffolds as knottins[129-132], fibronectin type III domain[133, 134], and hyperthermophilic DNA-binding protein Sso7p[135], as well as the surface presentation of several enzymes[136-140]; engineering of human immunological proteins and the major histocompatbility complex

were reported[141-143]. Furthermore epitope mapping of designed ankyrin repeat proteins (DARPins) against epidermal growth factor receptor ectodomains[144] and screening of human and insect cDNA libraries have been performed[145, 146].

2.2.1. Immunoglobulin G (IgG)

Immunoglobulins or antibodies are one supporting pillar of the mammal immune system, which has evolved to protect the host from pathogens and toxic substances. They were first described by von Behring and Kitasato in 1890 by the observation that a compound of the blood was able to neutralize diphtheria toxin[147]. Further characterization of immunized serum was carried out by Tiselius and Kabat in 1939 through electrophoresis, size-exclusion chromatography and depletion experiments, revealing that Immunoglobulin G (IgG) is an immunologic active substance[148]. IgGs are a tool of the adaptive immune system which ensures the exquisite specificity for antigens. They are encoded by genes that are assembled by somatic rearrangement of germline gene elements to form B-cell antigen receptors, or IgGs respectively. The combination of a few hundred gene elements leads to the formation of a million IgGs with unique specificity against different antigens. IgGs bind to microbes or particles trigger their neutralization by recruiting phagocytic cells of the immune system as neutrophils, monocytes and macrophages. IgG producing B-cells represent 15 % of peripheral blood leukocytes and differentiate in the bone marrow from heamatopoietic stem cells[149]. B-cell lineage is induced by Interleukine-7 (IL-7) secreted by marrow stromal cells which is followed by sequential heavy and light chain gene rearrangement[150, 151].

Each IgG molecule is built-up of two identical heavy chains and two identical **κ** or **λ** light chains with a molecular weight of each about MW 50,000 and MW 25,000, respectively[152]. Crystal structure of a murine IgG is shown in figure 7. The heavy and the light chain are interconnected by a disulfide bridge. In detail, each light chain contains an amino-terminal variable (V) and one constant carboxyl-terminal domain (C) while the heavy chain constant domain contains three C domains. Each domain possesses 110 to 130 amino acid residues and shows an Ig-fold characterized by a sandwiched 3-strand/4-strand β-sheet intra-connected via a disulfide bridge[153]. The heavy chain additionally bears a hinge region in the linker between amino-terminal constant heavy chain domain (C_H) 1 and C_H2 where the heavy chains are interconnected by at least one disulfide bridge. Papain was found as a protease separating an IgG into two antigen binding fragments (Fab) consisting of V_H, C_H1, V_L and C_L domains as well as one crystallizable fragment (Fc) consisting of two C_H2 and two C_H3 domains[154]. Further separation of the Fab results in a variable fragment (Fv) consisting of V_H and V_L which are used as single chain Fv (scFv) in engineering approaches for recapitulating monovalent IgG characteristics[155]. Individual fragments of an IgG are indicated by bars in figure 7.
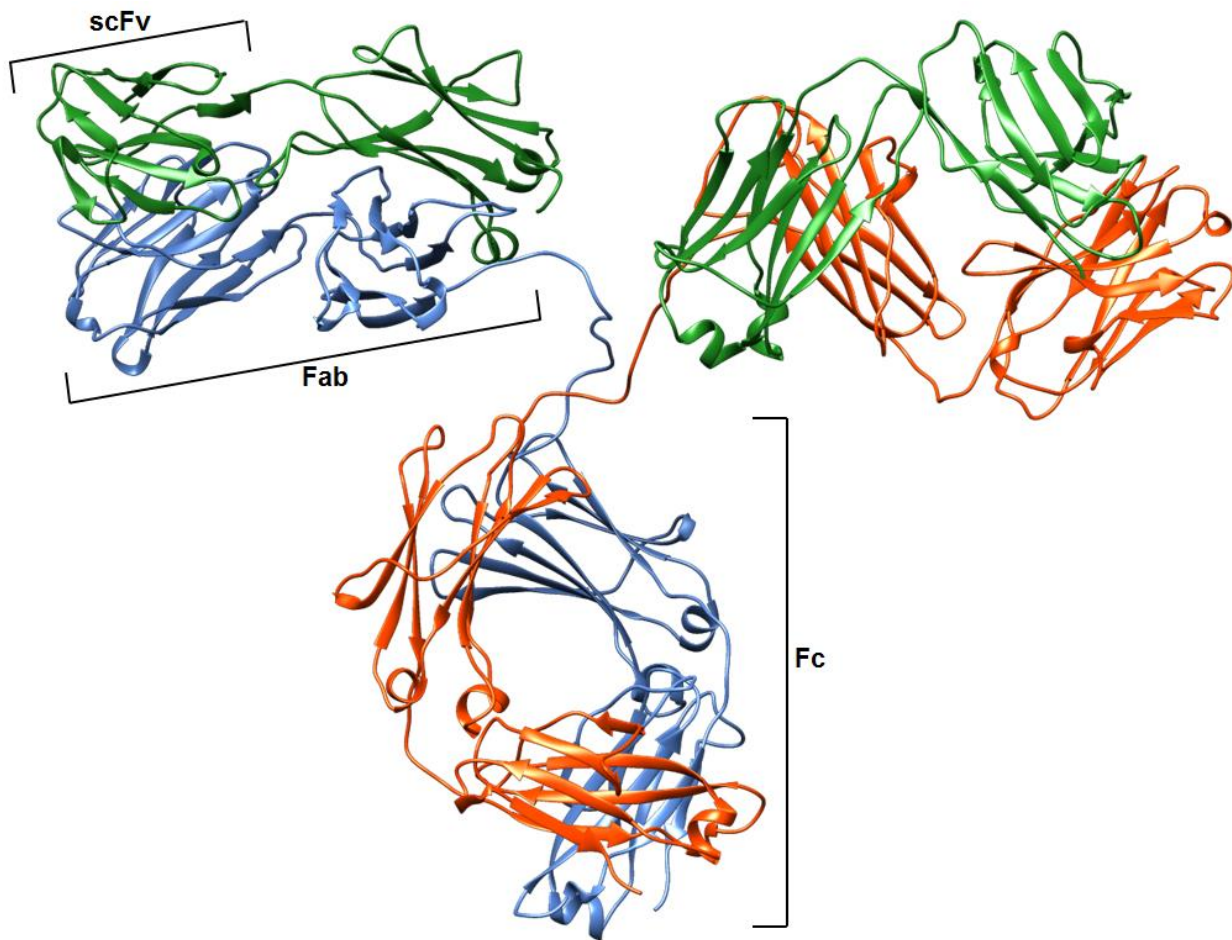
Figure 7 X-ray crystal ribbon structure of murine IgG (PDB entry 1IGT). The heavy chains are shown in blue and red, the light chains are shown in green. Bars indicate the IgG derived scaffolds Fc, Fab and scFv.

The variable parts of an IgG molecule responsible for antigen binding are located at the amino terminus of the heavy and the light chain designated as V_H, V_κ and V_λ. Each variable region is divided into three sub-regions, called complementarity-determining regions (CDRs) which are highly variable and form the antigen-binding site situated between four regions of stable sequence, called framework regions (FRs). In human Igs heavy and light chains genes are separated on different chromosomes and the individual V domains which constitute the CDRs are encoded by independent *VJ* elements for the two loci of the light chain and *VDJ* elements for the heavy chain while the C domains are encoded by individual gene elements each[156, 157]. Recombination of the V domains is a complex procedure and leads to highly diverse target affinities due to the complex and individual arrangement for λ, κ and H chain[94]. The ensemble of CDRs of the heavy and the light chain mediating antigen binding are designated as paratope while the counter part of the antigen involved in binding is designated as epitope. The majority of Igs are produced against intact antigens leading to the detection of a conformational epitope while the unfolded linear antigen sequence is not detected. The carboxyl terminal parts of the heavy and the light chain are constant for each class of Ig whereas the heavy **chain's constant part is responsible for most Ig's effector functions mediated through the family of** different Fc receptors (FcR) on effector cells or activating other immune mediators, such as complement[158]. Thus, alterations in the Fc region lead to significant changes in the response of antibody-antigen interaction. Additionally the Fc part influences the binding properties of V domains against an antigen[159]. There are five different constant parts of antibodies allowing a classification into IgA, IgD, IgE, IgG and IgM isotypes differing in their properties including size, complement activation, FcR binding and antigen interaction. Isotype switching is influenced by the localization, the antigen and the activated downstream signaling pathways[160, 161]. IgG is the most abundant Ig existing in the human body where it shows the longest serum half-life of all Igs making it the most interesting starting

point for antibody therapeutics. There are four subclasses of IgG (IgG1, IgG2, IgG3 and IgG4) differing in their constant region domains C_H1 and C_H3 resulting in structural, functional and antigenic differences. IgG subclasses were ranked according to their distribution in the human body whereas IgG1 is the most abundant. The IgG subclasses differ in the flexibility of the Fab because of the different C_H1 domains which results in an altered interaction with potential antigens. IgG subclasses distinguish themselves in their ability of complement activation or in secondary antibody response where IgG1 and IgG3 are predominantly expressed for protein antigens while IgG2 and IgG4 are expressed for antigens associated with polysaccharides. Another difference is their ability to bind the three classes of FcγRs (FcγRI, II and III). While IgG1 and IgG3 bind to all FcγRs, IgG4 only binds FcγRI and FcγRII as well as IgG2 only binds FcγRII. There is an additional FcR, the neonatal FcR (FcRn), which regulates the serum level of IgG by endocytosis after binding. For higher IgG serum level the IgG bound by FcRn in the endosom is recycled or for a lower IgG serum titer IgG-FcRn is neutralized by the lysosome.

Moreover, Igs are glycosylated especially in the Fc region, which has been shown to influence antibody function. **This glycosylation patterns differ with the antibody's isotype**[162]. Although all CH2 domains of IgGs heavy chain correspond in glycosylation site Asn297, the glycosylation extent alters by different sugars in different positions leading to 32 unique glycosylation patterns. IgG structure is stabilized through glycosylation, giving a longer serum half-life. Degree of stabilization changes with different glycosylation patterns[163, 164]. Beyond that, it was shown that IgG glycosylation is indispensable for binding to FcRs. The two main effector functions mediated through FcR for IgGs (FcγR) are antibody-dependent cellular cytotoxicity (ADCC), in which antibody-labeled antigens activate immune cells like monocytes or natural killer cells and complement-dependent cytotoxicity (CDC), where IgG is binding to C1q an initial key player of the complement system. For both effector functions a specific glycosylation pattern is crucial[165-167].

The fully mature Igs have an additional carboxyl-terminal transmembrane domain allowing surface presentation named Igα and Igβ which enables an intracellular signaling of the presenting B-cell after antigen binding[168, 169]. These presented antibodies of naïve B-cells are the isotypes IgM and IgD constructed by alternative splicing of the same $V_HD_HJ_H$ exon to the μ and δ heavy chain exons resulting in a membrane-bound variant. This alternative splicing called class-switch recombination (CSR) allows the B cell to switch all isotypes between membrane-bound and secreted Igs by a DNA rearrangement mediated by several enzymes, which is induced by T cell-derived cytokines and T helper cells. This allows a grafting of a functional $V_HD_HJ_H$ binding unit to different antibody isotypes with the same antigenic specificity[170]. T cell-derived IL-10 causes switching to IgG1 and IgG3 isotype, while Interferon-γ (IFN-γ) and other molecules from T helper cells causes switching to IgG2, for example. Parallel to CSR the B cell introduces actively random mutations in the antigen-binding segments mediated by activation-induced cytidine deaminase, uracil DNA glycolyase, APE1 and DNA repair enzymes[171]. A mutation resulting in a loss of antigen binding results in a loss of growth signals important for survival and in opposite mutations leading to increased binding affinity to the antigen results in signaling molecules for proliferation of the B cell[172]. The consequence of this is a clonal selection of B cells expressing antibodies with a high affinity and specificity located in the center of the secondary lymphoid tissue like the spleen, adenoids, tonsils and the skin[173]. Most often T cells induce activation and maturation of B cells as well as the isotype of antibody they produce. In case of repeated exposure to an antigen a T cell mediated maturation event occurs, which is called somatic hypermutation (SHM) and delivers 10^{-3} changes per base pair for each maturation round involving two mechanisms. On the one hand there is targeting of mutation hotspots made up by a *RGYW* (purine/G/pyrimidine/A) motif and on the other hand error-prone DNA synthesis[174, 175]. Besides CSR and SHM, T cells mediate differentiation of B cells into continuing plasma cells or into continuing memory B cells, the latter especially after a repeated antigen exposure[176]. This memory response is responsible for the extraordinary effect of vaccination. Without T cell stimulation B cells differentiate in short-living plasma cells with limited class switching opportunities emphasizing the importance of T cell communication.

2.2.2. Variable Domain of a Heavy Chain Antibody (VHH)

The members of the *Camelidae* family *Camelus dromedarius*, *Camelus bactrianus*, *Lama glama*, *Lama pacos*, *Lama guanicoe* and *Lama vicugna* show a unique feature in the mammal immune system concerning their IgGs. While IgGs usually consists of two heavy chains and two light chains, in the 1990s emerged an additional variant in camelids that only consists of two heavy chains, named heavy-chain antibodies (HCAbs)[177]. HCAbs, named isotypes IgG2 and IgG3 are delivered by B cells during a classical immunization reaction as well as common IgG molecules namely IgG1[177]. The ratio of HCAbs compared to IgGs varies from camels with around 50–80 % to lamas and alpacas with an amount of around 10–25 %[178]. The organization of the variable heavy chain (HV) is quite similar of both, common IgG and HCAb. Interestingly, a disorder was observed in humans leading to HCAbs constructed by genetic deletion events resulting in a pathological disorder[179, 180]. The important differences explaining the equivalent binding properties of an antigen by lack of a light chain is compensated by a more extended CDR1 and CDR3 compared with a classical IgG. Moreover, the canonical loop structures of the CDRs deviate in sequence and structure from hypervariable regions of VH in mouse and human[181, 182]. An extra conformational difference occurring mainly in dromedaries is an additional intramolecular disulfide bond of CDR1 and CDR3[183, 184]. Furthermore, the area of the heavy chain which is responsible for interaction with the light chain by highly conserved hydrophobic residues in framework 2 is substituted to ressemble a more hydrophilic surface[183-185]. Hence, these mutations show no conformational rearrangements of the Ig-fold but overcome instabilities and regain solubility resulting from the lack of a light chain[186, 187]. Another difference to IgGs is that the heavy chain consists only of three instead of four globular domains found in IgG, whereas the C_H1 domain is missing. The C_H2-C_H3 **domain is highly homologous to IgG's Fc which is directly** connected to V_H domain in HCAbs referred as variable domain of a heavy chain antibody (VHH)[188, 189]. It was shown that the VHH is a functional antigen binding unit[183-185, 189, 190].

The antigen binding unit of an HCAb, the VHH also called Nanobody (Nb) reveals a number of benefits compared to the Fab and scFv of classical antibodies. VHHs typically denature between 60-80 °C but there are also stable VHHs described resisting temperatures above 90 °C, demonstrating their high stability[191, 192]. Corresponding to this shelf life for months as well as incubations for several weeks at 37 °C do not reduce the antigen binding capacity[193]. Immunogenicity was not observed by injection of VHHs to human and mouse as it was supposed due to its stable behavior, high sequence homology to human VH and its small size leading to a rapid renal clearance[194-196]. Additionally, there are approaches for humanization of the non-homologous amino acid residues[197]. Its molecular weight (MW) of about 15,000 is half of the MW of the smallest antigen binding unit of classical antibodies, namely scFv and delivers a molecule able to protrude into cavities like active-sites of enzymes or buried epitopes, respectively. This ability is enhanced by its paratope architecture formed by the CDRs giving a preference for binding of cavities. These reasons making them interesting as scaffolds for affecting enzyme activity by designing inhibitors and activators[194, 198-203]. The small size further leads to a better tissue penetration compared with Igs with the consequence of better antigen neutralization[204-206]. Furthermore scFvs tend to dimerize in contrast to VHHs. Access to VHHs is easy because of their biotechnological handling, as multiple expression systems as bacteria, yeast, plants or mammalian cell lines in sufficient laboratory scales are described[207-210]. The most convenient strategy to obtain highly specific and affine VHH molecules is immunization of camelids followed by cloning into a directed evolution system as phage display[193, 211]. Moreover, synthetic and non-immunized libraries obtained and pooled from various individuals were described[212, 213]. Isolated VHHs usually display equilibrium dissociation constants in the sub-nanomolar range. There are published approaches where two VHHs with different specificity were genetically fused, resulting in bivalent molecules as well as bi- or multivalent fusions that enlarge binding affinity by avidity effects[91, 200, 214, 215]. Finally it was shown that fusions to the Fc combine the advantages of an Ig and the VHH which were previously described[216, 217]. These properties are crucial making VHHs an interesting molecule for various applications as research tools and in diagnostic and therapeutic applications[218-220]. In applications as research tools, VHHs were used to stabilize membrane proteins for structure determination by crystallization, or in subcellular localization and therapeutic target validation through intracellular co-expression[221-227]. The diagnostic

use of VHHs is fostered by its rapid renal clearance due to its small size. The resulting short plasma half-life in blood makes it possible to use radio-labeled VHHs as probes for *in vivo* imaging with positron emission tomography, which was already demonstrated by mouse xenograft experiments[228-231]. The most interesting field for VHHs is their therapeutic application because of the benefits compared to classical antibodies, while the disadvantages of short plasma half-life and missing effector functions can be overcome by pegylation, fusion to albumin binding units or Fc domains[232]. VHHs that are able to cross the blood-brain barrier or lead to transcytosis across epithelia are published[215, 233-235]. Furthermore, there are several VHH-based therapeutics in clinical phase I and II trials against IL6R, TNFα, RANKL or von Willebrand factor[236]. Finally, oral or inhalative administrations which are more patient-friendly are conceivable.

2.2.3. Variable Novel Antigen Receptor (vNAR)

Sharks are the oldest vertebrate taxon that possess the key components of an adaptive immune system as described for mammals. That includes the combination of detecting invading molecules by low affine receptors followed by their maturation to highly specific and affine neutralizing compounds. As previously described this task is fulfilled by TCRs, Igs, RAGs, MHC as well as somatic hypermutation occurring in specialized compartments as the primary and secondary lymphoid tissue[237]. After Greenberg discovered IgM molecules in sharks it was shown by Flajnik *et al.* that in nurse sharks which are members of the order Orectolobiforme, there also exist heavy chain antibodies. These Ig molecules characterized by the lack of a light chain were designated Immunoglobulin novel antigen receptor (IgNAR) and were found in sharks at an amount of around 30-fold less than IgM[238-240]. In detail IgNARs were found in spiny dogfish and in nurse shark which are separated phylogenetically by approximately 200 million years which indicates distribution over most elasmobranchs[241]. According to vertebrate antigen receptors there exist soluble and B-cell presented IgNAR molecules. Research on IgNARs revealed that the membrane bound variant has three or five domains while the soluble variant always consists of five domains[242]. Additionally there is an antigen driven selection mechanism indicated through a higher degree of mutations in the soluble variant[243]. Nevertheless IgNARs show only low sequence homology to human antibodies but also homology to cell adhesion molecules and TCRs[240]. Thus it is likely that IgNAR evolved independently of vertebrate antibodies by the elasmobranch immune system[244]. Similar to VHHs there are residue substitutions at the interface region of IgGs VH and VL domains, where hydrophobic residues are exchanged against hydrophilic amino acids. Combined with further differences like the extremely shortened CDR2 region the IgNAR binding domain, called variable domain novel antigen receptor (VNAR), is the smallest described independent antigen binding unit in animal kingdom. Besides these sequence differences there are different rarely replaced cysteine residues allowing a separation into three defined types of IgNAR (I, II, II)[245-247]. Type III was only observed in neonates, while Type I was exclusively observed in nurse sharks. Also in families of the same order there were only Type II IgNARs described. All Types share a highly conserved disulfide bond at residue 35 and 107 that stabilizes the Ig fold of the VNAR domain. Type I carries two further disulfides comprised by cysteines in framework 2 and 4 which are connected to two cysteines encoded by CDR3. Type II is connected by one additional disulfide bond encoded by CDR1 and CDR3. While CDR3 of Type I is bent down due to its two disulfides, the CDR3 of Type II is presented in a protruding manner, stabilized by the connection to CDR1 giving them completely different binding properties. As mentioned previously, there is no defined CDR2 in VNAR but there are two elements located between CDR1 and CDR3 which are similar to hypervariable loops (HV) 2 and 4 found in TCRs[248]. Studies revealed that Type I CDR3 is on average about six residues longer than Type II, while Type II shows higher frequency of mutations in CDR1. Moreover sequence variation of HV2 from Type I is greater compared with Type II[249].

Sharks have three heavy chains of which two (IgM and IgW) are combined with four light chain loci[238, 250]. The organization of these elements is different of that compared to the mammalian systems, because in sharks they are clustered[251]. In detail, sharks possess only one *V* segment which is combined in a cluster with at least one *D* segment, one *J* segment and a set of *C* segments which are rearranged exclusively by RAG recombinase[240, 252-258]. As a big difference compared with vertebrates there is no isotype switching between the clusters observed. The most effective mechanisms for the heterogeneity

of the naïve repertoire of shark antibodies are the N-addition and the *D*-region rearrangement. Additionally the 5' nucleotide addition mediated by TdT is highly similar to the mechanism in higher vertebrates[258]. The lack of a light chain in IgNARs is compensated by the number of recombination events and the presence of additional *D* segments[240]. Besides these recombination events there is also an extensive N and P nucleotide addition, which predominantly enhances naïve diversity of CDR3. Particularly important for secreted IgNAR selectivity and affinity is affinity maturation by somatic hypermutation. The mutational patterns are similar to those of mammals but unusual base changes occur in tandem[245]. Besides affinity maturation, sharks possess a secondary feature of an adaptive immunity, the memory of recognized antigens. An antigen-specific response was observed in different elasmobranch species when challenged by IgM serum analysis[239, 259-261]. Similar to IgM an adaptive response was shown for IgNAR by repeated immunizations with hen egg lysozyme (HEL) with an expression plateau after 4 months. In further re-immunizations antigenic-memory was proved[262]. Interestingly, sharks are the only vertebrates with an adaptive immune system which shows no class switch recombination. The epigonal organ attached to the gonads and the Leyding organ, which is localized at the oesophagus, are the critical tissues for lymphopoiesis in elasmobranches that possess at least one of them. These organs are composed and organized like the primary lymphoid tissue in higher vertebrates[263]. The epigonal organ exhibits large numbers of secretory B-cells in adult sharks suggesting an analog function to mammalian bone marrow. Although there are no germinal centers for B-cell activation observed, it is highly indicative that the spleen is the compartment for B-cell activation due to its mammalian like structure[264].

vNAR domains combine many interesting features, among them high stability against denaturing agents and the capability to refolding after heat denaturation. Due to high urea concentrations in sharks blood, vNARs are extremely stable and according to their hydrophilic surface they are highly soluble resulting in high expression levels already in bacterial expression systems[265-267]. They are slightly smaller than VHHs giving them the opportunity to access buried epitopes and binding pockets. Having a significantly different binding loop composition compared to VHHs, they are not only an alternative to VHHs but also an additional scaffold for designing proteins with high specificity and affinity for difficult to address target molecules and for recessed epitopes such as the active site of enzymes[266, 268-272]. A vNAR phage display library constructed of nurse shark RNA previously immunized with HEL allowed the isolation of vNAR variants in the nanomolar range against HEL. Sequences of HEL binding vNARs were analyzed and mutations were separated into those occurred through somatic hypermutation and to class switch recombination[253]. Additionally, crystal structures of a matured vNAR and its germline ancestor in complex with HEL revealed positions important for highly specific and affine binding[254]. Another approach using the naïve repertoire of wobbegong sharks combined with random mutagenesis delivered a selective IgNAR against Gingipain K protease[273]. Additionally, vNARs from naïve and semi-synthetic libraries from spiny dogfish delivered binding molecules against cholera toxin and ricin in the nanomolar range[265]. vNARs can be produced in various formats and strategies already used for VHHs or other scaffold proteins such as dimerization can be applied[274]. Oligomerization of binding molecules specific for different targets, is interesting for enlarging the specificity to a neoplastic cell that overexpress surface receptors that are not unique on the cell for example. Another strategy is to enlarge serum half-life of molecules by fusion to polyethylene glycol, serum albumin binding molecules or Fc parts. For the above-mentioned reasons it is beneficial to have small and stable monomeric molecules because of an easier expression with higher yields of active molecules with high stability for chemical or biological conjugation compared with classical antibodies. The phylogenetical distance of 400 million years to the mammalian adaptive immune system results in little sequence homology, which makes them a powerful alternative to VHHs which clearly evolved from antibodies.

2.2.4. *Momordica cochinchinensis* Trypsin Inhibitor II (McoTI-II)

Momordica cochinchinensis Trypsin Inhibitor II belongs to the family of knottins. These peptides of 28 to 35 amino acids in length are connected by three disulfide bridges, resulting in a defined three-dimensional structure leading to the name cystine knot miniproteins. Knottins are found in many different kingdoms of nature as fungi, plants, insects, mollusci, mammalia and viruses with more than

2000 reported sequences until now[275-278]. The most interesting property of these molecules is the extremely high chemical and biological stability which results from their unique structure. It was shown that most members of this family are stable against boiling, storage at 65 °C over months or extremely unphysiological pH values (1 M HCl, 1 M NaOH). Additionally many of them are resistant against degradation of serum proteases[22, 279-281]. All cystine knot miniproteins share the same cystine pattern where cys #1 is connected to cys #4, cys #2 to cys #5 and cys #3 to cys #6. This results in a pseudo-knotted center, which is further defined by three antiparallel β-strands connected by loops that vary in sequence and length. Nevertheless the backbone of peptide bonds is highly structural rigid[282].Crystal structure of the open chain variant of knottin McoTI-II is shown in figure 8. Disulfide bridges and side chains of loop 1 residues are outlined.
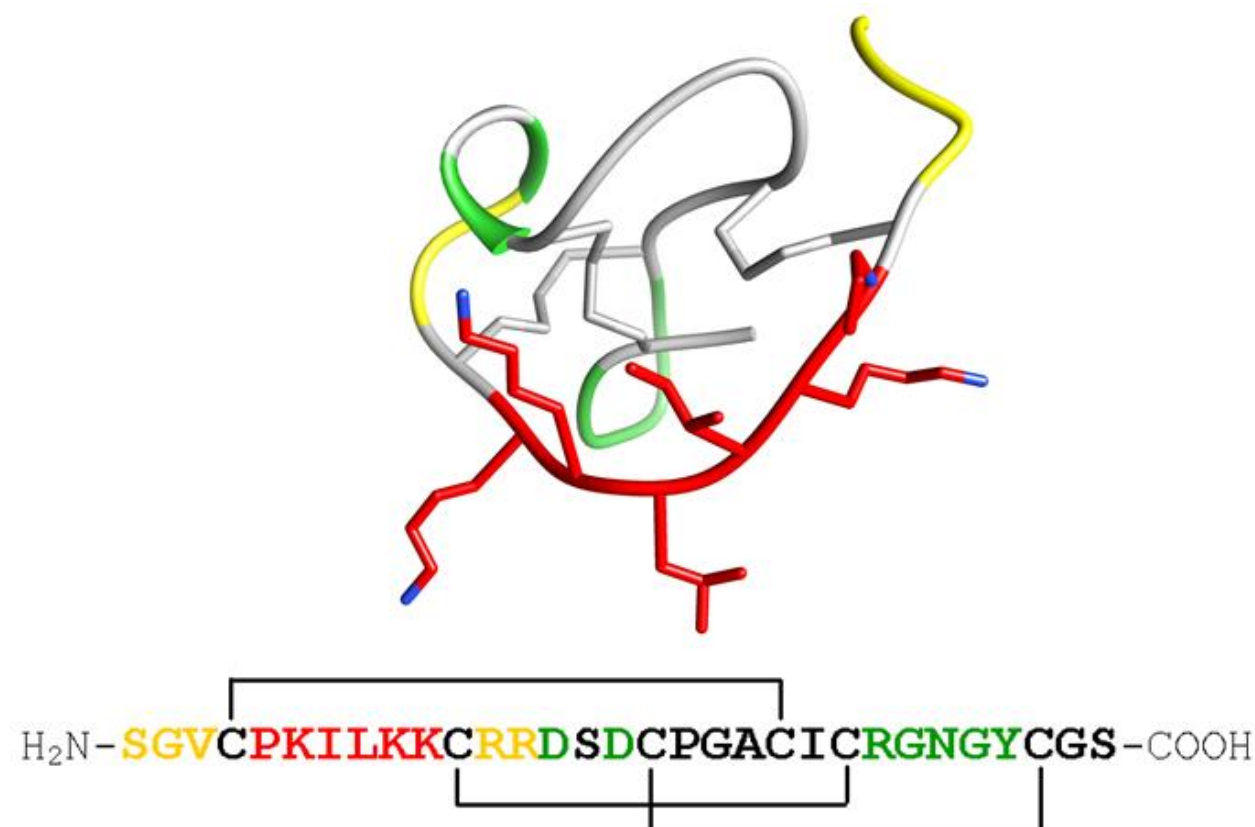

Figure 8 X-ray crystal structure (PDB entry 1HA9) of open chain variant of McoTI-II (top). Amino acid side chains of the inhibitor loop are shown in red. Disulfide bridges are shown in light grey. Color code belongs to amino acid sequence (bottom) that reflects the degree of randomization in a combinatorial library approach described in chapter 5.3 of this work. Cystines are indicated by black bars. Yellow letters 50 % randomisation, green letters 10 % ramdomization and red letters 100 % randomization of all 19 amino acids (without cysteine).

McoTI-II is a knottin that belongs to a special class of knottins, the cyclotides. These share an additional feature that is an additional loop that emerges by cyclization of the amino- and the carboxyl-terminus by a peptide bond[283-286]. McoTI-II is a trypsin inhibitor isolated from the seeds of the squash *Momordica cochinchinesis*[287]. Further cyclotides were observed in other plant families namely *Rubiaceae* and *Violaceae* with a broad range of biological properties such as insecticidal, antimicrobial and hemolytic activity[288-290]. Due to the biological function, McoTI-II is also grouped into the family of inhibitor cystine knots (ICK). Several members of this family such as EETI-II[291, 292] and CMTI[292, 293] are not cyclic but share extensive similarities in the three-dimensional structure[291-293]. The inhibitory activity against trypsin-like proteases is mediated by the loop located between cys #1 and cys #2 composed of 6 amino acid residues [21, 277]. Besides the structural conserved core, the solvent-exposed residues are susceptible for alterations of amino acids[277]. Thus, it becomes possible to generate variants with different biological activities by protein engineering approaches. These variants could serve as therapeutics or diagnostic agents in clinical applications[22, 279, 281, 294]. Accordingly, designed knottins

were reported that address targets of medical relevance such as a McoTI-II-based molecule that inhibits tryptase β which is involved in allergen driven asthma[131, 294-299]. Recently another McoTI-II-based variant was isolated from a combinatorial library by YSD against the tumor associated protease matriptase-1 with a sub-nanomolar inhibitory constant[129].

Interestingly, there was also a non-cyclic variant in the seeds of *Momordica cochinchinesis* abundant called McoTI-III. To make McoTI-II accessible for protein engineering, an open chain variant was synthesized with the result of a 10-fold loss in biological activity which was in opposite to the cyclotide kalata B1 where biological activity was completely lost after opening the cyclic structure[21]. The X-ray crystal structure of McoTI-II open chain variant (ocMcoTI-II) is shown in figure 8. A special advantage of knottins compared with other proteins is the accessibility to solid-phase peptide synthesis additional to recombinant expression[277, 300].

2.3. Aim of this Work

This work aimed at modulating the activity of human serine protease High Temperature Requirement A1 (HTRA1), because it is suggested to be involved in several diseases of high relevance[16-20]. Several approaches are conceivable for HTRA1 functional modulation, such as competitive binding to the active-site, allosteric disordering of the catalytic triad as well as allosteric stabilization of the enzyme's active state. At present there is only one single immunoglobulin derived inhibitor[335], but no proteogenic activator described, that act specifically at the catalytic domain. To close this gap, protein libraries of independent scaffold molecules should be screened by yeast surface display for obtaining binding molecules towards HTRA1.

However, HTRA1 is a protease with different and not well characterized higher oligomeric states. Preferably a monomeric variant should be used for screening in order to work with an easier to handle and more controllable target protein. Moreover, a stable monomeric HTRA1 variant with only minor alterations compared to native sequence would serve as a preferred target since molecules recognizing the oligomerization interfaces that would all be accessible in the monomeric variant could be identified. Such modulators of oligomerization would also most likely influence enzyme activity since it was shown for human HTRA1 that the oligomeric state of this enzyme has an impact on proteolytic activity[31]. As a consequence, one major goal of this work was the design of HTRA1 with reduced or preferably abolished oligomer forming properties.

Binders should be isolated from libraries based on the cystine knot, the VHH and the vNAR scaffold. Additionally, for molecules obtained from the vNAR library a stepwise affinity maturation should be applied to obtain high affinity binders[272] through variation of CDR1 and HV2 of obtained binding molecules with variant CDR3 regions and a combination of both.

Finally, successful candidates should be soluble expressed and characterized in view of the influence on HTRA1 proteolytic activity. Modulators of HTRA1 activity would become valuable tools for analysis of protease function and the evaluation, whether this enzyme might serve as a therapeutic target. Particularly, an activator would represent a novel tool for evaluation of HTRA1.

3. Material

3.1. Bacterial Strains, Yeast Strains and Cell Lines

3.1.1. Bacterial Strains

DH5α

F– Φ80*lacZ*ΔM15 Δ(*lac*ZYA-*arg*F) U169 *rec*A1 *end*A1 *hsd*R17 (rK–, mK+) *pho*A *sup*E44 λ– *thi*-1 *gyr*A96 *rel*A1

BL21 (DE3)

F– *omp*T *hsd*SB(rB–, mB–) *gal dcm* (DE3)

BMH 71-18

*supE thi Δ(lac -proAB) [mutS::*Tn*10] [F' proAB+ lacI*q *lacZ*ΔM15*]*

3.1.2. Yeast Strains

EBY100

MATa GAL1-AGA1::URA3 ura3-52 trp1 leu2_1 his3_200 pep4::HIS2 prb1_1.6R can1 GAL, Trp-Leu-

3.1.3. Human Cell Lines

HEK293EBNA1-6E (HEK293-6E)

Human embryonic kidney cells stably expressing EBNA1[301]

3.2. Cultural Media

dYT	Yeast extract 10 g/l, peptone/tryptone 16 g/l, NaCl 5 g/l h
LB	Yeast extract 5 g/l, peptone/tryptone 10 g/l, NaCl 10 g/l
YPD	Yeast extract 10 g/l, peptone/tryptone 20 g/l, dextrose 20 g/l
SD-CAA	Yeast nitrogen base without amino acids and ammonium sulfate 1.7 g/l, ammonium sulfate 5 g/l, casamino acids 5 g/l, dextrose 20 g/l, $NaH_2PO_4 \times H_2O$ 8.6 g/l, Na_2HPO_4 5.4 g/l
SG-CAA	Yeast nitrogen base without amino acids and ammonium sulfate 1.7 g/l, ammonium sulfate 5 g/l, casamino acids 5 g/l, galactose 20 g/l, $NaH_2PO_4 \times H_2O$ 8.6 g/l, Na_2HPO_4 5.4 g/l, polyethylene glycol 8000 10 % (w/v)

FreeStyle F17 Expression Medium   Life Technologies, Carlsbad, USA (add. 25–
                                         50 µg/ml G418, 4 mM L-glutamine)

3.3. Plasmids

3.3.1. pET21d

Figure 9 Vector map for bacterial expression plasmid based on pET21d-HTRA1-cd. Arrows indicate orientations of genetic elements encoding for: Bacterial origin of replication (F1 ori), ampicillin resistance (AmpR), lac operator of lac operon (LacO), human Htra1 catalytic domain (hHTRA1 cd), histidine tag (His(6)) and stop codon (Stop). NcoI and XhoI recognition sequences for restriction enzymes.

3.3.2. pCT
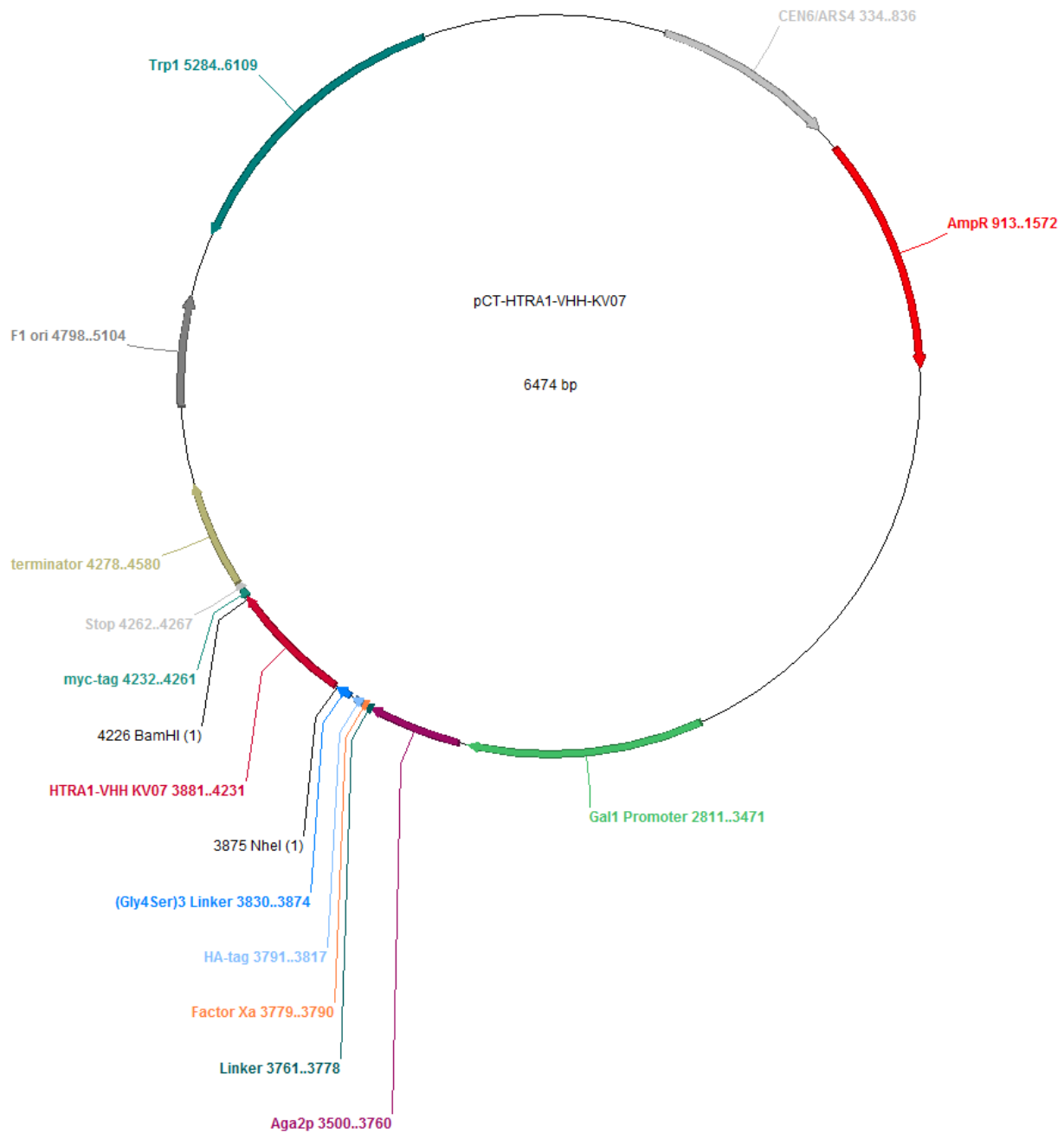
Figure 10 Vector map for yeast surface display plasmid based on pCT-HTRA1-VHH-KV07. Arrows indicate orientations of genetic elements encoding for: Yeast origin of replication (CEN6/ARS4), ampicillin resistance (AmpR), Galactose1 Promoter for protein expression in yeast (Gal1 Promoter), A-agglutinin-binding subunit 2 for presentation of fused protein by attachment to A-agglutinin-binding subunit 1 in the cell wall (Aga2p), Linker (Linker), recognition site for cleavage by Factor Xa (Factor Xa), hemagglutinin epitope (HA-tag), 3 repeats of 4 glycine 1 serine linker ((Gly4Ser)3 Linker), isolated HTRA1 binding VHH clone 7 (HTRA1-VHH KV07), myc epitope (myc-tag), stop codon (Stop), S. cerevisiae terminator of transcription (terminator), bacterial origin of replication (F1 ori) and auxotrophic selection marker (Trp1). NheI and BamHI recognition sequences for restriction enzymes.
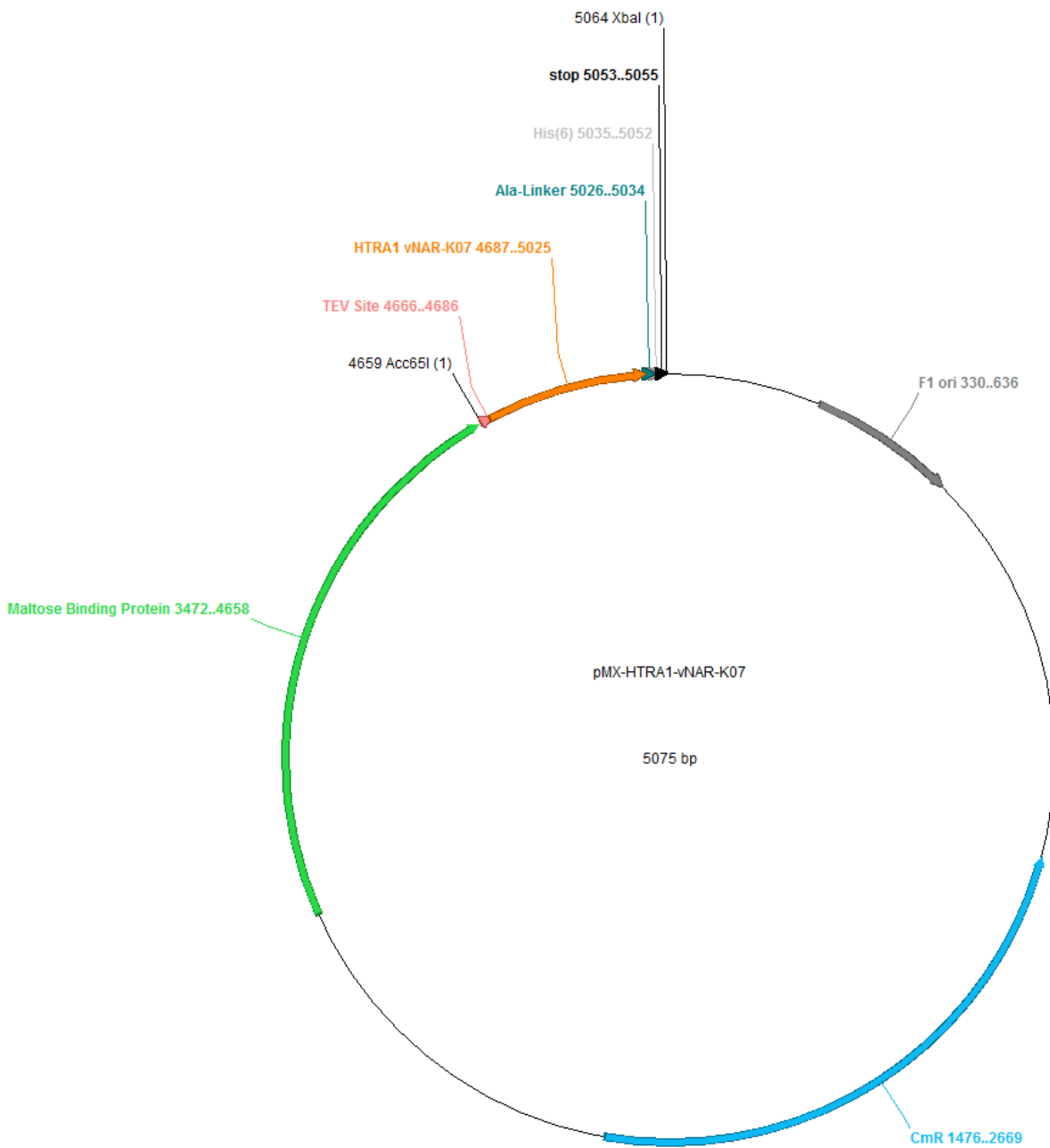
3.3.3. pMX

Figure 11 Vector map for Maltose-binding Protein-encoding plasmid based on pMX-HTRA1-vNAR-K07. Arrows indicate orientations of genetic elements encoding for: Chloramphenicol resistance (CmR), Maltose-binding Protein (Maltose-binding Protein), recognition site for tobacco etch virus protease (TEV Site), isolated HTRA1 binding vNAR clone 7 (HTRA1-vNAR-K07), spacer of three alanines (Ala-Linker), histidine tag (His(6)), stop codon (stop) and a bacterial origin of replication (F1 ori). Acc65I and XbaI recognition sequences for restriction enzymes.
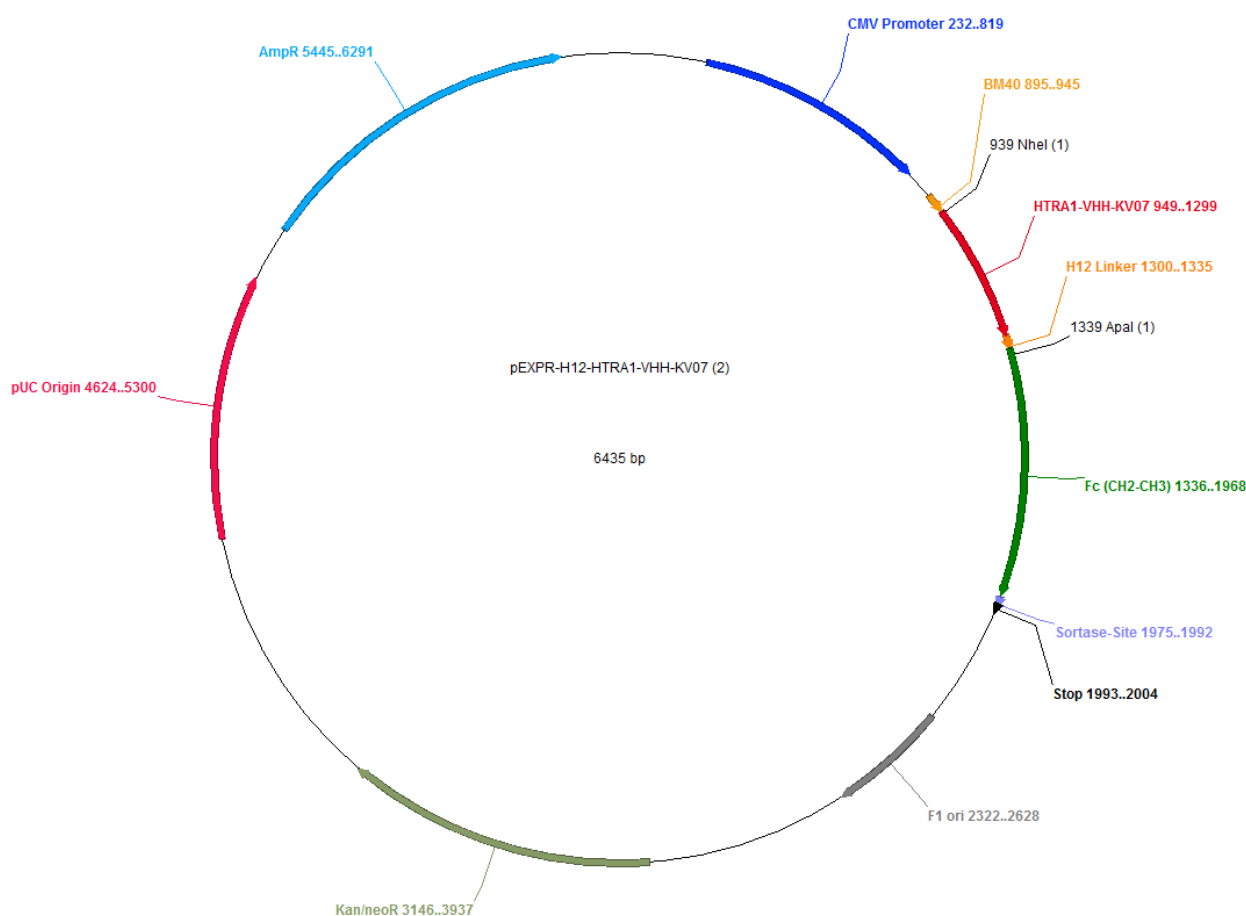
3.3.4. pExpress-Fc

Figure 12 Vector map for Fc-encoding plasmid based on pEXPR-H12-HTRA1-VHH-KV07. Arrows indicate orientations of genetic elements encoding for: Ampicillin resistance (AmpR), cytomegalovirus promoter (CMV promoter), signal sequence for protein secretion (BM40), isolated HTRA1 binding VHH clone 7 (HTRA1-VHH-KV07), IgG1 hinge region (H12 Linker), CH2 and CH3 domains of human IgG1 (Fc), sortase A recognition sequence (Sortase Site), stop codon (Stop), resistance against neomycin (Kan/neoR) and a bacterial origin of replication (pUC origin). NheI and ApaI recognition sequences for restriction enzymes.

3.4. Enzymes, Proteins, Protein Conjugates, Nucleic Acids and Standards

*Acc65*I	New England Biolabs, Beverly, USA
Albumin Fraktion V (pH 7,0) (BSA)	AppliChem GmbH, Darmstadt, Germany
Anti-Mouse IgG–Alkaline Phosphatase (goat)	Sigma-Aldrich, St. Louis, USA
Anti-Mouse IgG–Biotin (rabbit)	Sigma-Aldrich, St. Louis, USA
Anti-Mouse Ig–FITC (rabbit)	Sigma-Aldrich, St. Louis, USA
Anti-myc IgG (mouse)	Sigma-Aldrich, St. Louis, USA
*Apa*I	New England Biolabs, Beverly, USA
*Bam*HI	New England Biolabs, Beverly, USA
CutSmart® Buffer	New England Biolabs, Beverly, USA
dNTPs	Carl Roth GmbH, Karlsruhe, Germany
ExtrAvidin™-alkaline phosphatase conjugate	Sigma-Aldrich, St. Louis, USA
Gel Filtration HMW Calibration Kit	GE Healthcare, Little Chalfont, UK

Gel Filtration LMW Calibration Kit	GE Healthcare, Little Chalfont, UK
NcoI	New England Biolabs, Beverly, USA
NEBuffer 3.1	New England Biolabs, Beverly, USA
NheI	New England Biolabs, Beverly, USA
Lambda DNA *Eco47*I (*Ava*II) Marker	Fermentas, Vilnius, Lithuania
Lysozyme from chicken egg white	Sigma-Aldrich, St. Louis, USA
O'GeneRuler™ 100bp DNA Ladder	Fermentas, Vilnius, Lithuania
Oligonucleotides	Sigma-Aldrich, St. Louis, USA
Penta·His Alexa Fluor 488 conjugate	QIAGEN, Hilden, Germany
Penta·His Antibody, BSA-free	QIAGEN, Hilden, Germany
Phusion® High-Fidelity PCR Kit	New England Biolabs, Beverly, USA
Prestained Protein Marker, Broad Range 7-175 kDa	New England Biolabs, Beverly, USA
Protein A, HRP conjugate	Sigma-Aldrich, St. Louis, USA
Streptavidin-Allophycocyanin conjugate (SAPC)	eBioscience, San Diego, USA
Streptavidin-R-Phycoerythrin conjugate (SPE)	Sigma-Aldrich, St. Louis, USA
T4 DNA Ligase	New England Biolabs, Beverly, USA
T4 DNA Ligase Reaction Buffer (10x)	New England Biolabs, Beverly, USA
Taq-Polymerase	in-house
TEV-Protease	in-house
Trypsin-EDTA	Gibco, Karlsruhe, Germany
*Xba*I	New England Biolabs, Beverly, USA
*Xho*I	New England Biolabs, Beverly, USA
Yeast Lytic Enzyme	MP Biomedicals, Santa Ana, USA

3.5. Oligonucleotides

CDR1rand_up

ACCATCAATTGCGTCCTAAAA(X)$_5$TTGGGTAGCACGTACTGGTATTTCACAAAGAAG

FR1_up

ATGGCCGCACGGCTTGAACAAACACCGACAACGACAACAAAGGAGGCAGGCGAATCACTGACCATCAATTGCGTCCTAA

GR_up

GTGGTGGTGGTTCTGCTAGCATGGCCGCACGGCTTGAACA

GR_lo

ATAAGCTTTTGTTCGGATCCWTTCACAGTCASARKGGTSCCSCCNCC

hHtrA1_cd_NcoI_up

GCGCGCCCATGGGCCAAGGGCAGGAAGATCC

hHTRA1_cd_Y169A_F171A_NcoI_up

GCGCGCCCATGGGGCAGGAAGATCCCAACAGTTTGCGCCATAAAGCTAACGCTATCGCGG

hHTRA1_cd_XhoI_lo

CGCGCGCTCGAGTTTTCCTTTGGCC

hHTRA1_cd_F278A_SOE_lo

GGGCTTCCGATGGCGACCAC

hHTRA1_cd_F278A_SOE_up

CCGGGAGAGGCCGTGGTCGCCATCGGAAGCCCG

hHTRA1_PDZ_XhoI_lo

CGCGCGCTCGAGTGGGTCAATTTCTTCGGG

HV2_SOE_lo

GCCCTTCTTTGTGAAATACCA

HV2_SOE_rand_up

TGGTATTTCACAAAGAAGGGC(X)$_9$GCGGACGATACTCGGACACA

MASKO_rd5_VHH-K1_NheI_up

GCGCGCGCTAGCCGCTGAGGTGCAGCTGCAGGCGTCTGG

MASKO_rd5_VHH-K1/7_ApaI_lo

CGCGCGGGGCCCGCCCAGCAGTTCAGGGGCAGGGCTAGGGGGGCTGGTGTGGGATCCGCTGGAGACGGTGACC

MASKO_rd5_VHH-K7_NheI_up

GCGCGCGCTAGCCGCTGATGTTCAGTTGCAGGCGTCTGG

pCT_Seq_up

AGGACAATAGCTCGACGATT

pCT_Seq_lo

GCGCGCTAACGGAACGAAAAATAGAAA

pEXPR_Seq_for

GAGAACCCACTGCTTACTGGC

pEXPR_Seq_rev

TAGAAGGCACAGTCGAGG

pMX_seq_up

TGGTATGCCGTGCGTACTGC

pMX_seq_lo

TGAATTAGCTTGGAATTGCG

SloII_HTRA1_K1_NheI_up

GCGCGCGCTAGCCGCTATCACACTGTGCTTCTAC

SloII_HTRA1_K1_ApaI_lo

CGCGCGGGGCCCGCCCAGCAGTTCAGGGGCAGGGCTAGGGGGGCTGGTGTCCGAGGCCGAGCCGCAGT

T7_Pomoter_seq_up

TAATACGACTCACTATAGGG

T7_Terminator_seq_lo

TAGAGGCCCCAAGGGGTTAT

vNAR_Acc65I_TEV_up

GCGCGCGGTACCCGAAAACCTGTATTTTCAGAGCATGGCCGCACGGCTTGAACAA

vNAR_His_Stop_XbaI_lo:

CGCGCGTCTAGATCATTAATGATGATGATGATGATGATTCACAGTCACAAGGGTCCC

X: triplet codon for all natural amino acids without cysteine; K: G/T; N: A/G/C/T; R: A/G; S: G/C; W: A/T.

3.6. Chemicals

2-Mercaptoethanol	Carl Roth GmbH, Karlsruhe, Germany
3,3′,5,5′-tetramethylbenzidine (TMB)	Sigma Aldrich, St. Louis, USA
5-Bromo-4-chloro-3-indolyl phosphate (BCIP)	Carl Roth GmbH, Karlsruhe, Germany
7-(Carboxymethoxy)-4-methylcoumarin (MCA)	Sigma Aldrich, St. Louis, USA
Acetic Acid	Carl Roth GmbH, Karlsruhe, Germany
Acetonitrile	Carl Roth GmbH, Karlsruhe, Germany
Acrylamide/Bisacrylamide (37,5:1)	Carl Roth GmbH, Karlsruhe, Germany
Agar-Agar	Carl Roth GmbH, Karlsruhe, Germany
Agarose	Carl Roth GmbH, Karlsruhe, Germany
Ammonium acetate	Carl Roth GmbH, Karlsruhe, Germany
Ammonium hydrogene carbonate	Carl Roth GmbH, Karlsruhe, Germany
Ammonium sulfate	Carl Roth GmbH, Karlsruhe, Germany
Ampicillin, sodiumsalt	Carl Roth GmbH, Karlsruhe, Germany
Ammonium persulfate (APS)	Carl Roth GmbH, Karlsruhe, Germany
Anisole	Sigma Aldrich, St. Louis, USA
Bacillol plus	Carl Roth GmbH, Karlsruhe, Germany
Bromophenol blue	Carl Roth GmbH, Karlsruhe, Germany
Calcium chloride	Carl Roth GmbH, Karlsruhe, Germany
Casaminoacids	Becton Dickinson GmbH, Heidelberg, Germany
Chloramphenicol	Carl Roth GmbH, Karlsruhe, Germany
Citric acid	Carl Roth GmbH, Karlsruhe, Germany
Coomassie Brilliant Blue-R250	Carl Roth GmbH, Karlsruhe, Germany
Cupric sulfate penta-hydrate	Sigma Aldrich, St. Louis, USA
Dichloromethane (DCM)	Sigma Aldrich, St. Louis, USA
Diethyl ether	Sigma Aldrich, St. Louis, USA
Dimethyl sulfoxide (DMSO)	Sigma Aldrich, St. Louis, USA
Dimethylformamide (DMF)	Carl Roth GmbH und Co KG, Karlsruhe
Dithiothreitol (DTT)	Carl Roth GmbH, Karlsruhe, Germany
Disodium hydrogen phosphate	Carl Roth GmbH, Karlsruhe, Germany
Ethanol	Carl Roth GmbH, Karlsruhe, Germany

Ethidium bromide	Carl Roth GmbH, Karlsruhe, Germany
Ethylenediaminetetraacetic acid (EDTA)	AppliChem GmbH, Darmstadt, Germany
Fetal bovine serum	Sigma-Aldrich, St. Louis, USA
Fluorescein isothiocyanate	Sigma-Aldrich, St. Louis, USA
Fmoc-L-Lys(Boc)-Wang Resin	IRIS Biotech GmbH, Marktredwitz
Fmoc-Lys(Dnp)-OH	Merck Millipore, Darmstadt, Germany
Fmoc protected amino acids	IRIS Biotech GmbH, Marktredwitz
Galactose	Sigma-Aldrich, St. Louis, USA
Gel loading dye (6x)	New England Biolabs (NEB), Beverly, USA
Glucose	Carl Roth GmbH, Karlsruhe, Germany
Glycerin	Carl Roth GmbH, Karlsruhe, Germany
Glycine	Carl Roth GmbH, Karlsruhe, Germany
Glycerol	Carl Roth GmbH, Karlsruhe, Germany
Hydrochloric acid (HCl)	Carl Roth GmbH, Karlsruhe, Germany
Imidazole	Carl Roth GmbH, Karlsruhe, Germany
Isopropanol	Carl Roth GmbH, Karlsruhe, Germany
Isopropyl β-D-1 thiogalactopyranoside (IPTG)	Carl Roth GmbH, Karlsruhe, Germany
Lithium acetate	Carl Roth GmbH, Karlsruhe, Germany
L-Glutamine	Sigma Aldrich, St. Louis, USA
Magnesium chloride	Carl Roth GmbH, Karlsruhe, Germany
Meliseptol	B. Braun Melsungen AG, Melsungen
Methanol	Carl Roth GmbH, Karlsruhe, Germany
Nickel chloride	Merck KGaA, Darmstadt, Germany
Nitro blue tetrazolium chloride (NBT)	Sigma Aldrich, St. Louis, USA
Paraffin oil	Carl Roth GmbH, Karlsruhe, Germany
Piperazine-N,N'-bis(2-ethanesulfonic acid) (PIPES)	Carl Roth GmbH, Karlsruhe, Germany
Penicillin/Streptomycin (100x)	Life Technologies, Carlsbad, USA
Peptone/Tryptone	Carl Roth GmbH, Karlsruhe, Germany
Polyethylene glycol 8000	Carl Roth GmbH, Karlsruhe, Germany
Polyethylenimine, 25 kDa, linear (PEI)	Polysciences, Eppelheim, Germany
Potassium chloride	Carl Roth GmbH, Karlsruhe, Germany
Potassium dihydrogen phosphate	Carl Roth GmbH, Karlsruhe, Germany
Potassium hydrogen phosphate	Carl Roth GmbH, Karlsruhe, Germany
Potassium hydroxide	Carl Roth GmbH, Karlsruhe, Germany
Sucrose	Carl Roth GmbH, Karlsruhe, Germany
Sodium bicarbonate	Sigma Aldrich, St. Louis, USA

Sodium bicinchoninate	MP Biomedicals, Santa Ana, USA
Sodium carbonate	Sigma Aldrich, St. Louis, USA
Sodium chloride	Carl Roth GmbH, Karlsruhe, Germany
Sodium dihydrogen phosphate di-hydrate	Carl Roth GmbH, Karlsruhe, Germany
Sodium dodecyl sulfate (SDS)	Carl Roth GmbH, Karlsruhe, Germany
Sodium hydroxide	Carl Roth GmbH, Karlsruhe, Germany
Sodium tartrate	Sigma Aldrich, St. Louis, USA
Sorbitol	Carl Roth GmbH, Karlsruhe, Germany
Sulfo-NHS-LC-Biotin	Thermo Fisher Scientific, Geel, Belgium
SYPRO Orange	Sigma Aldrich, St. Louis, USA
Tetramethylethylenediamine (TEMED)	Merck KGaA, Darmstadt, Germany
Triethylsilane	Sigma Aldrich, St. Louis, USA
Trifluoroacetic acid (TFA)	Carl Roth GmbH und Co KG, Karlsruhe
Tris(hydroxymethyl)aminomethan (Tris)	Carl Roth GmbH, Karlsruhe, Germany
Trisodium citrate	Carl Roth GmbH, Karlsruhe, Germany
Triton X-100	Carl Roth GmbH, Karlsruhe, Germany
Tri-sodium citrate	Carl Roth GmbH, Karlsruhe, Germany
Trypan Blue Solution, 0.4 %	Life Technologies, Carlsbad, USA
Tryptone	Becton Dickinson GmbH, Heidelberg, Germany
Tryptone/Peptone	Carl Roth GmbH, Karlsruhe, Germany
TWEEN-20	Carl Roth GmbH, Karlsruhe, Germany
Yeast extract	Carl Roth GmbH, Karlsruhe, Germany
Yeast Nitrogen Base	Becton Dickinson GmbH, Heidelberg, Germany

3.7. Solutions and Buffers

AP-Buffer	Tris 100 mM, NaCl 100 mM, MgCl$_2$ 50 mM (pH 9)
APS-stock	10 % (w/v)
BCA-stock 1	Sodium bicinchoninate (BCA) 10 g/l, sodium carbonate 20 g/l, sodium tartrate 1.6 g/l, NaOH 4 g/l, and sodium bicarbonate 9.5 g/l, pH 11.25, adjusted with NaOH
BCA-stock 2	Cupric sulfate penta-hydrate 40 g/l
BCIP-stock	50 g/l in 70 % DMF
dNTP Mix	Adenine 2.5 mM, Cytosine 2.5 mM, Guanine 2.5 mM, Thymine 2.5 mM
Ethidiumbromide-stock	1 g/l

IMAC EDTA Solution	EDTA 100 mM
IMAC Elution Buffer	Imidazol 1 M in Protease Buffer (pH 8)
IMAC Nickel chloride solution	Nickel chloride 100 mM
IPTG-stock	IPTG 1 M
LiAc/DTT buffer	Lithium acetate 100 mM, Dithiothreitol 10 mM
NBT-stock	75 g/l in 70 % DMF
PAGE Buffer A (4x)	Tris/HCl 3 M (pH 8.85), SDS 4 g/l
PAGE Buffer B(4x)	Tris/HCl 0.5 M (pH 6.8), SDS 4 g/l
PAGE Destaining Solution	Acetic acid 10 % (v/v), Isopropanol 25 % (v/v)
PAGE Running Buffer (5x)	Tris 50 mM, Glycin 190 mM, SDS 1 g/l
PAGE Staining Solution	Acetic acid 10 % (v/v), methanol 40 % (v/v), Coomassie brilliant blue R250 0.25% (w/v)
PEI-stock	Polyethylenimine 1 g/l, pH 7.5 adjusted with HCl
Phosphate Buffered Saline (PBS)	NaCl 8.1 g/l, KCl 0.75 g/l, Na_2HPO_4 1.13 g/l and KH_2PO_4 0.27 g/l, (pH 7.4)
PBST	PBS, Tween-20 0.05 % (v/v)
Periplasm Prep Buffer	Sucrose 0.5 M, Tris/HCl 0.1 M, EDTA 1 M
Protease Buffer	Tris 100 mM, NaCl 150 mM (pH 8)
Protein A Elution Buffer (pH 2.2)	Glycine 0.1 M (pH 2.2)
Protein A Neutralization Buffer (pH 9.0)	Tris/HCl 1 M (pH 9.0)
Protein A Running Buffer	Sodium dihydrogen phosphate dihydrate 1.08 g/l, Disodium hydrogen phosphate 1.72 g/l (pH 7.0)
Protein Loading Buffer (5x)	Tris/HCl 0.25 M (pH 8), SDS (7.5 % (w/v), Glycerin 25 % (w/v), bromphenol blue 0.25 mg/ml, 2-mercaptoethanol 12.5 % (w/v)
TAE Buffer (Agarosegelectrophoresis)	Tris 2 M, acetic acid 1M, EDTA 0.1 M
Taq Buffer (10x)	Tris 100 mM, KCl 500 mM, $MgCl_2$ 25 mM, Triton X-100 1 % (v/v) (pH 8.8)
TEV-Protease Buffer (10x)	Tris 500 mM, NaCl 1.5 M, (pH 7.5)
Trypan blue solution	Trypan blue 4 % (w/v)
Western blot Transfer Buffer	Tris 25 mM, glycine 192 mM, methanol 20 % (v/v)
Yeast electroporation buffer	Sorbitol 1 M, calcium chloride 1 mM
Yeast freezing solution	Glycerol 2 % (v/v), yeast nitrogen base 0.67 % (w/v)

Yeast Lysis Buffer   Sorbitol 1 M, PIPES 10 mM (pH 6.5)

All buffers and solutions were solved in di-distilled H_2O. Buffers and solutions were autoclaved or sterile filtered.

3.8. Laboratory Materials and Kits

Amicon Ultra-15, miscellaneous	Merck Millipore, Darmstadt, Germany
Centrifuge tubes (50 ml) with screw caps	Carl Roth GmbH, Karlsruhe, Germany
Corning cell culture flasks (25 or 75 cm^2)	Sigma-Aldrich, St. Louis, USA
Corning Erlenmeyer cell culture flasks	Sigma-Aldrich, St. Louis, USA
Electroporation cuvettes	Bio-Rad, München, Germany
Filtropure filter devices	Sarstedt, Nümbrecht, Germany
Glassware	Schott AG, Mainz, Germany
Glass-beads (500 μm)	Carl Roth GmbH, Karlsruhe, Germany
HiLoad Superdex 200 pg 16/60, SEC column	GE Healthcare, Little Chalfont, UK
HiLoad Superdex 75 pg 16/60, SEC column	GE Healthcare, Little Chalfont, UK
HisTrap HP, 1 ml column	GE Healthcare, Little Chalfont, UK
HiTrap Protein A HP, 1 ml column	GE Healthcare, Little Chalfont, UK
Nitrocellulose membrane	Carl Roth GmbH, Karlsruhe, Germany
Nunc MaxiSorp ELISA plates	eBioscience, San Diego, USA
Microscope slides	Carl Roth GmbH, Karlsruhe, Germany
Parafilm® "M"	Laboratory Film American National Can., Chicago, USA
PD-10 Desalting Columns	GE Healthcare, Little Chalfont, UK
Petri dishes, miscellaneous	Sarstedt, Nümbrecht, Germany
Pierce Polyacrylamide Spin Desalting Columns	Thermo Fisher Scientific, Waltham, USA
Pipet tips, miscellaneous	Sarstedt, Nümbrecht, Germany
Reaction tubes, miscellaneous	Sarstedt, Nümbrecht, Germany
RP-HPLC columns, miscellaneous	Phenomenex Aschaffenburg, Germany
Seals AirOtop	BioSilta Oy, Oulu, Finnland
Sphero™ rainbow calibration particles	Spherotech Inc, Lake Forest, USA
Superdex 200 10/300 GL, SEC column	GE Healthcare, Little Chalfont, UK
Syringes, miscellaneous	B. Braun Melsungen AG, Melsungen
Ultra-Yield flask, miscellaneous	BioSilta Oy, Oulu, Finnland
Whatman® chromatography paper	Carl Roth GmbH, Karlsruhe, Germany
Wizard® SV Gel and PCR Clean-Up System	Promega, Fitchburg, USA
Wizard® Plus SV Midipreps DNA Purification System	Promega, Fitchburg, USA

Wizard® Plus SV Minipreps DNA Purification System	Promega, Fitchburg, USA
Zellu Trans dialysis membranes, miscellaneous	Carl Roth GmbH, Karlsruhe, Germany

Further materials comprised common laboratory equipment.

3.9. Equipment

Äkta Basic UV900 P900 Frac 900, Unicorn 3.1 software	GE Healthcare, Little Chalfont, UK
Äkta Purifier UPC-900 P900 Frac-920, Unicorn 5 software	GE Healthcare, Little Chalfont, UK
B 5061 EC/CO_2 incubator	Heraeus, Hanau, Germany
BioPhotometer	Eppendorf, Hamburg, Germany
Bio-Rad 96CFX Connect qPCR detection system	Bio-Rad Laboratories, Hercules, USA
BioSpec-nano Micro-volume UV-Vis Spectrophotometer	Shimadzu, Kyoto, Japan
BIOWIZARD SilverLine BlueSeries	Kojair, Vilppula, Finland
Cell Disrupter	Constant Systems Ltd, Daventry, UK
Centrifuge 6K15	Sigma-Aldrich, St. Louis, USA
Centrifuge Eppendorf 5415 R	Eppendorf, Hamburg, Germany
Centrifuge Heraeus Megafuge 1.0	Heraeus Holding GmbH, Hanau, Germany
Fluorescence Activated Cell Sorter (FACS), MoFlo® Cytometer with Cyclone sorting unit, Summit® v4.3 Software package	Dako Cytomation, Fort Collins, USA
Gel documentation system, Gel Jet Imager	INTAS Science Imaging Instruments GmbH, Göttingen
Gene Pulser Xcell und pulse controller	Bio-Rad Laboratories, Hercules, USA
Incubator CertomatR BS-1	Sartorius AG, Göttingen, Germany
MCO-19AICUV CO_2 incubator	Panasonic, Kadoma, Japan
Microscope Axioskop	Carl Zeiss Microscopy GmbH, Jena, Germany
Operating Manual Freeze Dryer ALPHA 2-4 LSC	Martin Christ GmbH, Osterode am Harz, Germany
PCR Cycler Eppendorf Mastercycler	Eppendorf, Hamburg, Germany
Peptide synthesizer CEM Liberty	CEM GmbH, Kamp-Lintfort, Germany
Plate reader **GENios™**	Tecan, Männedorf, Switzerland
Plate reader Infinite M1000	Tecan, Männedorf, Switzerland
Puranity PU 20 Basic Water purification system	VWR, Radnor, USA
Shimadzu LCMS-2020 with Phenomenex Jupiter 5µ C4 LC column	Shimadzu, Kyoto, Japan
Varian LC920 System with Phenomenex	Varian Medical Systems GmbH, Darmstadt,

Synergi 4µ Hydro-RP   Germany

Varian LC 940 System with Phenomenex Luna   Varian Medical Systems GmbH, Darmstadt,
C18 column   Germany

Wisd WiseShake SHO-2D   Witeg, Wertheim, Germany

Further instruments comprised common laboratory equipment.

4. Methods

4.1. Expression, Purification and Characterization of HTRA1 Variants

4.1.1. Cloning of HTRA1 Variants

HTRA1 catalytic domain was provided by Prof. M. Ehrmann in expression vector pET21d[31]. Human full-length HTRA1 clone was supplied by Imagenes (Berlin). Catalytic and PDZ domain (HTRA1 cd+PDZ) were amplified using primers hHtrA1_cd_NcoI_up and hHTRA1_PDZ_XhoI_lo. PCR protocol was as followed: 95 °C for 5 min, 35 cycles of 30 s at 95 °C, 30 s at 52 °C and 60 s at 72 °C, followed by 72 °C for 5 min.

PCR product was purified using Wizard® SV Gel and PCR Clean-Up System (Promega) followed by digestion with 2 units of *Nco*I and *Xho*I for 1 h at 37 °C in suggested buffer. After heat inactivation for 10 min at 70 °C the PCR product was ligated with T4 DNA Ligase into Wizard® SV Gel and PCR Clean-Up System (Promega) gel purified vector pET21d HTRA1 after digestion with *Nco*I and *Xho*I.

E. coli cells were grown to OD_{600} of 0.6 and prepared for electroporation by washing 3-times with ice-cold distilled water. 5 µl of ligated vector was mixed with electro-competent *E. coli* DH5α in an electroporation cuvette on ice. Transformation protocol was the preset for bacteria on the Gene Pulser XcelI (Bio-Rad). Cells were incubated immediately after pulsing in 1 ml dYT media for 1 h at 37 °C. Afterwards cells were plated out on LB-Agar containing ampicillin (100 mg/l) and incubated over night at 37 °C.

Single clones were verified by colony PCR using insert specific primer and T7_Terminator_seq_lo. Positive clones were incubated in dYT media containing ampicillin (100 mg/l) over night at 37° C and 180 rpm. Plasmids were isolated using Wizard® Plus SV Minipreps DNA Purification System (Promega). Sequences were analyzed by Sanger sequencing (seqlab, Göttingen) using primer T7_Promoter_seq_up or T7_Terminator_seq_lo.

Mutants HTRA1 cd-mono2 and HTRA1 cd-mono3 were generated using pET21d-HTRA1 cd+PDZ as template. First the mutations for HTRA1 cd-mono2 were introduced by PCR using primers hHTRA1_cd_Y169A_F171A_NcoI_up and hHTRA1_cd_XhoI_lo. PCR protocol was as followed: 95 °C for 5 min, 35 cycles of 30 s at 95 °C, 30 s at 52 °C and 60 s at 72 °C, followed by 72 °C for 5 min. Finally the mutant was cloned into pET21d as described above and verified by sequencing.

The additional mutation for HTRA1 cd-mono3 was introduced by amplification of HTRA1 cd-mono2 in two parts using primer sets hHTRA1_cd_Y169A_F171A_NcoI_up / hHTRA1_cd_F278A_SOE_lo and hHTRA1_cd_F278A_SOE_up / hHTRA1_cd_XhoI_lo. PCR products were gel purified with Wizard® SV Gel and PCR Clean-Up System (Promega). Then PCR products were mated in a PCR without primers while 1 µl of each product of previous PCR was inserted into reaction. After 10 cycles primers hHTRA1_cd_Y169A_F171A_NcoI_up and hHTRA1_cd_XhoI_lo were added. Protocol for first and second PCR was as followed: 95 °C for 5 min, 45 cycles of 30 s at 95 °C, 30 s at 52 °C and 60 s at 72 °C, followed by 72 °C for 5 min. Finally the mutant was cloned into pET21d and verified by sequencing as described above.

4.1.2. Expression of HTRA1 Variants

E. coli cells were grown to OD_{600} of 0.6 and prepared for electroporation by washing 3-times with ice-cold distilled water. 1 µl of sequence verified pET21d of each HTRA1 variant was mixed with electro-competent *E. coli* BL21 in an electroporation cuvette on ice. Transformation protocol was the preset for bacteria on the Gene Pulser XcelI (Bio-Rad). Cells were incubated immediately after pulsing in 1 ml dYT media for 1 h at 37° C. Afterwards cells were plated out on LB-Agar containing ampicillin (100 mg/l) and incubated over night at 37° C.

A single clone was incubated in 50 ml dYT media containing ampicillin (100 mg/l) over night at 37° C and 180 rpm. 10 ml of culture were used for starting production culture in 1 L LB media containing ampicillin (100 mg/l) at 180 rpm at 37° C. Optical density at 600 nm (OD_{600}) was measured until

OD$_{600}$ between 0.8-1. Then temperature was decreased to 16 °C and 1 mM IPTG was added to induce protein expression for 24 h.

4.1.3. Purification of HTRA1 Variants and Determination of Oligomeric States

Cells were harvested using a centrifuge (Sigma) for 20 min at 16000 g and 4 °C. After decanting the supernatant cells were resuspended on ice with 30-40 ml Protease Buffer and lysed using a Multi Shot cell disruptor (Constant Systems Ltd). Lysis was done by 5 repeats with 35 kpsi. Suspension was centrifuged at 19000 g at 4°C for 20 min. Supernatant containing soluble protein was filtered using 0.45 µm syringe filter (Sarstedt) and applied on an equilibrated HisTrap column (GE Healthcare) using Äkta FPLC-System (GE Healthcare). Bound protease was washed with Protease Buffer and eluted using a linear gradient by addition of IMAC Elution Buffer. Eluted protein was collected using automated fractionator Frac900 (GE Healthcare). Fractions containing HTRA1 variant were concentrated by ultra-filtration using Amicon Ultra-15 10000 (Merck Millipore).

Evaluation and separation of different oligomeric states was done using a HiLoad Superdex 200 16/60 pg (GE-Healthcare) size-exclusion chromatography column on an Äkta FPLC-System (GE-Healthcare). Different oligomeric states were collected separately and concentrated by ultra-filtration using Amicon Ultra-15 10000 (Merck Millipore).

Recombinant expressed proteins were analyzed by SDS-PAGE and Western blot. Pooled fractions were applied on SDS gel (15 % v/v) after incubation with 5x Protein Loading Buffer for 10 min at 95 °C. After electrophoresis gel was either stained with PAGE Staining Solution or electrically blotted on a nitro-cellulose membrane by usage of Western Blot Transfer Buffer. Expressed proteins were detected by monoclonal anti-penta-His antibody (QIAGEN), followed by anti-mouse alkaline phosphatase conjugate. Antibodies were solved in 1:10000 dilution in PBS milk powder solution (1 % w/v) and incubated for 1 h each. After first and secondary antibody membrane was washed 10-times with PBST. Membrane was washed with water before addition of 30 ml AP-Buffer, 12.5 µl NBT and 70 µl BCIP solution for developing the Western blot. Reaction was stopped by washing with water.

After concentration determination by photometric and BCA-Assay (4.1.5), HTRA1 variants were aliquoted and stored at -80°C.

Stability of different oligomeric states that were collected separately was analyzed using analytical gel filtration column Superdex 200 10/300 GL (GE Healthcare) in combination with Äkta FPLC-System (GE Healthcare).

4.1.4. Melting Curve Analysis of HTRA1 Variants and Isolated Binding Molecules

For determination of thermal stability of expressed proteins the melting temperatures were measured. Purified proteins were diluted with Protease Buffer to 1 mg/ml if being concentrated above. Samples were mixed with SYPRO Orange (Sigma-Aldrich) to a final dye concentration of 1:1000. For each duplicate two times 25 µl were used for analyses in a real-time PCR Cycler CFX Connect (Bio-Rad). Gradient was from 30° C to 95° C with a ramp rate of 0.5 °C/min. Data was evaluated using CFX Manager software (Bio-Rad).

4.1.5. Protein Concentration of HTRA1 Variants and Isolated Binding Molecules by BCA-Assay and Optical Density

For determination of protein concentration by Bicinchoninic Acid (BCA) Assay 100 volumes of BCA Solution A were mixed with 2 volumes of BCA Solution B to obtain a working solution. Then 1 ml of working solution was mixed with 20 µl sample and incubated for 30 min at 60° C. After cooling sample to room temperature 200 µl were used for measurement of absorption at 562 nm using multi-plate reader Infinite M1000 PRO (Tecan). Protein concentration was determined according to a standard curve of serial dilutions of Bovine Serum Albumin. When concentration of sample was above highest concentration of standard curve the sample was diluted with Protease-Buffer.

4.1.6. Labeling of HTRA1 Variants

HTRA1 variants were labeled with fluorescein or biotin for isolation of binding molecules via yeast surface display and characterization of isolated clones. Buffer of GFC purified protease variants was exchanged using 0.5 ml 7K Zeba™ Spin Desalting Columns (Thermo Fisher) or PD-10 Desalting Columns (GE Healthcare).

For fluorescein labeling by fluorescein isothiocyanate (FITC)[302] the protease was eluted in 100 mM sodium carbonate buffer (pH 9.0) and adjusted to a concentration of 2 mg/ml. FITC was solved in DMSO at a concentration of 2 mg/ml. 20 µl of FITC solution were slowly added to each milliliter of protein solution. Reaction was carried out for 8 h at 4 °C in the dark. Afterwards protease was purified using 0.5 ml 7K Zeba™ Spin Desalting Columns (Thermo Fisher) or PD-10 Desalting Columns (GE Healthcare). Buffer was exchanged against Protease Buffer.

For biotin labeling by NHC-LC-Biotin[303] the protease was eluted in 100 mM sodium phosphate, 150 mM NaCl buffer (pH 7.5) and adjusted to a concentration of 2 mg/ml. NHC-LC-Biotin was solved in DMF to a concentration of 40 mg/ml. 5 µl of NHS-LC Biotin solution were slowly added to each milliliter of protein solution. Reaction was carried out for overnight at 4 °C. Afterwards protease was purified using 0.5 ml 7K Zeba™ Spin Desalting Columns (Thermo Fisher) or PD-10 Desalting Columns (GE Healthcare). Buffer was exchanged against Protease Buffer.

Labeled protease variants were aliquoted and stored at -80 °C.

4.1.7. Activity Measurements of HTRA1 Variants and Isolated Binding Molecules

For determining functionality of expressed protease variants and the effect of binding molecules the proteolytic activity of HTRA1 variants was measured using substrate H2Opt-K (Mca-IRRVSYSF(Dnp)KKK). H2Opt-K is based on H2Opt[53] and was chemically synthesized by automated solid-phase peptide synthesis according to Merrifield synthesis strategy[304] using a Liberty Synthesizer (CEM). Coupling of amino carboxymethoxy-methylcoumarin was according to the protocol of Knight *et al*[305]. Only difference was using a lysine pre-loaded resin for addition of an additional carboxyl–terminal lysine. After cleavage from resin peptide substrate was purified by reversed-phase HPLC (Varian) using a C18 column (Phenomex) followed by lyophilization. Synthesized substrate was verified by LC ESI-MS (Shimadzu).

Activity measurement was carried out using a multimode microplate reader Infinite M1000 PRO (Tecan). Substrate was solved in Protease Buffer and mixed with HTRA1 variants to described concentrations using a black 384-well microtiter plate. Final volume of 40 µl was adjusted with Protease Buffer. Reaction was started by addition of substrate followed by measurement immediately at 18-20 °C. Wavelength for measurement was 328 nm for excitation and 393 nm for emission. For measuring the influence of isolated molecules on HTRA1 activity, protease was incubated with each molecule 15 min at RT previous to addition of substrate.

4.2. Library Screening

4.2.1. Serum Titer

For evaluation of the immunization of Llama, it was checked if antibodies against HTRA1 were produced. Therefore serum before and after immunization were analyzed for their ability to bind HTRA1 variants. Thus 100 ng of HTRA1 cd and 1 mg of BSA were immobilized in separate wells of a maxi-sorb microtiter plate (Nunc) over night at 4 °C. Then wells were blocked with 2 % milk powder for 1 h and washed 3-times with an automated plate washer (Tecan). Afterwards wells were incubated for 1 h with serial dilutions of sera containing 1 % milk powder. Then wells were washed 10-times with PBS and incubated for 1 h with Protein A-HRP conjugate in 1:10000 dilution containing 1 % milk powder. Then wells were washed 10-times with PBS followed by addition of 100 µl TMB One solution (Promega). Reaction was stopped with 100 µl HCl (0.1 %) and absorption was measured using a plate reader (Tecan).

4.2.2. Screening of McoTI-II, VHH and vNAR Libraries as well as vNAR Sub-Libraries

For induction of library presentation on the yeast cell surface the cells of the different libraries were incubated overnight with 180 rpm at 30 °C in SD-CAA media and then transferred into SG-CAA media with 180 rpm at 20 °C for 1-2 days.

For isolation of antigen-specific binding molecules from different libraries the cells were double labeled with biotinylated or fluorescein conjugated antigen HTRA1 and additionally for myc epitope to check surface presentation of full-length construct. Biotin and fluorescein conjugation to HTRA1 variants is described in section 4.1.6. For the first rounds of enrichment the quantity of cells of library or sub-library size were labeled with monoclonal anti-myc antibody (in-house), washed with 1 ml ice-cold Protease Buffer and then labeled with 1:10 dilution of secondary anti-mouse antibody (Sigma-Aldrich) that was biotinylated or conjugated with fluorescein, respectively. After labeling with biotinylated secondary antibody cells were washed with 1 ml ice-cold Protease Buffer and labeled with streptavidin-allophycocyanin conjugate (eBioscience) in 1:10 dilution. After labeling of myc epitope cells were washed with 1 ml ice-cold Protease Buffer and labeled with different concentrations of biotinylated or fluorescein conjugated HTRA1 variant. After labeling with biotinylated HTRA1 variant cells were washed with 1 ml ice-cold Protease Buffer and labeled with streptavidin-allophycocyanin conjugate (eBioscience) in 1:10 dilution. Finally cells were washed with 1 ml ice-cold Protease Buffer. All incubation steps were incubated for 10 min on ice. For Successive rounds of screening lower quantity of cells were labeled, but at least 100-fold excess of cells than isolated in the previous round.

Labeled cells were kept on ice until screening by using a fluorescence activated cell sorter (FACS) (DakoCytomation) that was controlled by Summit software version v4.3. After sorting the efficiency was determined by dilution plating. Cells were incubated in SD-CAA medium with 180 rpm at 30 °C and used for successive rounds.

4.2.3. Single Clone Analysis of Isolated Clones

For analyses of single clones for antigen binding the single clones from dilution plating were incubated and induced for surface presentation in SD-CAA media and SG-CAA media, respectively. Single clones were labeled as described for library screening (4.2.2) whereby about 10^6 cells were labeled. Analyses were carried out using fluorescence activated cell sorter (DakoCytomation) that was controlled by Summit software version v4.3. *S. cerevisiae* single clones binding to antigen were lysed in 20 µl Yeast Lysis Buffer with a final concentration of 1 mg/ml yeast lytic enzyme (MP-Biomedicals) at 37 °C for 30 min. Then 5 µl were added to PCR using primers pCT_Seq_up and pCT_Seq_lo. PCR protocol was as followed: 95 °C for 5 min, 35 cycles of 30 s at 95 °C, 30 s at 52 °C and 60 s at 72 °C, followed by 72 °C for 5 min. PCR product was verified by gel electrophoresis and cleaned using Wizard® SV Gel and PCR Clean-Up System (Promega). Sequences were analyzed by Sanger sequencing (seqlab, Göttingen) using primer pCT_Seq_up or pCT_Seq_lo.

4.2.4. Binding of Single Clones for Different HTRA1 Variants

For evaluation if isolated McoTI-II and vNAR derived molecules also bind HTRA1 variants that were not used during screening the yeast single clones were labeled with these variants on the cell surface. Here only single labeling by antigen was performed after previous analysis of myc presentation, which was labeled as described in section 4.2.2. For HTRA1 labeling around 10^6 cells per clone were labeled with 1 µM of each variant, followed by washing with 1 ml ice-cold Protease Buffer. Then cells were labeled with Alexa488 conjugated anti-Penta His antibody (QIAGEN) that was 1:10 diluted, followed by washing with 1 ml ice-cold Protease Buffer. All incubation steps were incubated for 10 min on ice. Analyses were carried out using fluorescence activated cell sorter (FACS) (DakoCytomation) that was controlled by Summit software version v4.3.

4.2.5. Affinity Titration of Isolated VHH, vNAR and McoTI-II Derived Molecules

Affinities towards antigens of isolated molecules were determined by affinity titration using yeast single clones as reported by Chao *et al.* [111, 306]. Only yeast cells expressing sufficient amounts of myc epitope were included into calculation of equilibrium dissociation constant (K_D) by gating with

evaluation software Summit v4.3. Thus, around 10^7 cells were labeled with anti-myc antibody, secondary anti-mouse antibody and streptavidin-allophycocyanin conjugate as described in section 4.2.2. Then cells were divided on 10^6 cells each and incubated with decreasing concentrations of fluorescein conjugated HTRA1 for 15 min on ice. Finally cells were washed with 100 µl ice-cold Protease Buffer directly before analyses. Analyses were carried out using fluorescence activated cell sorter (FACS) (DakoCytomation) and mean fluorescence of fluorescein signal (FL1) was used in equation: $y = y_{min} + (y_{max}{}^*x/(x+K_D))$ for determination of K_D.

4.2.6. Affinity Maturation of Isolated vNAR Molecules (HV2, CDR1, HV2+CDR1)

Affinity maturation of initial binding molecules of HTRA1 was performed by isolating plasmids of populations after promising rounds of enrichment by FACS. Cells were grown in SD-CAA media for 1 day at 180 rpm at 30 °C. After incubation 1 ml yeast suspension was centrifuged and resuspended in 250 µl Cell Resuspension Buffer from Wizard® Plus SV Minipreps DNA Purification System (Promega). Glass beads were added and cell suspension was vortexed for 5 min. Then liquid was transferred into a new reaction tube and plasmids were isolated according to the kits manual.

CDR1 matured library was constructed using isolated plasmids as template with primers CDR1rand_up and GR_lo. This was followed by two sequential PCRs using primers FR1_up / GR_lo for the second and GR_up / GR_lo for the third elongation. PCR protocol for all elongation steps was: 95 °C for 5 min, 35 cycles of 30 s at 95 °C, 30 s at 55 °C and 40 s at 72 °C, followed by 72 °C for 5 min. Same strategy was applied for HV2 matured clones that were subsequently matured in CDR1.

For HV2 maturation CDR1 and CDR3 containing regions were amplified separately using primers HV2_SOE_rand_up and pCT_Seq_lo as well as pCT_Seq_up and HV2_SOE_lo, respectively. PCR protocol was as followed: 95 °C for 5 min, 35 cycles of 30 s at 95 °C, 30 s at 55 °C and 40 s at 72 °C, followed by 72 °C for 5 min. PCR products were gel purified using Wizard® SV Gel and PCR Clean-up System (Promega). Both fragments were mated in a PCR without primers while 1 µl of each product of previous PCR was inserted into reaction. After 10 cycles primers pCT_Seq_up and pCT_Seq_lo were added for amplification of full-length sequence. PCR protocol was the same as for the first step.

The PCR products of the three independent maturation approaches were each purified using Wizard® SV Gel and PCR Clean-up System (Promega).

The cloning of the constructs was done by homologous recombination into yeast cells according to the protocol of Benatuil *et al.*[110]. Therefore 250 µl pCT vector with a concentration of 20 ng/µl were linearized by 100 U of restriction enzymes *Nhe* I and *Bam* HI (NEB) according to the manufacturers protocol. Yeast cells were made competent for electroporation according to the protocol of Benatuil *et al.* and mixed with 2 µg of linearized plasmid and 10 µg of PCR product. Gene Pulser XcelI (Bio-Rad) was used for electroporation with settings 2.5 kV and 25 µF which resulted in time constants between 3.0 to 4.5 ms. After transformation yeast cells were incubated for 2 days at 180 rpm and 30 °C in SD-CAA media. Cells were harvested by centrifugation and resuspended in yeast freezing solution for storage at -80 °C.

Library size was determined by serial dilution plating 2 days after electroporation.

For induction of yeast surface presentation yeast cells were incubated overnight with 180 rpm at 30 °C in SD-CAA media and then transferred into SG-CAA media with 180 rpm at 20 °C for 1-2 days.

4.3. Expression, Purification and Characterization of Isolated VHH and McoTI-II Derived Molecules in HEK293 Cells

4.3.1. Cloning of Isolated VHH and McoTI-II Derived Molecules as Fc Fusion Protein

Isolated VHH and McoTI-II derived molecules binding HTRA1 were soluble expressed as amino-terminal Fc-fusion proteins for evaluation. Plasmids of isolated clones containing VHH and McoTI-II derived molecules were isolated from single clones from 1 ml yeast SD-CAA culture that was grown over-night at 180 rpm and 30 °C. Cells were harvested by centrifugation that was followed by resuspension of yeast cells with 250 µl Cell Resuspension Buffer from Wizard® Plus SV Minipreps DNA

Purification System (Promega). Glass beads were added and cell suspension was vortexed for 5 min. Then liquid was transferred into a new reaction tube and plasmids were isolated according to the kits manual.

Sequences were amplified from plasmids in a 3-step PCR with following protocol: 95 °C for 5 min, 35 cycles of 30 s at 95 °C, 30 s at 52 °C and 40 s at 72 °C, followed by 72 °C for 5 min. The primers MASKO_rd5_VHH-K1_NheI_up, MASKO_rd5_VHH-K7_NheI_up, MASKO_rd5_VHH-K1/7_ApaI_lo, SloII_HTRA1_K1_NheI_up and SloII_HTRA1_K1_ApaI_lo were used for amplification and addition of restriction sites *Nhe*I and *Apa*I. PCR products were purified using Wizard® SV Gel and PCR Clean-Up System (Promega) followed by digestion with 2 units of *Nhe*I and *Apa*I for 1 h at 37 °C in suggested buffer. The PCR product was ligated with T4 DNA Ligase into vector pExpress-Fc containing McoTI-II wild-type sequence[307]. Vector was previously digested with 2 units of each *Nhe*I and *Apa*I for 1 h at 37 °C and gel purified with Wizard® SV Gel and PCR Clean-Up System (Promega). *E. coli* cells were grown to OD_{600} of 0.6 and prepared for electroporation by washing 3-times with ice-cold distilled water. 5 µl of ligated vector were mixed with electro-competent *E. coli* DH5α in an electroporation cuvette on ice. Transformation protocol was the preset for bacteria on the Gene Pulser XceII (Bio-Rad). Cells were incubated immediately after pulsing in 1 ml dYT media for 1 h at 37 °C. Afterwards cells were plated out on LB-Agar containing ampicillin (100 mg/l) and incubated over night at 37 °C. Single clones were verified by colony PCR using primers pEXPR_Seq_for and MASKO_rd5_VHH-K1/7_ApaI_lo. Positive clones were incubated in dYT media containing ampicillin (100 mg/l) over night at 37 °C and 180 rpm. Plasmids were isolated using Wizard® Plus SV Minipreps DNA Purification System (Promega). Sequences were analyzed by Sanger sequencing (seqlab, Göttingen) using primer pEXPR_Seq_for or pEXPR_Seq_rev.

4.3.2. Expression of Isolated VHH and McoTI-II Derived Molecules as Fc Fusion Protein

Mammalian HEK293 cells were cultured at 37 °C at 5 % CO_2 and 100 rpm in Freestyle™ 293 media. About 10^6 cells/ml were grown in 25 ml media for 24 h. Transfection was done with 25 µg plasmid and 75 µg PEI that were diluted to a total volume of 2.5 ml with Freestyle™ 293 media followed by incubation for 15 min at room temperature. Then mixture was added slowly to the cells and incubated at 37 °C at 5 % CO_2 and 100 rpm for 24 h. Afterwards 700 µl tryptone solution (20 % in Freestyle™ 293 media) was added and cells were incubated for another 4 days.

4.3.3. Purification of Isolated VHH and McoTI-II Derived Molecules as Fc Fusion Protein

For purification of Fc fusion proteins the expression culture was centrifuged at 4500 g for 10 min at 4 °C. Supernatant was applied on a HiTrap Protein A HP column (GE-Healthcare) using an Äkta FPLC-System (GE-Healthcare). Column was washed with 5 volumes PBS, followed by elution with Protein A Elution Buffer (pH 2.2). Eluted fractions of 1 ml were collected in tubes that contain 200 µl Protein A Neutralization Buffer (pH 9.0). Purification process was monitored using Unicorn Software (GE-Healthcare) by measurement of absorption at 280 nm. Collected fractions containing Fc-fusion protein were pooled and dialyzed (ZelluTrans, Carl Roth GmbH, MWCO 3500) against 5 L Protease Buffer (pH 8.0) overnight at 8 °C. Protein purity was evaluated by SDS-PAGE (4.1.3) and quantity was determined by photometric measurement (4.1.5).

4.3.4. ELISA of Fc Fusion Proteins of Isolated VHH and McoTI-II Derived Molecules

For evaluation of binding properties of isolated VHH and McoTI-II derived molecules an ELISA was performed with soluble expressed Fc-fusion proteins. Thus 100 ng of HTRA1 cd, HTRA1 cd-mono3 and lysozyme were immobilized in separate wells of a maxi-sorb microtiter plate (Nunc) over night at 4°C. Then wells were blocked with 2 % milk powder for 1 h and washed 3-times with Protease Buffer using a plate washer (Tecan). Afterwards wells were incubated for 1°h with serial dilutions of purified Fc-fusion proteins containing 1 % milk powder. In the next step wells were washed 10-times with Protease Buffer and incubated for 1 h with Protein A-HRP conjugate (Sigma-Aldrich) in 1:10000 dilution containing 1 % milk powder. Then wells were washed 10-times with Protease Buffer. After washing 100 µl TMB One solution (Promega) was added to each well. Finally reaction was stopped

using 100 µl HCl (0.1 %) and absorption was measured using a plate reader (Tecan). All proteins and blocking solution were solved and/or diluted in Protease Buffer.

4.4. Expression, Purification and Characterization of Isolated vNAR Molecules

4.4.1. Cloning of Isolated vNAR Molecules as MBP Fusion Protein

For evaluation of isolated vNAR molecules they were soluble expressed as Maltose-binding Protein (MBP) fusion proteins. Plasmids containing isolated vNAR molecules were isolated from single clones from 1 ml yeast SD-CAA culture that was grown over-night at 180 rpm and 30 °C. Cells were harvested by centrifugation that was followed resuspension of yeast cells with 250 µl Cell Resuspension Buffer from Wizard® Plus SV Minipreps DNA Purification System (Promega). Glass beads were added and cell suspension was vortexed for 5 min. Then liquid was transferred into a new reaction tube and plasmids were isolated according to the kits manual.

Sequences were amplified from plasmids in a 3-step PCR with following protocol: 95 °C for 5 min, 35 cycles of 30 s at 95 °C, 30 s at 52 °C and 40 s at 72 °C, followed by 72 °C for 5 min. The primers vNAR_Acc65I_TEV_up and vNAR_His_Stop_XbaI_lo were used for amplification and addition of restriction sites *Acc65*I and *Xba*I. PCR products were purified using Wizard® SV Gel and PCR Clean-Up System (Promega) followed by digestion with 2 units of *Acc65*I and *Xba*I for 1 h at 37 °C in suggested buffer. The PCR product was ligated with T4 DNA Ligase into Wizard® SV Gel and PCR Clean-Up System (Promega) gel purified vector pMX-EETI that was previously digested with *Acc65*I and *Xba*I.

E. coli cells were grown to OD_{600} of 0.6 and prepared for electroporation by washing 3-times with ice-cold distilled water. 5 µl ligated vector were mixed with electro-competent *E. coli* DH5α in an electroporation cuvette on ice. Transformation protocol was the preset for bacteria on the Gene Pulser XceII (Bio-Rad). Cells were incubated immediately after pulsing in 1 ml dYT media for 1 h at 37 °C. Afterwards the cells were plated out on LB-Agar containing chloramphenicol (25 mg/l) and incubated over night at 37 °C. Single clones were verified by colony PCR using primers vNAR_Acc65I_TEV_up and pMX_seq_lo. Positive clones were incubated in dYT media containing chloramphenicol (25 mg/l) over night at 37 °C and 180 rpm. Plasmids were isolated using Wizard® Plus SV Minipreps DNA Purification System (Promega). Sequences were analyzed by Sanger sequencing (seqlab, Göttingen) using primer pMX_seq_up or pMX_seq_lo.

4.4.2. Expression of Isolated vNAR Molecules as MBP Fusion Protein

E. coli BMH 71-18 cells were grown to OD_{600} of 0.6 and prepared for electroporation by washing 3-times with ice-cold distilled water. Then 1 µl plasmid was mixed with electro-competent *E. coli* BMH 71-18 in an electroporation cuvette on ice. Transformation protocol was the preset for bacteria on the Gene Pulser XceII (Bio-Rad). Cells were incubated immediately after pulsing in 1 ml dYT media for 1 h at 37 °C. Afterwards cells were plated out on LB-Agar containing chloramphenicol (25 mg/l) and incubated over night at 37 °C.

A single clone was selected and incubated in 50 ml dYT media containing chloramphenicol (25 mg/l) overnight at 37 °C and 180 rpm. Then 1 L LB-media containing chloramphenicol (25 mg/l) was inoculated with 20 ml of overnight culture and grown until OD_{600} of 0.8 at 37 °C at 180 rpm. At an OD_{600} about 0.8, protein expression was induced by addition of IPTG to a final concentration of 1 mM for 24 h at 30 °C and 180 rpm.

4.4.3. Purification of Isolated vNAR Molecules as MBP Fusion Protein

After expression of MBP fusion proteins the *E. coli* cells were harvested by centrifugation at 16000 g for 15 min at 4 °C. Cells were resuspended in ice-cold Periplasm Prep Buffer containing Lysozyme (100 mg/l). Cells were incubated on a tumbling shaker for 30 min on ice followed by centrifugation at 19000 g for 15 min at 4 °C. Supernatant was sterile filtered before it was applied on a HisTrap column (GE Healthcare) using an Äkta FPLC-System (GE-Healthcare). Column was washed with 5 volumes PBS, followed by elution with a linear gradient of PBS/PBS 1 M imidazole. Eluted protein was

collected in fractions of 1 ml each. Purification process was monitored using Unicorn Software (GE-Healthcare) by measurement of absorption at 220 nm.

For cleavage of vNAR from MBP with tobacco etch virus protease (TEV protease) the collected fractions were pooled and 10-fold TEV Buffer was added as well as TEV protease in a ratio of 1:10. Cleavage of fusion protein was carried out overnight at 8 °C.

For separation of both proteins the cleavage reaction was concentrated by ultra-filtration with Amicon Ultra-15 10000 (Merck Millipore). Then cleavage mix was applied on a gel filtration column HiLoad Superdex 75 pg 16/60 (GE-Healthcare) that was equilibrated with Protease Buffer. Eluted vNAR molecules were collected in fractions of 1 ml and pooled. Protein purity was evaluated by SDS-PAGE (4.1.3) and quantity was determined by photometric measurement (4.1.5).

5. Results

5.1. Expression and Purification of HTRA1 Variants

To investigate the influence on activity of the different oligomeric states of HTRA1, variants were generated that lack amino acid residues important for trimerization. In contrast to oligomers, monomers present surfaces that are masked in the oligomeric state. Molecules that bind to that region might therefore stabilize the monomeric state and preclude oligomer formation. This type of molecules might be valuable tools for the study of HTRA1 function. Moreover, exploratory experiments revealed no enrichment of specific binders from VHH nanobody libraries using oligomeric HTRA1 as target, neither in phage display, nor in yeast display screens (results not shown). Only nonspecifically binding or unstable VHH molecules were obtained by screening of a phage display library of naïve VHH domains (results not shown). Likewise, in yeast surface display problems occurred during rounds of enrichment. In detail, HTRA1 oligomer particles were detectable in the cell sorter upon common side scatter triggering that is used for cell detection, complicating FACS screening of yeast cells (results not shown). Thus mainly protein particles were isolated and not cells needed for following rounds. These findings strongly supported the motivation to design a monomeric variant of HTRA1.

The gene for the protease domain of HTRA1 was provided by Prof. M. Ehrmann in expression vector pET21d with a carboxyl-terminal His-tag[31]. Residues that were identified by inspection of the 3D structure to be involved in trimerization[31] were replaced by alanine to generate a monomeric variant. The three hydrophobic residues that are suggested to mediate trimerization of catalytic domains are shown in figure 4b. For the first variant HTRA1 cd-mono2 the two amino-terminal residues tyr169 and phe171 were substituted by alanine using site-directed mutagenesis. The second variant HTRA1 cd-mono3 additionally replaced phe278 by an alanine and was generated through splicing by overlap extension (SOE) PCR using HTRA1 cd-mono2 as template. Additionally a variant HTRA1 cd+PDZ was amplified from the human HTRA1 full-length clone *IRATp970G0933D* delivered from GenomeCube that additionally contains the carboxyl-terminal Post Synaptic Density, Discs Large and Zonula Occludentes-1 domain (PDZ) but is lacking the native amino-terminal Insulin-like Growth Factor Binding Protein (IGFPB) and Kazal-like Inhibitor Domain (KI). The schematic illustration in figure 13 shows the domain arrangement of the human full-length HTRA1 and the variants generated in this work.
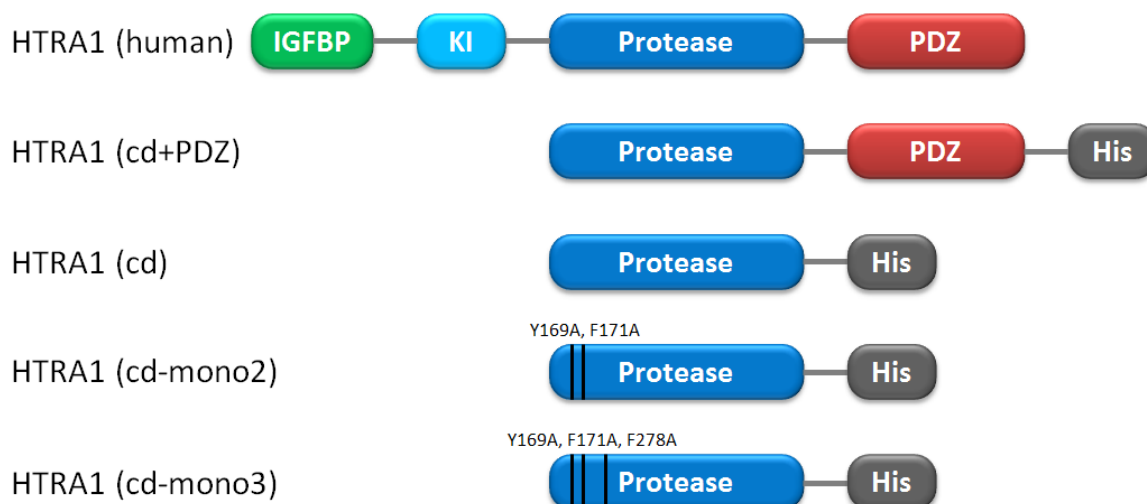
Figure 13 Schematic domain arrangement of human full-length HTRA1 and its recombinant derived variants. Insulin-like Growth-Factor Binding Protein (green), Kazal-like Inhibitor Domain (light blue), Trypsin-like Protease Domain (blue), Post Synaptic Density, Discs Large and Zonula Occludentes-1 domain (red) and 6 Histidine-Tag (grey). Amino acid exchanges are indicated by black bars in the protease domain with position and residue above.

All constructs were cloned into pET21d vector by *Nco*I and *Xho*I cleavage sites, verified by sequencing and transformed in expression host *E. coli* BL21. Expression was carried out for 24 h at 16 °C in Low

Broth (LB) media under continuous shaking at 180 rpm. After harvesting cells they were lysed using cell-disruptor instrumentation followed by removing cell debris through centrifugation. HTRA1 variants were isolated from the supernatant by immobilized metal ion affinity chromatography (IMAC) using ÄKTA FPLC system with Hi-Trap columns. Fractions containing eluted protease were pooled, concentrated by ultra-filtration and further separated by preparative size-exclusion chromatography (SEC). SEC chromatograms for different expressed HTRA1 variants are shown in figure 14. For determination of size of different fractions calibration proteins were purified on SEC column. For each variant an oligomeric population was observed eluting with the dead volume of the used column at around 45 ml indicating an apparent molecular weight of approximately (MW) 500,000. A second elution peak was observed at 78 ml for HTRA1 cd and its mutants indicating to an apparent molecular weight of 75,000. A third elution peak was observed for the two mutants of HTRA1 cd at 90 ml indicating to an apparent molecular weight of MW 25,000. For HTRA1 cd+PDZ three elution peaks additionally to the first were observed at 54 ml, 67 ml and 84 ml in preparative SEC (Figure 14).

Pooled fractions were further analyzed by SDS-polyacrylamide gel electrophoresis (PAGE). PAGE of standardized protein concentrations is shown in figure 17a in section 5.1.3. PAGE confirmed the molecular weight of the denatured monomeric protein of MW 25,000 for HTRA1 cd and both mutants, as well as of 37,000 for HTRA1 cd+PDZ as expected. Some fractions contain co-purified proteins from IMAC and fragments that most likely result from the HTRA1 proteolytic activity. Additionally it was confirmed by Western blot with an anti-His antibody that purified proteins of correct size are His-tagged molecules (results not shown).

For the variant HTRA1 cd the detected apparent molecular weight of 75,000 corresponds to the trimer as well as for HTRA1 cd+PDZ the detected apparent molecular weight of 110,000. These results confirm the two different oligomeric states (trimer and higher oligomer) previously reported[31]. For the mutants of HTRA1 cd additionally monomeric states with apparent molecular weight of 25,000 were detected and isolated, but still higher oligomers and trimers are present. HTRA1 cd-mono3 shows a similar peak pattern compared with HTRA1 cd-mono2. Interestingly ratios of the peak-areas which correlate to the amount of protein are shifted from trimer to monomer by the additional mutation of HTRA1 cd-mono3. Through multiple SEC runs, sufficient amounts of the three different HTRA1 cd-mono3 fraction could be collected.
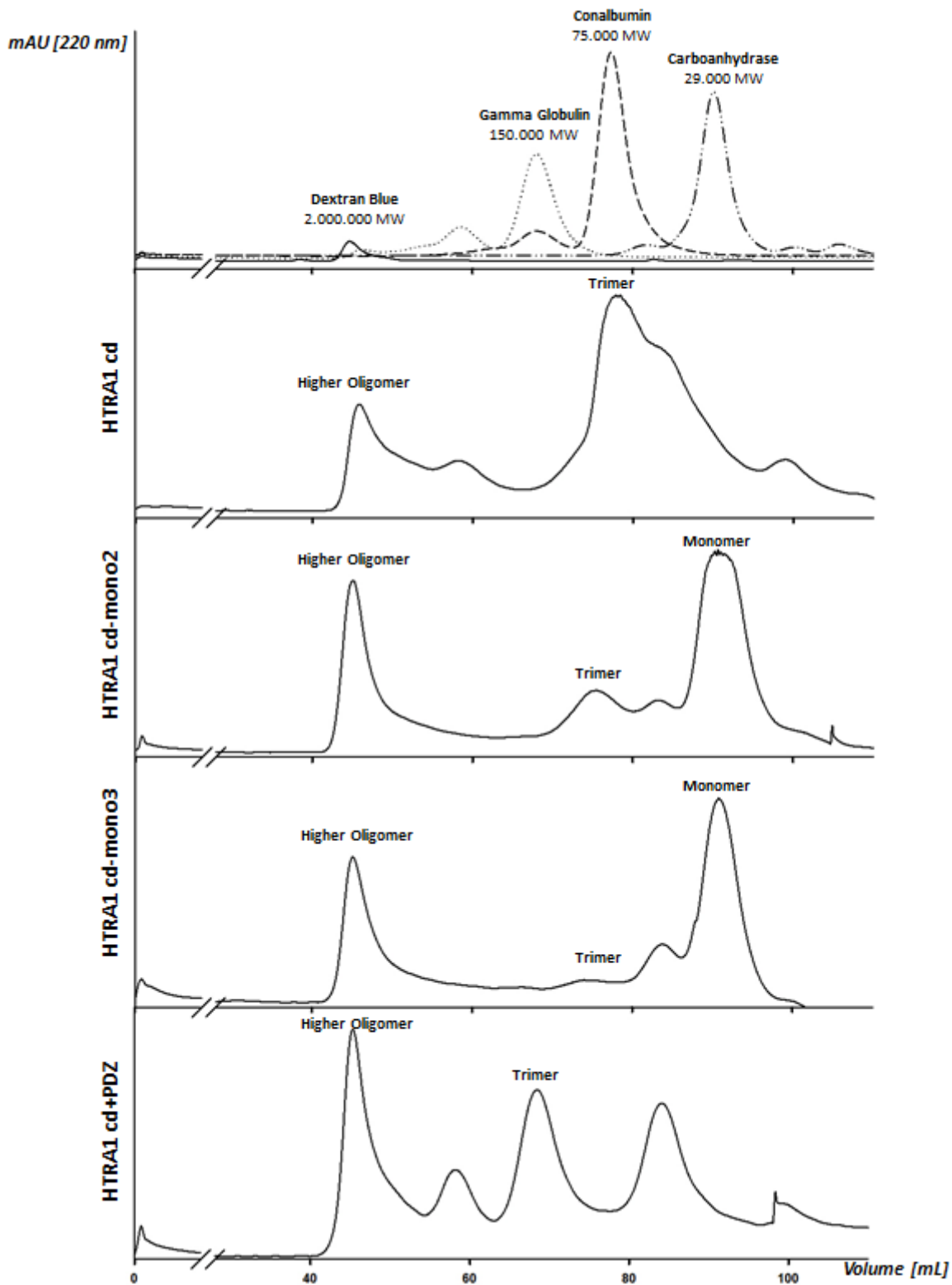
Figure 14 Size-exclusion chromatography (SEC) of his-tagged HTRA1 variants after immobilized metal ion affinity chromatography (IMAC). Chromatograms of calibrator proteins, HTRA1 cd, HTRA1 cd-mono2, HTRA1 cd-mono3, HTRA1 cd+PDZ (from top to bottom). Different HTRA1 fractions that were confirmed by SDS-PAGE are indicated by their oligomeric states. Detection was at 220 nm wavelength.

5.1.1. Determination of Stability of HTRA1 Oligomeric States by SEC

Preparative SEC analysis in section 5.1 (figure 14) revealed that the ratio of the amount of different oligomeric states altered by the exchange of residues residing at the trimer interface.

To determine whether separated oligomeric states are stable or equilibrate upon storage, the different fractions obtained from SEC separation were frozen at -20 °C and thawed after 24 h followed by storage at 8 °C for 7 days. Subsequently an analytical SEC was performed using the ÄKTA FPLC system with an analytical column. Figure 15 shows the SEC plot of all four variants and their different oligomeric states. All higher oligomeric fractions and the monomeric fractions of the mutants of HTRA1 cd that were previously purified were found to be stable and no gross re-equilibration was observed. Nevertheless trimer fraction of HTRA1 cd and HTRA1 cd+PDZ showed a slight shift towards a lower molecular weight fraction. This may be due to proteolytic degradation. While the monomeric fraction of HTRA1 catalytic domain mutant variants remained monomeric upon storage, the trimer fractions showed some equilibration between the trimeric and the monomeric states.
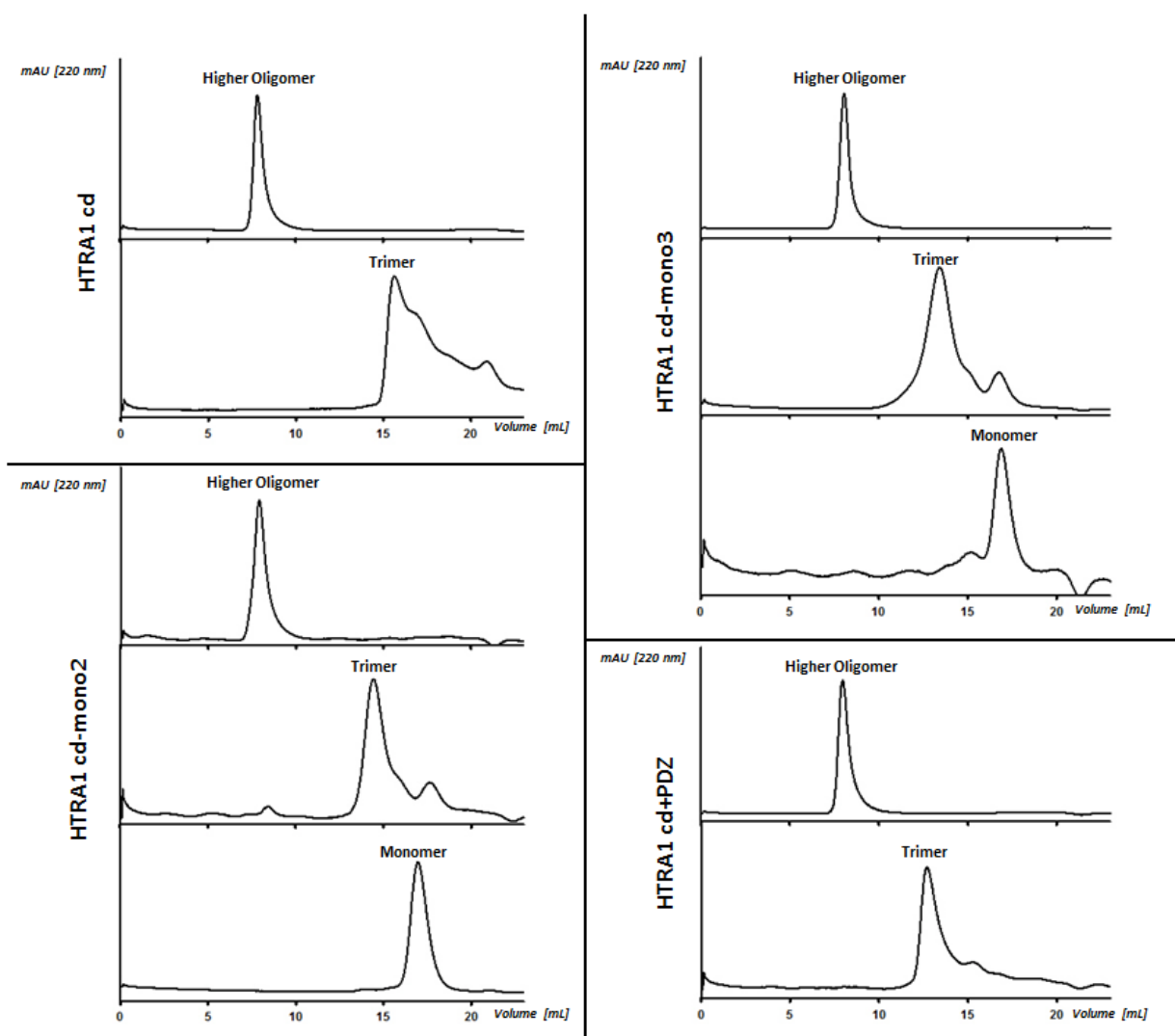
Figure 15 Plots of size-exclusion chromatography (SEC) of previously separated HTRA1 variant fractions of different oligomeric states. Chromatograms of HTRA1 cd (top-left), HTRA1 cd-mono2 (bottom-left), HTRA1 cd-mono3 (top-right), HTRA1 cd+PDZ (bottom-right). Specific oligomeric states are indicated. Detection was at 220 nm wavelength.

5.1.2. Melting Curves of HTRA1 Variants

To determine the thermal stability of the expressed HTRA1 variants, thermal melting was measured using SYPRO-Orange. Temperature gradient and data recording were carried out on a real-time PCR instrument. SYPRO-Orange that provides fluorescence excitation and emission after intercalation with hydrophobic patches of proteins was added before HTRA1 variants were exposed to the temperature gradient. All variants show denaturation in a temperature range between 54-63 °C (figure 16). The trimeric fraction of HTRA1 cd displayed a melting point of 62 °C as well as the trimeric fraction of HTRA1 cd-mono3 and HTRA1 cd+PDZ with around 60 °C. The melting points of the monomeric fractions of HTRA1 cd-mono2 and cd-mono3 were 8-10 °C lower than the one for the trimeric fractions. This indicates that the generated variants are stable as monomers. Additionally, trimerization enhanced thermal stability of the monomeric folding unit. The higher oligomeric fraction of HTRA1 cd-mono3 is with 62 °C comparable with the trimeric fractions of HTRA1 cd and HTRA1 cd+PDZ with respect to melting temperature.
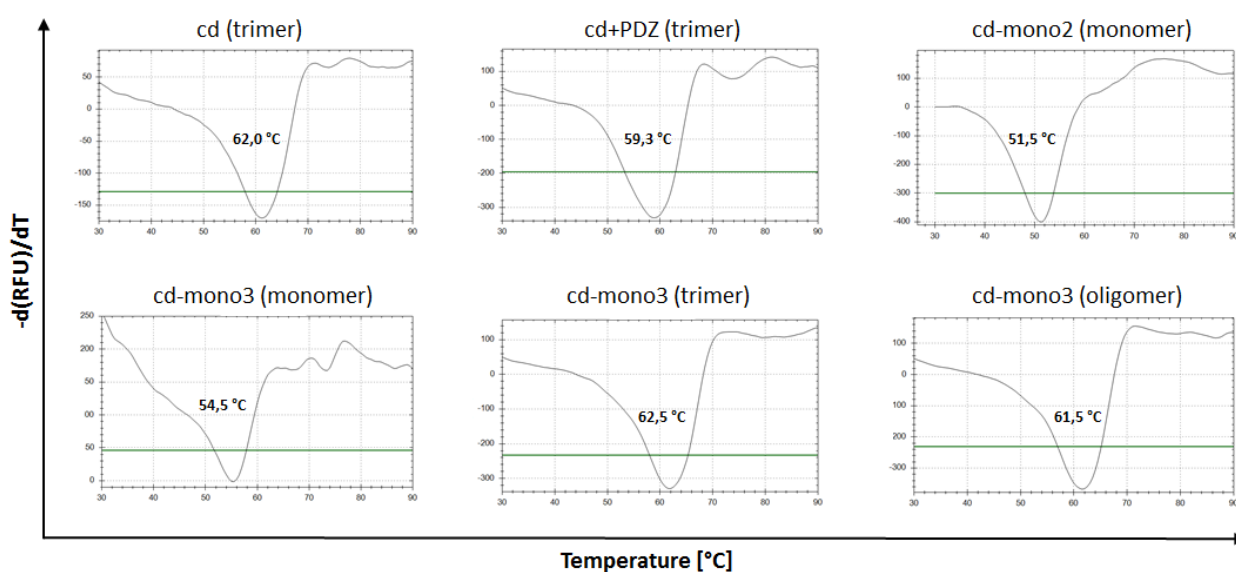
Figure 16 Melting curve analysis of HTRA1 variants using SYPRO-Orange. Melt points (Tm) were measured in duplicates and values are indicated in the plots.

5.1.3. Protein Concentration of HTRA1 Variants (BCA/OD$_{280}$)

After SEC the pooled fractions were concentrated by ultra-filtration and concentrations were determined using measurement of optical density (OD) at 280 nm with specific extinction coefficient (ε) of the different variants. Specific ε was calculated using algorithm of vector NTI Software (Invitrogen)[308]. Due to a high divergence of protein amount of different HTRA1 variants that was observed in SDS-PAGE after normalization according to OD$_{280}$ indicating presence of contaminants absorbing at 280 nm, a bicinchoninic acid assay (BCA) was executed (figure 17a). By this method a colorimetric signal is measured that is proportional to distinct amino acids and peptide bonds. The normalization based on BCA assay indicated similar concentrations for tri- and monomeric fractions while the higher oligomeric fractions were much lower concentrated as shown by SDS-PAGE (figure 17a). Additionally the SDS-PAGE revealed several impurities at the higher oligomeric fractions. These were possibly co-purified by HTRA1 during purification due to unspecific binding to the protease as well as degradation products. The concentration of the relatively pure HTRA1 cd-mono3 was determined under consideration of its specific ε280 of 3840 M^{-1}cm^{-1} to be 2 mg/ml. With a volume of about 6 ml the total yield for HTRA1 cd-mono3 monomeric fraction was after two-step purification (IMAC and SEC) approximately 12 mg per Liter. For the other HTRA1 variants and their different monomeric and trimeric fractions the yield was lower, but at least 2.5 mg per Liter for trimeric HTRA1

cd-mono2 and HTRA1 cd-mono3 could be isolated. Due to the impurities no yields for the higher oligomeric fractions were calculated.
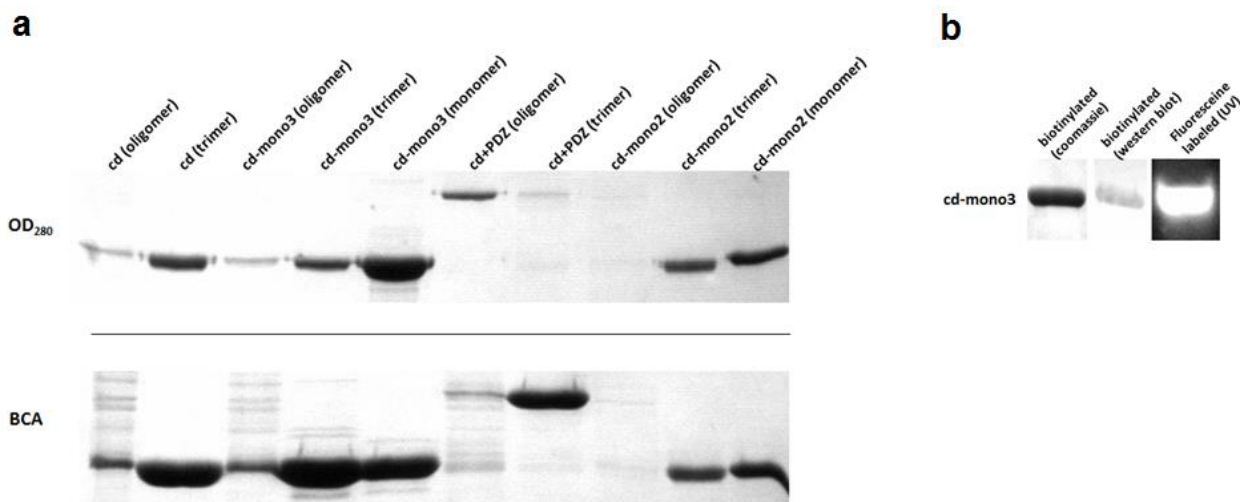
Figure 17 HTRA1 variants after separation by size-exclusion chromatography (SEC). Standardization of protease amount on optical density (OD280) (top) and BCA-Assay (bottom) (a). Verification of labeling with biotin by Western blot (middle) and labeling with fluorescein by PAGE under UV-light (right) (b).

5.1.4. Labeling of HTRA1 Variants

For the directed evolution method of yeast surface display that is carried out on a fluorescence activated cell sorter (FACS), it is necessary to label the target molecule with a fluorescence dye. One possibility for covalent labeling is the linkage mediated by an amine reactive group. In this work fluorescein was coupled through an isothiocyanate moiety (FITC) to HTRA1, whereas biotin was coupled through N-hydroxysuccinimide moiety (NHS-LC-Biotin). Biotin is strongly bound by streptavidin which is commercially available as a conjugate to many prominent fluorescent dyes such as phycoerythrin or allophycocyanin. Both moieties are amine reactive, so they react with lysine as well with the amino-terminus of a polypeptide. The labeling procedure was carried out as described in section 4.1.6.

For labeling of HTRA1 cd-mono3 purification buffer was exchanged by gravity desalting columns to obtain optimal reaction conditions for labeling. The ratio for both labeling approaches was 5 labeling molecules per target molecule. Although not all labeling reagents are attached during the labeling process a low ratio was chosen to prevent loss of protease activity by extensive protein modification. FITC labeling was verified by SDS-PAGE which was exposed to UV-light. NHS-biotin labeling was verified by SDS-PAGE followed by Western blot using an ExtrAvidin™-alkaline phosphatase conjugate. Both results are shown in figure 17b in the previous section (5.1.3). Labeling of HTRA1 variants was successful for both reagents although it remains unclear how many molecules are attached to a protease molecule and whether each protease molecule is at least labeled once.

5.1.5. Measurement of HTRA1 Activity

To determine, whether expressed HTRA1 cd+PDZ, HTRA1 cd and its mutants are active enzymes an activity assay was performed. The most sensitive reported substrate is a quenched fluorogenic peptide substrate named H2Opt. This substrate was originally found by screening a substrate library against human HTRA2, but it was shown that it also works well with HTRA1[30, 53]. The substrate was synthesized using automated solid phase peptide synthesis (SPPS), purified by reversed-phase HPLC and verified by LC ESI-MS (results not shown). Its sequence is Mca-IRRVSYSF(Dnp)KK, where m-coumaric acid (Mca) is amino-terminally attached as a fluorophore and dinitrophenol linked to a lysine side-chain is introduced as a quencher. After cleavage of the peptide bond between these molecules excitation of the fluorophore with 328 nm results in emission of light with a wavelength of

393 nm. The synthesized substrate was modified compared to the literature[53] by introducing an additional lysine at the carboxyl-terminus to enhance the solubility and was designated as H2Opt-K.

For measurement of proteolytic activity, a protease concentration of 0.625 µM was found to be optimal when using 12.6 µM of H2Opt-K (results not shown). Measurement was performed for 1 h at room temperature using a microtiter plate reader. Substrate background fluorescence was recorded without addition of protease to verify that no autolysis of the substrate occurs (results not shown). For all measurements a double determination was performed and the average value is shown in all plots, as well as the standard deviation by error bars. The plots for the three different purified HTRA1 fractions are shown in figure 18a, b and c. The higher oligomeric fractions showed high activity since a significant fraction of the substrate was cleaved already prior to start of recording. For higher oligomeric fractions it is important to note that the actual concentration of HTRA1 most likely is underestimated due to presence of contaminating impurities, a fact that corroborates the notion that higher oligomeric HTRA1 displays higher proteolytic activity compared to trimeric HTRA1.

The trimeric fractions of HTRA1 cd and HTRA1 cd+PDZ showed similar activity towards substrate H2Opt-K. However, HTRA1 cd-mono2 and cd-mono3 are inactive at comparable concentrations, as well as monomeric fractions of both mutant variants. Due to this observation all monomeric fractions of HTRA1 cd-mono3 were measured again using higher substrate and/or higher protease concentrations. At 63.5 µM substrate concentration the trimeric fraction showed substrate processing comparable to higher oligomeric fraction at 12.6 µM when using a protease concentration of 0.625 µM (figure 18d). Interestingly, the monomeric fraction showed comparable activity when substrate concentration is raised to 63.5 µM and additionally protease concentration is raised to 10 µM. Nevertheless standard deviation for HTRA1 cd-mono3 monomeric fraction is extremely high. No further experiments were performed aimed at investigating, whether monomeric HTRA1 variants re-equilibrate at high protein concentrations to for trimers or higher oligomers.
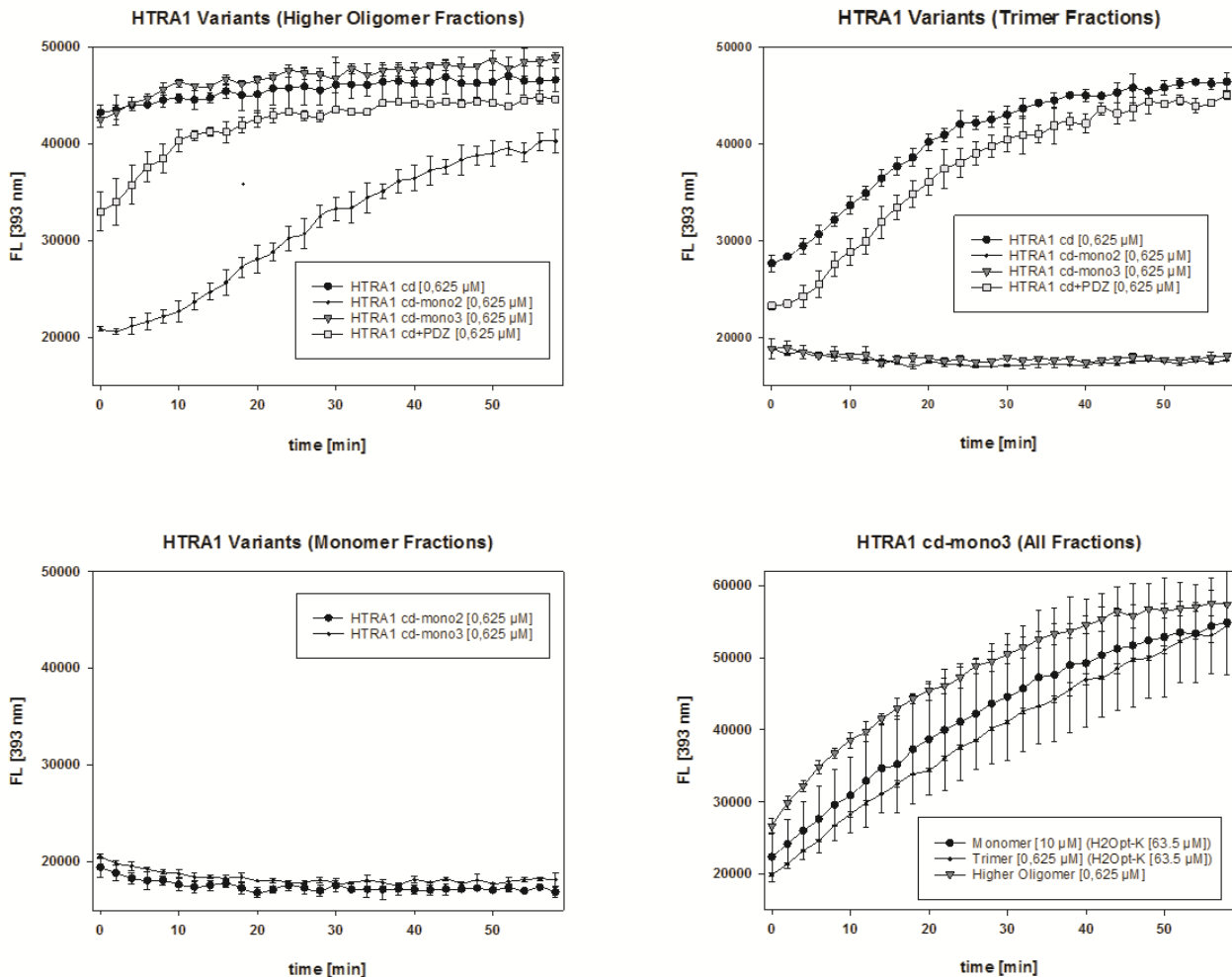
Figure 18 Activity measurement of HTRA1 variants and their different oligomeric states. Higher oligomeric states (a), trimeric states (b), monomeric states (c) and HTRA1 cd-mono3 with its 3 fractions with different protease and substrate concentrations (d). Activity was measured with H2Opt-K as fluorescence substrate over time in duplicates. Substrate concentration is increased for trimeric and monomeric fraction to 63.5 µM. Protease concentration of monomeric fraction is increased to 10 µM. For all plots only every second data point is shown.

5.2. Screening of an Immunized Llama VHH Library

In 2011, a llama was immunized with four different disease-related proteins initiated by the workgroup of Prof. Harald Kolmar[309]. The immunization was done with 1 mg of each protein followed by two boosting steps after several weeks. In this immunization, trimeric fraction of HTRA1 cd was administered. After the second boost blood was collected and B-cells were isolated bearing the information of matured IgG and as well as VHH molecules. RNA was isolated and transcribed with VHH specific primers in cDNA that serves as a template for the construction of a variant library in yeast cells that could be displayed on the cell surface.

5.2.1. Serum Titer against HTRA1

To verify whether the immunization against trimeric fraction of HTRA1 cd was successful the titer of antibodies against the protease was determined. To this end, HTRA1 cd trimeric fraction and BSA as negative control were immobilized on the surface of a microtiter plate (MTP). In the next step cavities were incubated with serial dilutions from 1:10-1:1000 of serum collected before and after immunization. The binding of antibodies was detected using a protein A horseradish-peroxidase conjugate and TMB One as substrate. The chart for antibody titer is shown in figure 21a in section 5.2.3. The pre-immune serum showed no specific binding in any dilution. The post-immune serum showed strong signal against HTRA1 cd trimeric fraction in 1:10 dilution as well as clear signal in 1:100 dilutions. In 1:1000 dilutions no signal was observed. This indicates a concentration-dependent

binding of antibody molecules induced by immunization of llama. However, it is important to note that this assay does not allow one to distinguish between classical antibodies and single domain antibodies recognizing HTRA1.

5.2.2. Library Generation and Screening

The VHH library used in this work was obtained by immunization of a llama with a combination of four different antigens including a trimeric fraction of protease domain of human HTRA1 which was recombinantly expressed in *E. coli*. The collection of blood was performed 54 days post immunization. Approximately 100 ml whole blood was collected with two different methods, either by extracting and stabilizing mRNA directly after collection, or stabilizesing the blood until mRNA extraction in the laboratory was performed. After reverse transcription by oligo(dT)$_{20}$ and random hexamer primers VHH genes were amplified with addition of homologous ends for library generation in yeast[110] (4.2.6). Library size was estimated to be approximately 2.8×10^8 independent clones.

Using biotinylated HTRA1 cd for library screening caused unexpected problems. Obviously, the target protein formed large aggregates that were detectable by FACS hampering the isolation of labeled yeast cells. As a consequence, in following experiments monomeric fraction of HTRA1 cd-mono3 was exclusively used for library screening.

Additionally to fluorescein labeled monomeric fraction of HTRA1 cd-mono3 a carboxyl-terminal myc epitope that is expressed by each variant was used for detection of VHH expression and cell surface presentation using a second fluorescent label addressing the myc epitope. The FACS allows for isolation of variants from the library that show both features, which are cell surface presentation and target binding. The isolated yeast cells can be amplified by culturing and screened again for several rounds until a population of binders emerges. Ideally, the enriched population should contain full-length VHH molecules with the ability of binding the HTRA1 variant used for screening.

For the isolation of VHHs recognizing the monomeric HTRA1 cd-mono3 fluorescein labeled protease and a biotinylated anti-myc antibody were used for the first two rounds of enrichment. While fluorescein has an emission maximum around 520 nm the biotinylated antibody was stained using a streptavidin-allophycocyanin (SAPC) conjugate with an emission maximum around 680 nm. In the next three rounds staining of the yeast cells, the mode of cell detection was inverted by using a combination of an anti-myc antibody labeled with a fluorescein conjugated anti-mouse antibody and the biotinylated HTRA1 cd-mono3 monomeric fraction, followed by cell labeling with SAPC. For all five enrichment steps the protease concentration was 1 μM. The alternation of the labeling strategy should prevent enrichment of yeast cells that present VHHs binding to the secondary antibody, streptavidin or fluorophores as well as misinterpretation of artefacts. The two dimensional (2D) consideration of binding properties allows an emphasis of distinction between surface presentation and target binding.

After the incubation steps with the different labeling agents the yeast cells were washed finally and sorted with the FACS at a rate of about 30,000 cells per second. After sorting of the fourth round an additional resorting was performed directly. Besides demonstrating that enrichment was successful this resorting removes false sorted cells and enlarges enrichment success. The histograms of the sorts and resorts of the different rounds are summarized in figure 19. The gate that resembles the decision for region of sorted cells was chosen arbitrarily. The fraction of isolated cells is displayed as percentage in the gate.
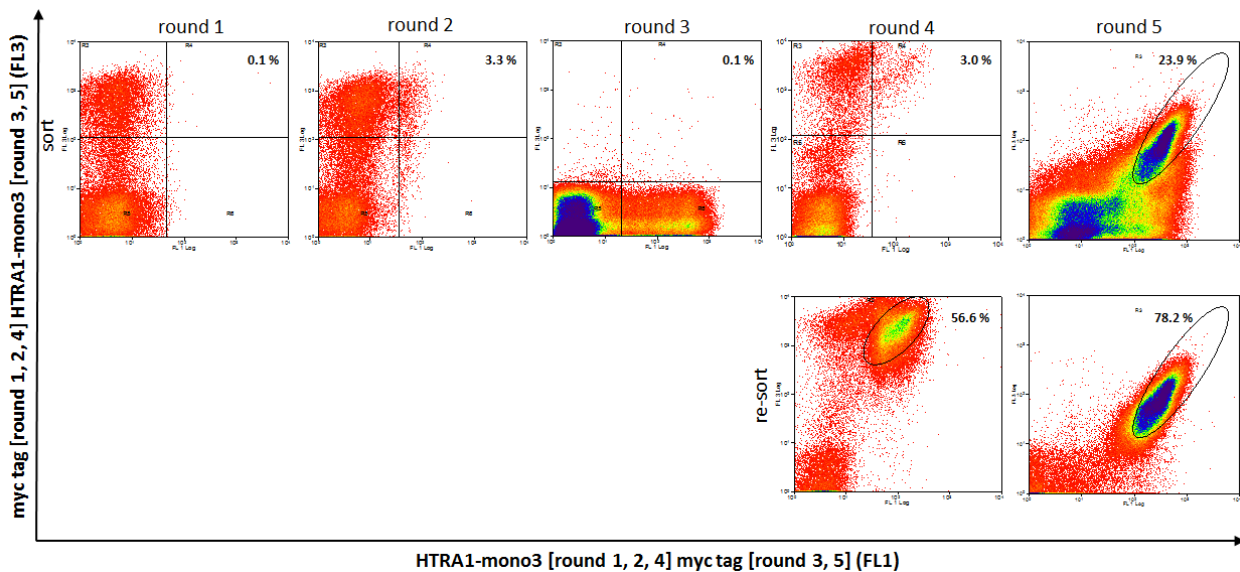
Figure 19 Histograms of enrichment of HTRA1 cd-mono3 binding cells presenting VHH library. Sorting rounds 1-5 (top) and resorts of round 4 and 5 (bottom). FL1 channel for HTRA1 cd-mono3 (round 1, 2 and 4) and myc-tag (round 3 and 5) on the x-axis. FL3 channel for myc-tag (round 1, 2 and 4) and HTRA1 cd-mono3 (round 3 and 5) on the y-axis. Gates for sorted cells are indicated by percentage of events that were isolated.

In the first round $2x10^8$ cells were screened and 0.13 % were collected on the basis of a trade-off between surface presentation and binding to HTRA1 cd-mono3. In the second round slight enrichment of HTRA1 cd-mono3 binding molecules in fluorescence channel 1 (FL1) was observed, since 3.3 % of the cells were found to be in the sorting window. The altered cell staining procedure in round three showed significantly less binding of HTRA1 compared to round two (0.07 %). Staining was altered again in the fourth as well as in the fifth round. About 3 % of the cells were sorted out in the fourth round. The successive resort revealed a strong enrichment since 56.6 % of the cells were found in the selection gate. Finally, a fifth sorting round revealed a high degree of enrichment of target binding cells as well as surface presentation (23.9 % in the sorting gate). A resort was performed to control successful enrichment process of this final round resulting in a population of 78.2 %.

For determination of the properties of enriched clones, 12 single clones were randomly picked from plates and cultured after the fifth sorting round. The induced cells were labeled with an anti-myc antibody and with HTRA1 cd-mono3 to investigate, whether their corresponding VHH is displayed in full-length and has the ability to bind to HTRA1 cd-mono3 monomeric fraction. About 50,000 cells of each labeled single clone were analyzed using FACS. By using a target concentration of 1 µM as it was used during the initial rounds of enrichment it could be qualitatively determined whether the isolated clones present a VHH variant that binds HTRA1 cd-mono3. 10 of the 12 clones showed presentation of myc-tag as well as target binding (Results not shown).

Sanger sequencing of the HTRA1 cd-mono3 binding clones revealed two unique sequences (figure 20). Sequence of clone KV01 was found six times, while clone KV07 was found four times. The amino acid sequence alignment of both clones is shown in figure 20. To find more sequences of HTRA1 cd-mono3 binding VHH molecules additionally 10 clones of the fourth round were sequenced. This only resulted in same sequences with a similar distribution. Both clones showed totally different framework residues in many positions. The CDRs show little conserved areas such as a methionine in position 6 of CDR1, an alanine in position 2 of CDR2 and a glycine in position 6 of CDR3. The CDR3 of KV07 is with only seven residues about five residues shorter than CDR3 of KV01.

```
KV01|rd5|VHH-MASKO|6/10    MAEVQLQASGGGLVQPGGSLRLSCATSGFTFTEYWMHWVRQAPGKGLEWV
KV07|rd5|VHH-MASKO|4/10    MADVQLQASGGGSVQTGGSLRLSCTASGDTDCISMMAFYRQAPGKGREFV

STINTGGFKTYYADSVKGRFLISRDNGENTLYLQMDSLKPEDTALYYCYAETYEYGDERDYSGPGTLVTVSSGS
ASITWTRGTIHYQESVKGRFTISRDNVTSTAYLQMNSLKPEDTAVYYCNALGPLWG-----WGQGTLVTVSSGS
```

Figure 20 Amino acid sequence alignment of HTRA1 cd-mono3 binding VHH molecules isolated by FACS. Clone name, selection round and occurrence are designated for each clone Positions that are unique in framework are indicated in red. CDR1 is shown in light grey, CDR2 in dim grey and CDR3 in black.

5.2.3. Characterization of Isolated VHH Molecules

By cell labeling using varying concentrations of the target protein, a binding curve can be generated by plotting mean fluorescence versus target protein concentration that allows for a calculation of the equilibrium dissociation constant (K_D). For this affinity titration (4.2.5), cells of clones KV01 and KV07 were stained for myc-tag and HTRA1 binding using decreasing concentrations of protease. The mean fluorescence of the labeled HTRA1 cd-mono3 cells from the gated population of cells with equivalent levels of VHH surface accumulation was recorded and correlated with labeling concentration of protease. K_D values were determined by fitting method of K. D. Wittrup using Sigma Plot Software[306]. The plots are shown in Appendix A and the K_D values in table 1 (5.4.4). Both VHH molecules showed K_D values in the triple-digit nano-molar range against HTRA1 cd-mono3 monomeric fraction when being presented on the yeast surface.

Both VHH variants were additionally expressed as Fc fusion proteins in HEK293 cells described in detail in section 5.5.2 of this work. Only expression of KV07 resulted in amounts that were sufficient for further investigations.

First an ELISA for Fc-fused KV07 was performed with immobilized HTRA1 cd trimeric fraction and HTRA1 cd-mono3 monomeric fraction. In the next step cavities were incubated with serial dilutions of cell culture supernatant of HEK293 cells producing KV07-Fc fusions from 1:10-1:1000, followed by incubation with a protein A horseradish-peroxidase conjugate. Presence of HTRA1 binding Fc-VHH fusion was detected by incubation with horseradish-peroxidase substrate TMB. The chart is shown in figure 21b. Interestingly, only the monomeric variant of HTRA1 is detected by KV07-Fc in a concentration dependent manner. HTRA1 cd trimeric fraction and the negative control showed no signal, even at the highest KV07-Fc concentration.

Additionally for Fc-fused KV07 an activity measurement towards HTRA1 cd trimeric fraction in presence of purified KV07-Fc was carried out (Figure 21c). An Fc lacking a fused VHH was used as negative control. Conditions were the same as for determination of activity of HTRA1 variants described in section 5.1.5 of this work (0.625 µM protease; 12.6 µM substrate). Concentration of Fc and KV07-Fc was 14 µM. No influence on activity of HTRA1 cd was observed in presence of KV07-Fc.

Due to the observation in ELISA that KV07 selectively binds HTRA1 cd-mono3, but not HTRA1 cd an activity measurement of HTRA1 cd-mono3 monomeric fraction in presence of purified KV07-Fc was carried out (figure 21d). Conditions were the same as for HTRA1 cd trimeric fractions. In this experiment, it was investigated whether KV07 binding allosterically activates HTRA1 cd-mono3 monomeric fraction, as for the substrate and protease concentration chosen no activity was observed for this variant. No allosteric modulation of HTRA1 activity was detected upon co-incubation with KV07.
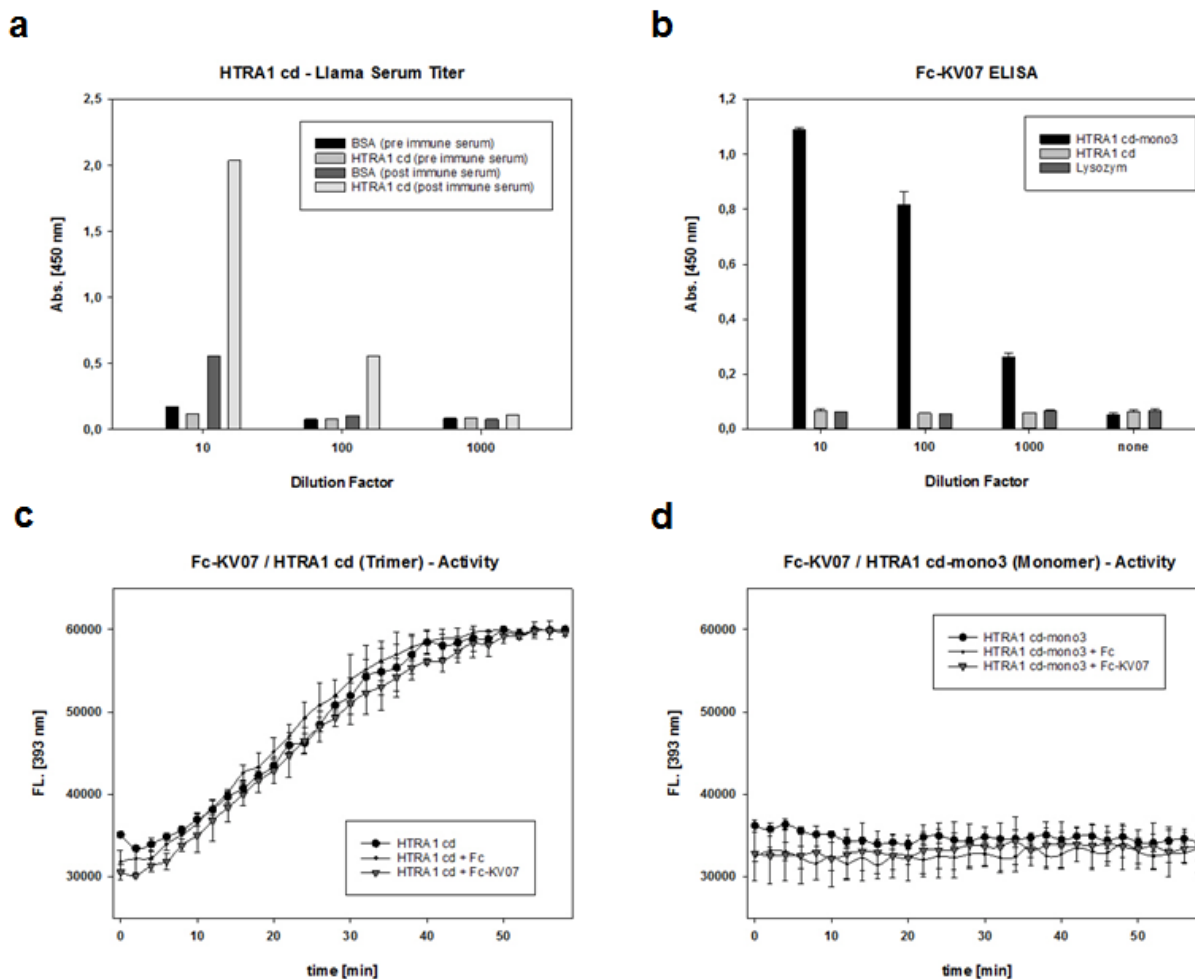
Figure 21 Analysis of HTRA1 cd-mono3 binding VHH. Titer of Llama Serum against HTRA1 cd (Trimer) previous to building library (a), ELISA of Fc fusion KV07-Fc against HTRA1 cd (Trimer) and HTRA1 cd-mono3 (Monomer)(b), Activity measurement of HTRA1 cd (Trimer) with addition of KV07-Fc (c) and activity measurement of HTRA1 cd-mono3 (Monomer) with addition of KV07-Fc (d). Cleavage of fluorescence quenched substrate H2Opt-K was recorded over time in duplicates. Only every second data point is shown.

5.3. Screening of a Combinatorial McoTI-II Library

The screening of the library of VHH variants from an immunized llama only revealed one characterized single clone that recognized the monomeric HTRA1 variant, albeit with low affinity. Since no inhibition of proteolytic activity was observed, we concluded that its binding site does not overlap with the active-site. In an effort to obtain inhibitors of HTRA1 proteolytic activity, a library of variants derived from the cystine-knot miniprotein McoTI-II was screened using the same display and screening format as described in the previous chapter.

To this end, a miniprotein library was used that was successfully applied previously to the isolation of binders against several targets[129, 310]. In this library, the protease inhibitor loop that consists of six residues was fully randomized for all natural occurring amino acids except cysteine with an equal distribution (figure 8). Due to the SlonoMax™ technology it is possible to generate different ratios of mutations on different positions of a protein. Thus the rims of the inhibitor loop were randomized with 50 % frequency, while 50 % were kept with wild-type codon. The fourth and last loop containing five residues was randomized by only 10 % frequency. Two further exposed positions in loop two were changed by 50 % frequency. The combinatorial library was amplified by PCR with addition of homologous regions for recombination in cell surface presentation vector pCT resulting in a library diversity of 2.4×10^8 clones which was determined by serial dilutions on cultural plates[129]. Predicted

structure and primary sequence with a color-coded randomization are shown in figure 8 in section 2.2.4.

5.3.1. Screening of the McoTI-II Library

For isolation of McoTI-II derived molecules binding HTRA1 cd-mono3 the screening procedure was performed as described for VHH molecules (4.2.2). In this enrichment process labeling of myc-tag and HTRA1 cd-mono3 was not alternated during the successive rounds as it was performed for VHH library. Thus for all rounds of enrichment the FITC labeled protease was used with additional staining of myc-tag by biotinylated anti-myc antibody and streptavidin-allophycocyanin conjugate. The histograms of the sorting rounds are shown in figure 22. In the first three rounds the target concentration was kept at 1 µM. $3x10^8$ cells were analyzed in the first round and the gate for sorting covered 0.5 % of total events. For each round a resort was performed, resulting for the first round in 8.9 % of cells in the sorting gate. In the second round approximately $5.3x10^7$ cells were analyzed and 1.2 % of cells were isolated. The resort resulted in an accumulation of cells in the sorting gate of 25.2 %. In the third round 3.2 % of cells were isolated and enriched to 42.9 % of the cells in the sorting gate after resort. In the fourth round, the target concentration was decreased to 100 nM resulting in 1.2 % of isolated cells with 30.8 % positive cells in the resort. A fifth round with 40 nM target concentration was finally executed which resulted in a cell population that displayed miniprotein expression (shown by myc-tag/SAPC labeling), but no target labeling (results not shown).
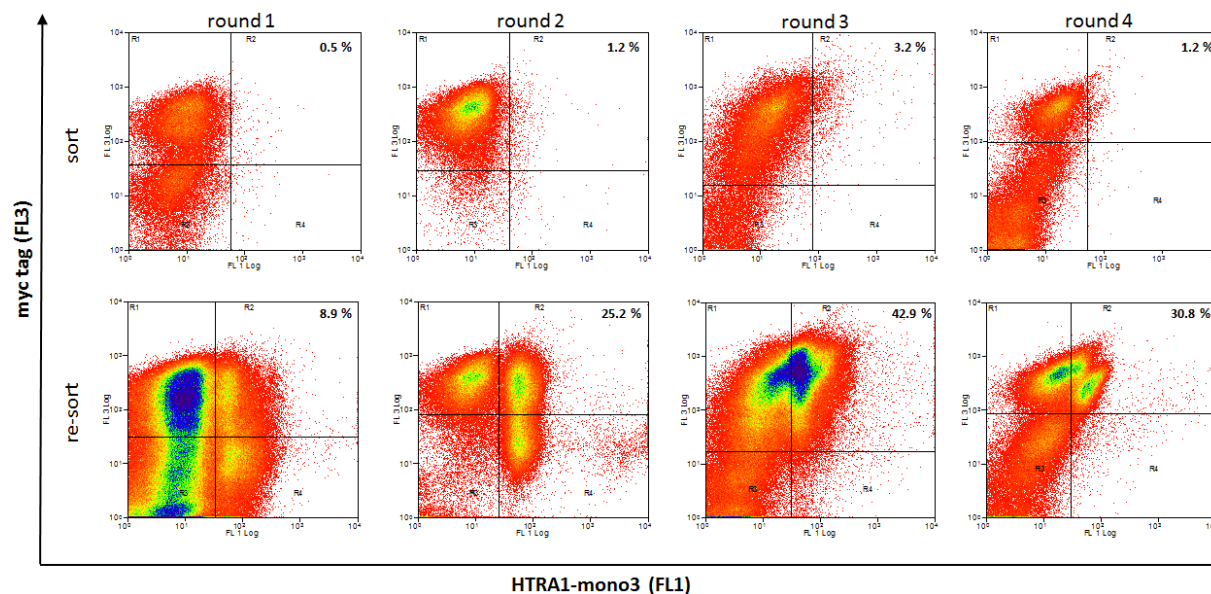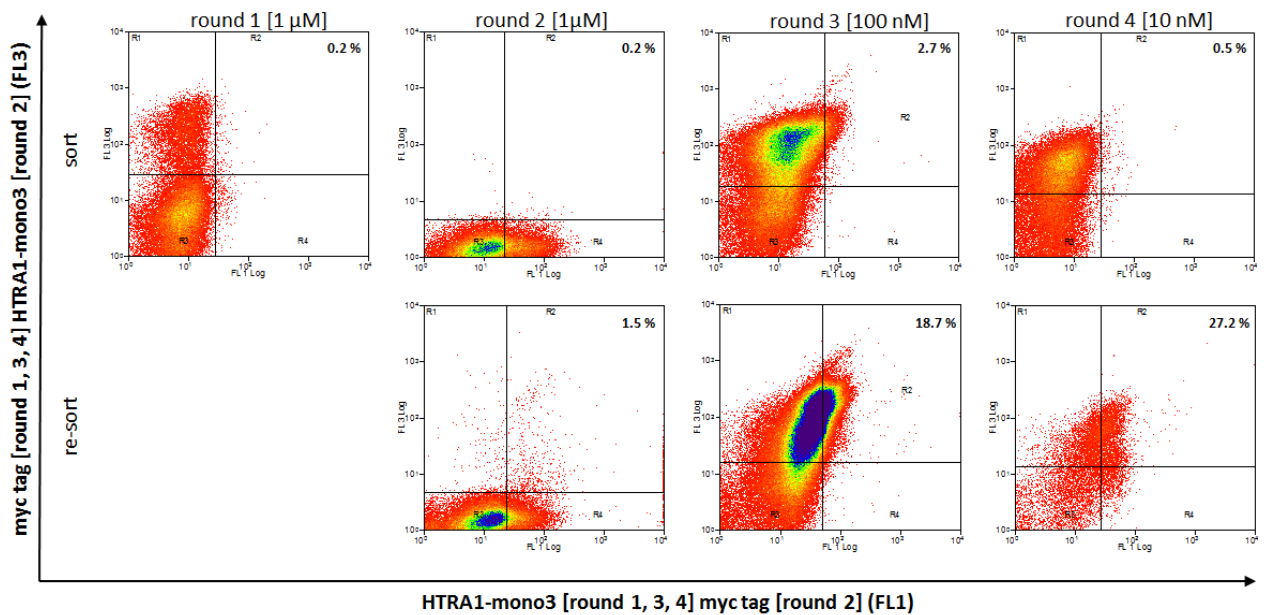

Figure 22 Histograms of enrichment of HTRA1 cd-mono3 binding cells presenting McoTI-II derived library. Sorting rounds 1-4 (top) and corresponding resorts (bottom). FL1 channel for HTRA1 cd-mono3 on the x-axis and FL3 channel for myc-tag on the y-axis. Gates for sorted cells are indicated by percentage of events that were isolated.

Due to the negative result of the fifth round, 10 clones of round four were randomly chosen. After induction of gene expression by cell incubation in galactose containing media, cells were double labeled for detection of full-length presentation by myc-tag and binding of HTRA1 cd-mono3. All clones showed target binding as well as a myc-tag presentation (results not shown). DNA sequences of these clones revealed that all 10 analyzed clones were identical. The unique sequence is shown in figure 23. The isolated McoTI-II derived molecule, called KS01, contains four aromatic amino acids out of six residues in the inhibitor loop. Its amino-terminal rim region of three residues is completely changed by two large aliphatic residues separated by threonine. All further randomized positions remained unchanged.

```
wild-type|ocMcoTI-wt      SGVCPKILKKCRRDSDCPGACICRGNGYCGS
KS01 |rd4|ocMcoTI-SloII   ITLCFYSFWECRRDSDCPGACICRGNGYCGS
```

Figure 23 Amino acid sequence alignment of HTRA1 cd-mono3 binding McoTI-II derived molecule KS01 isolated by FACS. Loop 1 with 100 % randomization is highlighted in black, fourth loop and two positions in the second loop with 10 % randomization are highlighted in light grey. Flanking regions of loop 1 with 50 % randomization are highlighted in dim grey.

5.3.2. Characterization of Isolated McoTI-II Derived Molecule

For determination of the affinity of KS01 an affinity titration was executed (4.2.5). As for isolated HTRA1 cd-mono3 binding VHH molecules (5.2.3), a single clone was stained for myc-tag and decreasing concentrations of FITC labeled target protease. The plot in Appendix A shows relative fluorescence signal against protease concentration. The transition point indicated an equilibrium dissociation constant (K_D) of 650 nM for KS01. The results of affinity titration of all isolated molecules in this work are summed up in table 1 in section 5.4.4.

Additionally cells presenting KS01 were stained with 10 µM fluorescein labeled HTRA1 cd, HTRA1 cd+PDZ and HTRA1 cd-mono3 as well as unlabeled cells as negative control. Interestingly, only HTRA1 cd-mono3 showed KS01 binding. The merged histograms are shown in figure 24d.
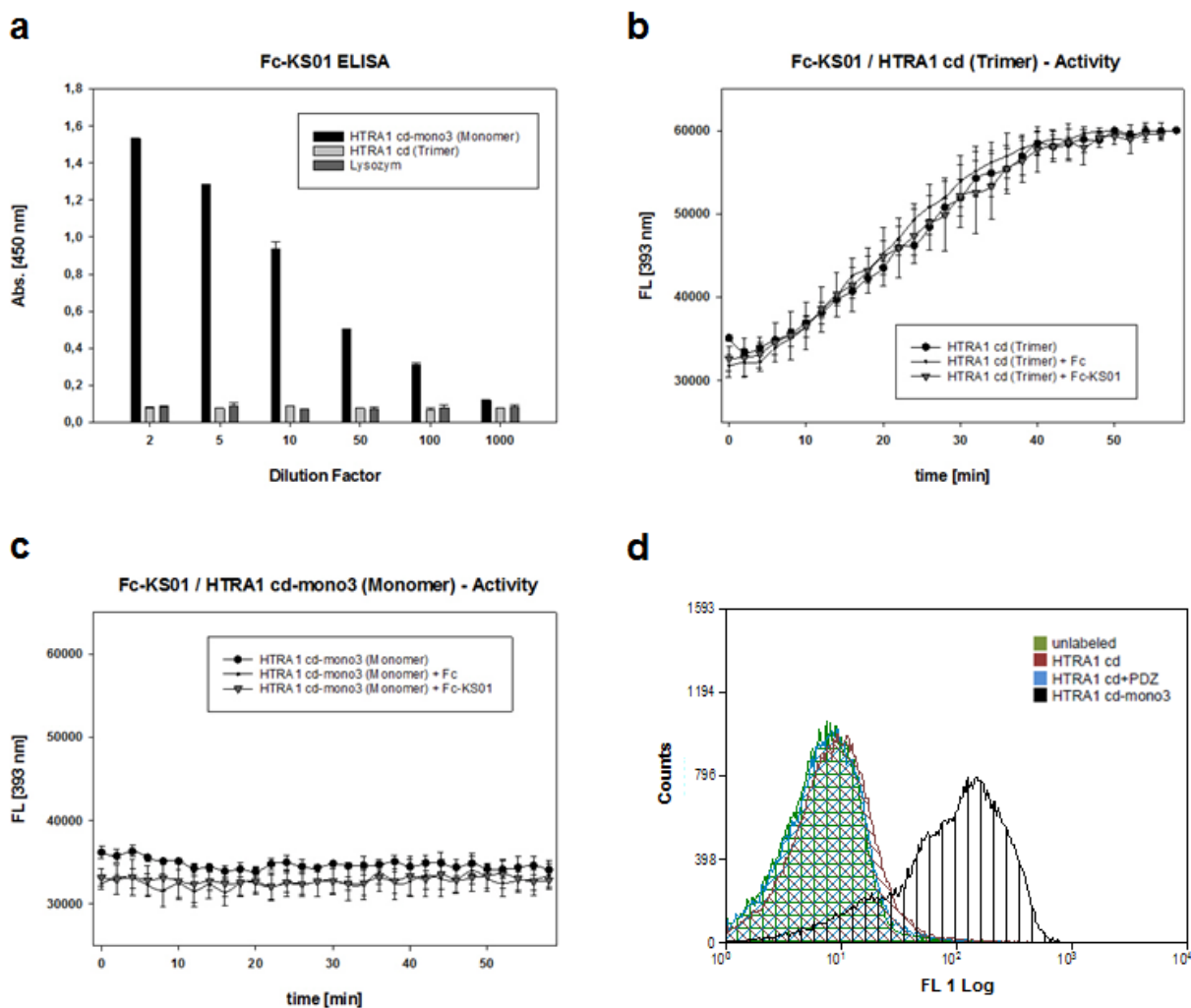
Figure 24 Analysis of HTRA1 cd-mono3 binding McoTI-II derived molecule KS01. ELISA of Fc fusion KS01-Fc against HTRA1variants (a), Activity measurement of HTRA1 cd (Trimer) with addition of KS01-Fc (b) and activity measurement of HTRA1 cd-mono3 (Monomer) with addition of KS01-Fc (c). Cleavage of fluorescence quenched substrate H2Opt-K was recorded over time in duplicates. Only every second data point is shown. Histogram of presented KS01 on the yeast surface labeled with HTRA1 cd-mono3 (black), HTRA1 cd (red), HTRA1 cd+PDZ (blue) and unlabeled (green). Relative fluorescence intensity is on the x-axis and counts are on the y-axis (d).

Finally, isolated KS01 was produced as Fc fusion protein in HEK293 cells as described in detail in section 5.5.2 of this work.

For functional characterization, an ELISA was performed with immobilized HTRA1 cd trimeric fraction and HTRA1 cd-mono3 monomeric fraction. In the next step cavities were incubated with serial dilutions of cell culture supernatant from 1:2-1:1000. The chart is shown in figure 24a. As found for the cell surface exposed KS01, only monomeric variant is bound by the Fc fusion of KS01 in a concentration-dependent manner. HTRA1 cd trimeric fraction and the negative control showed no signal, even at highest KS01-Fc concentration.

Finally, an activity measurement of HTRA1 cd trimeric fraction in presence of purified KS01-Fc was carried out (Figure 24b). As negative control wild type ocMcoTI-II fused to Fc was used. Conditions were the same as for determination of activity of HTRA1 variants described in section 5.1.5 of this work (0.625 µM protease; 12.6 µM substrate). Concentration of both Fc fusion molecules was 14 µM each. No influence on activity of HTRA1 cd was observed in presence of KS01-Fc.

Analogous to VHH molecule KV07, the isolated KS01 selectively binds HTRA1 cd-mono3, but not HTRA1 cd as observed by flow cytometric analyses with cells presenting KS01 (Figure 24d). According to this, an activity measurement of HTRA1 cd-mono3 monomeric fraction in presence of purified KS01-Fc was carried out (Figure 24c). Conditions were the same as for HTRA1 cd trimeric fractions. In this assay, it was investigated whether KS01 binding allosterically activates HTRA1. For the substrate and protease concentration chosen no enzyme activity was observed (5.1.5). Hence, as for the isolated VHH variant KV07 no activation of HTRA1 was observed.

5.4. Screening of a Synthetic vNAR Library Followed by Affinity Maturation

Another interesting scaffold for generating target-specific binders is the antigen binding domain of single chain antibodies of cartilaginous fish (vNAR). This binding unit shares structural similarity with mammalian antibodies like VHH domains, although they are only comprised of CDR1 and CDR3. The library was assembled by using the whole framework of a non-immunized bamboo shark[272]. After reverse transcription of mRNA CDR3 composed of 12 residues was randomized synthetically by codon-based oligonucleotide mixtures. The 12 residue CDR3 length corresponds to the most frequent loop length found in bamboo sharks as revealed by next-generation sequencing of the vNAR repertoire of three non-immunized bamboo sharks[272, 311]. After introducing randomization in CDR3 the DNA construct was extended by PCR to the full length of the vNAR gene and additional nucleotides were added for homologous recombination in yeast. Transformation of *S cerevisiae* EBY100 together with the expression plasmid resulted in $2x10^8$ independent yeast clones. This library was successfully used by Zielonka *et al.* for the isolation of binders against several targets[272, 311]. Since only a single loop is randomized, low to medium affinity binders in the triple digit nanomolar to micromolar range are commonly obtained. Hence, for the isolation of high affinity antibodies the population of binders obtained from library screening is further randomized in CDR1 or another neighboring loop HV2 in an effort of affinity maturation and clones with elevated affinity are subsequently isolated by several rounds of FACS screening with steadily decreasing target protein concentrations[312, 313].

5.4.1. Screening of the Synthetic vNAR Library

For isolation of vNAR-based molecules binding to HTRA1 cd-mono3 the screening procedure was performed as previously described for VHH and McoTI-II derived molecules. In the first round 1 µM FITC labeled target was used for staining in combination with anti-myc antibody, biotinylated secondary antibody and SAPC. $2x10^8$ cells were analyzed and the sorting gate covered 0.2 % of cells (figure 25). A resort was not performed after the initial round. For the second round induced yeast cells were alternatively labeled (as described before 4.2.2) resulting in an accumulation of 0.2 % of the cell population in the sorting window. The resort of this population indicated a successful enrichment (1.5 %). In the third and fourth round staining was switched back to FITC labeled target. The target concentration in these rounds was successively decreased to 100 nM and 10 nM, respectively. About 2.7 % of analyzed cells were isolated in the third round and the resort revealed 18.7 % positive cells. In the fourth round 0.5 % and in the successive resort about 27.2 % of cells were isolated.

Figure 25 Histograms of enrichment of HTRA1 cd-mono3 binding cells presenting CDR3 randomized library of vNAR scaffold. Sorting rounds 1-4 (top) and corresponding resorts (bottom). FL1 channel for HTRA1 cd-mono3 (round 1, 3 and 4) and myc-tag (round 2) on the x-axis. FL3 channel for myc-tag (round 1, 3 and 4) and HTRA1 cd-mono3 (round 2) on the y-axis. Gates for sorted cells are indicated by percentage of events that were isolated.

Fifteen single clones after the fourth round were analyzed by staining for surface presentation and target binding as described previously for VHH and McoTI-II based scaffolds. Of these, thirteen revealed HTRA1 cd-mono3 binding (Results not shown). Sequences of these clones were obtained from analysis of DNA sequencing after previous amplification by PCR of the respective vNAR coding sequence. Six different variants were found, while clone K10 appeared five times, K03 was found twice as was K07 and K09. Clone K13 and K14 were only found once in the thirteen analyzed sequences. Sequences are shown in figure 26. Besides different CDR3 regions also different framework residues were observed. Sequences were all individual over all twelve residues allowing no deviation of a consensus sequence regarding HTRA1 cd-mono3 binding. In position 2 large aliphatic residues were present in four individual clones. In position 4 an asparagine was observed 3 times. In position 6 there was two times a negatively charged aspartic acid as well as two times a positively charged lysine present. Further on position 3, 7, 10 and 12 aromatic amino acid residues were observed. Clones K09 and K10 share the sequence motif "HM" in position 7-8. Additionally K03 and K14 show motif "TW" in position 11-12 and position 10-11, respectively. Motif "NT" was also found twice in position 4-5 of K09 and position 9-10 of K14. Besides these small stretches of sequences identity no significant similarities were found.

Figure 26 Alignment of unique amino acid sequences of HTRA1 cd-mono3 binding CDR3 randomized vNAR molecules isolated by FACS. Clone name, selection round, randomized region and occurrence are designated for each clone. Framework mutations are indicated in red, CDR1 is indicated in dim grey, HV2 in grey and CDR3 in black.

Cells from all unique clones except K14 were stained with 10 µM fluorescein labeled HTRA1 cd, HTRA1 cd+PDZ and HTRA1 cd-mono3, respectively. Cells were additionally labeled and gated for myc-tag presentation using primary and secondary antibodies in combination with SAPC. Merged histograms of myc-tag gated cell populations are shown in figure 27. All analyzed clones showed a clear shift in fluorescence intensity for all different targets compared with negative controls. Cell populations of clones K03, K10 and K13 showed the highest mean fluorescence when labeled with HTRA1 cd-mono3 while the native variants displayed lower levels of cell staining. Interestingly, the mean fluorescence for K09 is the highest for HTRA1 cd, while HTRA1 cd-mono3 and HTRA1 cd+PDZ display the same level of cell staining. For K07 the mean fluorescence is similar for all HTRA1 variants. Afterwards an affinity titration was performed. Results are described in section 5.4.4.
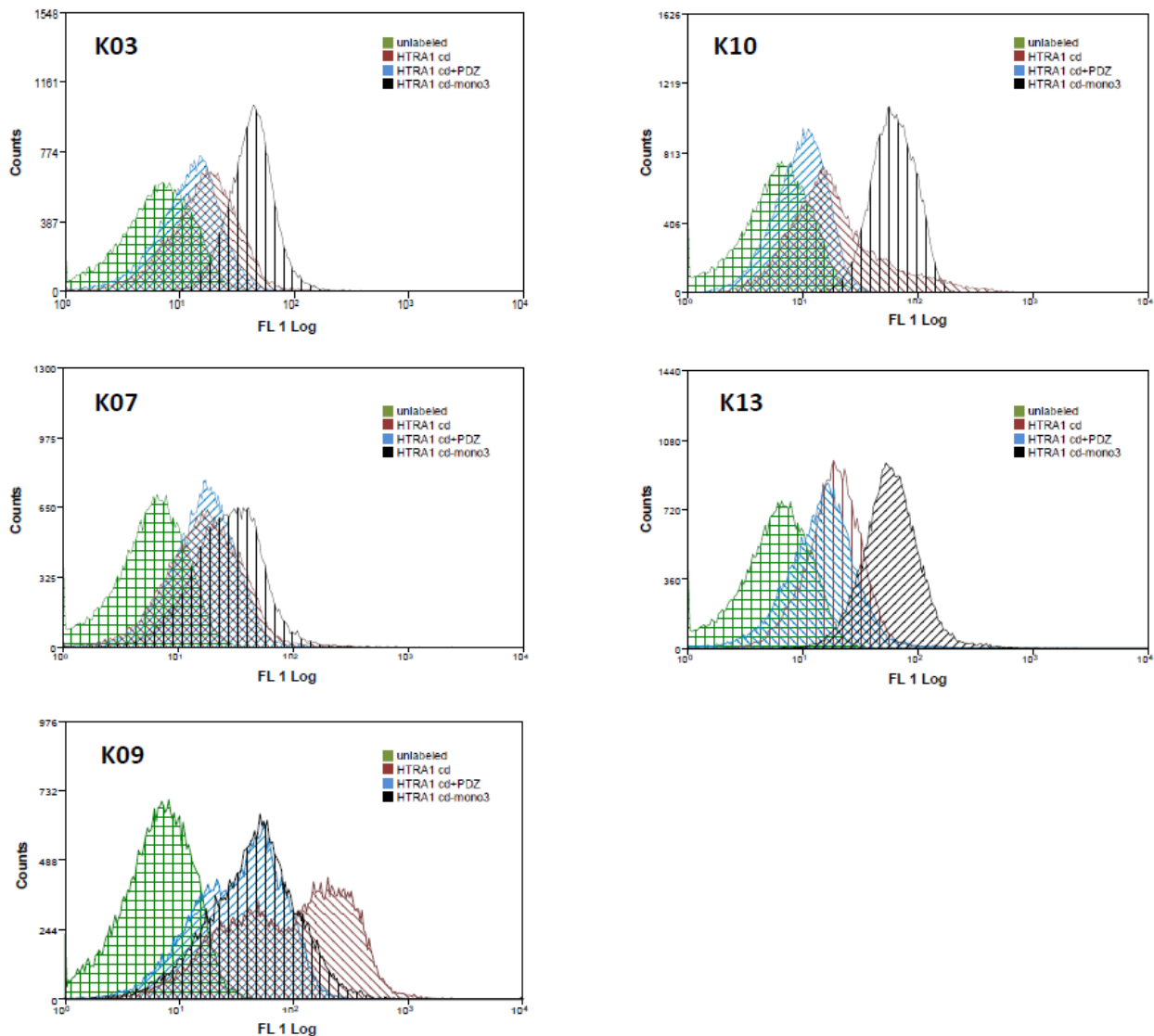
Figure 27 Histograms of clone K03, K07, K09, K10 and K13 labeled with HTRA1 cd-mono3 (black), HTRA1 cd (red), HTRA1 cd+PDZ (blue) and unlabeled (green). Relative fluorescence intensity is on the x-axis and counts are on the y-axis.

5.4.2. Affinity Maturation of CDR1 and HV2 and Screening

The total repertoire of cells from the third sorting round was used as template for randomization of CDR1 and HV2, respectively aimed at isolating clones with enhanced affinity. The naturally observed lengths of these regions were maintained with five residues each. For generation of the HV2 library the motif "ATKKA" was chosen for CDR1, as it was found in the initial library of immunized shark, to maintain a stable fold. Further the identified framework variability of the amino-terminus was kept by

using a set of different oligonucleotides, to preserve the natural properties of the library. Both sub-libraries covered a low diversity of about 50,000 independent clones.

The enrichment of CDR1 and HV2 sub-libraries were performed by labeling and sorting as described previously (4.2.2) with the modification that in each round FITC-labeled HTRA1 cd-mono3 was used for cell staining. In the first round, the target concentration was kept at 100 nM as in the third round of CDR3 screening which was used for sub-library construction. This strategy was chosen for getting rid of vNAR molecules that could not be displayed anymore in full-length as well as those that lost their ability to bind HTRA1 cd-mono3 by misfolding caused by newly introduced amino acids. Approximately 10^7 cells were screened for each sub-library.

For the enrichment of CDR1 matured clones the gate for cells sorted out was selected to cover 1.1 % of cells. In the resort the dual labeled population made up about 15.1 % of cells. In a second round target concentration was dropped to 10 nM. In this round the gate for cells sorted out was selected to cover 4.3 % of cells. In the resort the population made up about 18.8 % of cells. The histograms of the CDR1 maturation screening are shown in figure 28a.

For the enrichment of HV2 matured clones the gate for cells sorted out was selected to cover 1.4 % of cells. In the resort the dual labeled population made up about 56.8 % of cells. In a second round target concentration was dropped to 10 nM, as it was done for CDR1 sub-library. In this round the gate for cells sorted out was selected to cover 5.2 % of cells. In the resort the population made up about 30.4 % of cells. The histograms of the CDR1 maturation screening are shown in figure 28b.
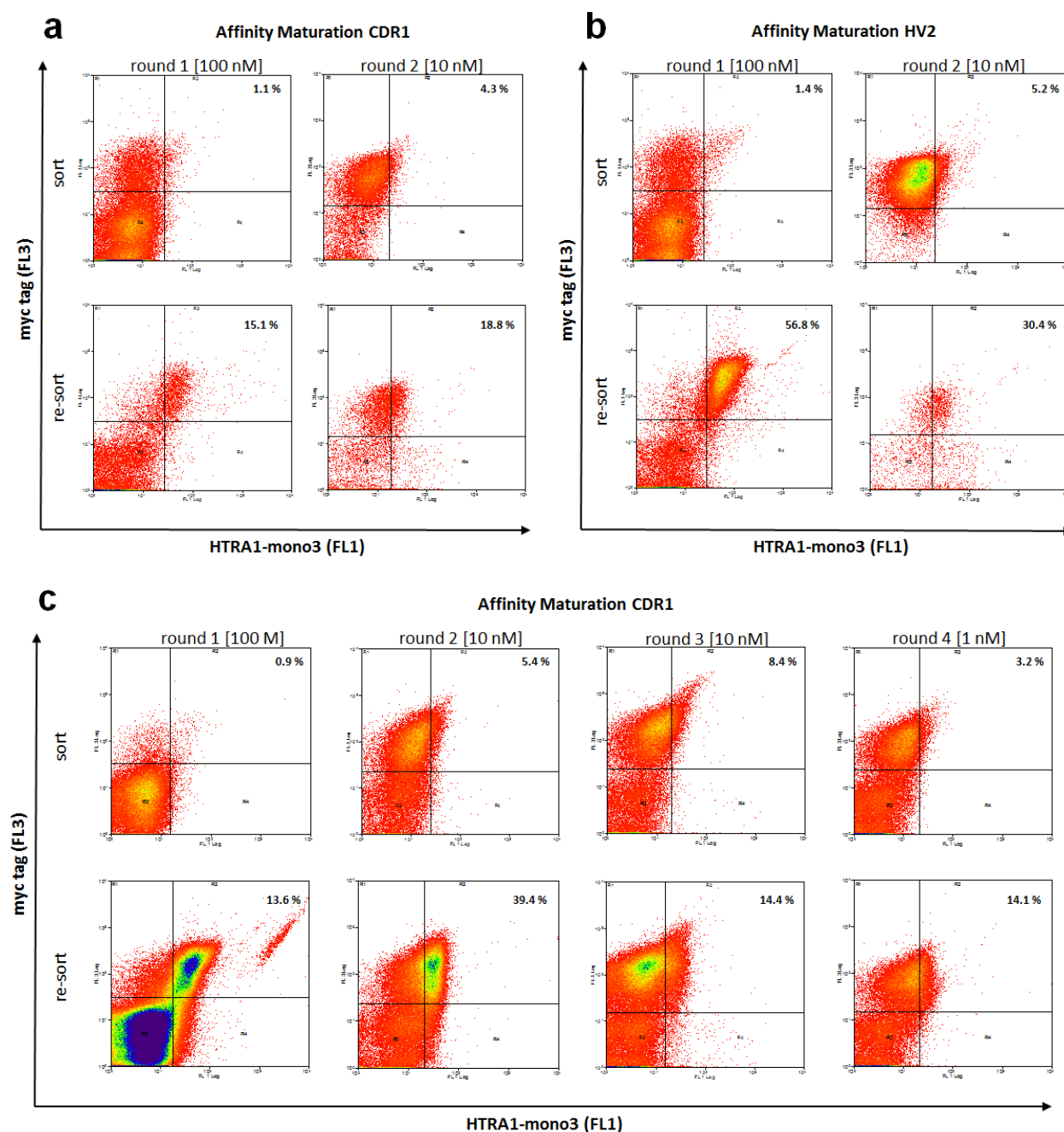
Figure 28 Histograms of enrichment of HTRA1 cd-mono3 binding cells presenting matured CDR1 (a) and HV2 (b) vNAR scaffolds. Histograms for cells presenting CDR1 matured vNAR molecules binding HTRA1 cd-mono3 previously matured in HV2 (c). Sorting rounds 1 and 2 (top) and corresponding resorts (bottom). FL1 channel for HTRA1 cd-mono3 is shown on the x-axis. FL3 channel for myc-tag is shown on the y-axis. Gates for sorted cells are indicated by percentage of events that were isolated.

After the second sorting round five clones of each affinity maturation were tested for presentation of full-length construct as well as for HTRA1 cd-mono3 binding. For CDR1 and HV2 four out of five clones displayed target binding. Positive clones KH01-03 and KH05 for HV2 and KC01-03 and KC05 for CDR1 were amplified by PCR and sequenced. Sequences of CDR1 matured clones are shown in figure 29a. The CDR3 of CDR1 matured clones KC01, KC02 and KC05 are derived from clone K07. In KC03 CDR3 sequence of K14 was found. No consensus sequence in CDR1 could be derived. Interestingly the framework of the three molecules derived from K07 showed single exchanges indicating that they are not derived from the same parental molecule. Additionally the motif "AYA" that is present in CDR1 of KC02 in position 3-5 is also found in CDR1 of HV2 matured clone KH05 at the same position. "YA" was additionally found in CDR1 of KH01 also in position 4-5. Although CDR1

was not randomized for HV2 sub-library the oligonucleotides for elongation introduced different residues derived from the naïve repertoire.

a

```
KC01|rd2|vNAR-CDR3-CDR1|1/4    MAARLEQTPTTTTKEAGESLTINCVLKTPQLWLGSTYWYFTKKGAT
KC02|rd2|vNAR-CDR3-CDR1|1/4    MAARLEQTPTTTTKEAGESLTINCVLKHWAYALGSTYWYFTKKGAT
KC03|rd2|vNAR-CDR3-CDR1|1/4    MAARLEQTPTTTTKEAGESLTINCVLKVKEQALGSTYWYFTKKGAT
KC05|rd2|vNAR-CDR3-CDR1|1/4    MAARLEQTPTTTTKEAGESLTINCVLKFGNWILGSTYWYFTKKGAT
```

```
KKASLSTGGRYSDTKNTASKSFSLRISDLRVEDSGTYHCEAMVVPYDWGAIGMIEGGGTIVTVKGS
KKASLSPGGRYSDTKNTASKSFSLRISDLRVEDSGTYHCEAMVVPYDWGAIGMIEGGGTLLTVKGS
KKASLSTGGRYSDTKNTASKSFSLRISDLRVEDSGTYHCEARHKFKTYLTRPIIEGGGTLLTVNGS
KEASLSTGGRYSDTKNTASKSFSLRISDLRVEDSGTYHCEAMVVPYDWGAIGMIEGGGTILTVKGS
```

b

```
KH01|rd2|vNAR-CDR3-HV2|1/4    MAARLEQTPTTTTKEAGESLTINCVLKGSGYALGITYWYFTKKGQTW
KH02|rd2|vNAR-CDR3-HV2|1/4    MAARLEQTPTTTTKEAGESLTINCVLKGSGYVLGRTYWYFTKKGHRH
KH03|rd2|vNAR-CDR3-HV2|1/4    MAARLEQTPTTTTKEAGESLTINCVLKGSGYGLGSTYWYFTKKGNWQ
KH05|rd2|vNAR-CDR3-HV2|1/4    MAARLEQTPTTTTKEAGESLTINCVLKGSAYALGKTYWYFTKKGIPH
```

```
FQSLSTGGRYSDTKNTASKSFSLRISDLRVEDSGTYHCEAMVVPYDWGAIGMIEGGGTTLTVKGS
MISLSTGGRYSDTKNTASKSFSLRISDLRVEDSGTYHCEAMVVPYDWGAIGMIEGGGTTLTVKGS
SGSLSTGGRYSDTKNTASKSFSLRISDLRVEDSGTYHCEAMVVPYDWGAIGMIEGGGTILTVNGS
WKSLSTGGRYSDTKNTASKSFSLRISDLRVEDSGTYHCEAMVVPYDWGAIGMIEGGGTLVTVKGS
```

c

```
KHC01|rd4|vNAR-CDR3-HV2-CDR1|1/10    MAARLEQTPTTTTKEAGESLTINCVLKEWQLYLGSTYWYF
KHC02|rd4|vNAR-CDR3-HV2-CDR1|1/10    MAARLEQTPTTTTKEAGESLTINCVLKQPGYYLGSTYWYF
KHC03|rd4|vNAR-CDR3-HV2-CDR1|1/10    MAARLEQTPTTTTKEAGESLTINCVLKQHVVYLGSTYWYF
KHC04|rd4|vNAR-CDR3-HV2-CDR1|1/10    AAARLEQTPTTTTKEAGESLTINCVLKVYYVVLGSTYWYF
KHC06|rd4|vNAR-CDR3-HV2-CDR1|1/10    AAARLEQTPTTTTKEAGESLTINCVLKWPEVYLGSTYWYF
KHC07|rd4|vNAR-CDR3-HV2-CDR1|1/10    MAARLEQTPTTTTKEAGESLTINCVLKAPHIYLGSTYWYF
KHC08|rd4|vNAR-CDR3-HV2-CDR1|1/10    MAARLEQTPTTTTKEAGESLTINCVLKNKQSMLGSTYWYF
KHC11|rd4|vNAR-CDR3-HV2-CDR1|1/10    MAARLEQTPTTTTKEAGESLTINCVLKSERHILGSTYWYF
KHC12|rd4|vNAR-CDR3-HV2-CDR1|1/10    AAARLEQTPTTTTKEAGESLTINCVLKDGEWILGSTYWYF
```

```
TKKGDKSPQSLSTGGRYSDTKNTASKSFSLRISDLRVEDSGTYHCEAMVVPYDWGAIGMIEGGGTLVTVNGS
TKKGSNSPQSLSTGGRYSDTKNTASKSFSLRISDLRVEDSGTYHCEAMVVPYDWGAIGMIEGGGTLVTVKGS
TKKGSTVPMSLSTGGRYSDTKNTASKSFSLRISDLRVEDSGTYHCEAMVVPYDWGAIGMIEGGGTLLTVNGS
TKKGQEAAQSLSTGGRYSDTKNTASKSFSLRISDLRVEDSGTYHCEAMVVPYDWGAIGMIEGGGTLLTVKGS
TKKGQEAAQSLSTGGRYSDTKNTASKSFSLRISDLRVEDSGTYHCEAMVVPYDWGAIGMIEGGGTLVTVNGS
TKKGQEAAQSLSTGGRYSDTKNTASKSFSLRISDLRVEDSGTYHCEAMVVPYDWGAIGMIEGGGTLLTVNGS
TKKGBLEWQSLSTGGRYSDTKNTASKSFSLRISDLRVEDSGTYHCEAMVVPYDWGAIGMIEGGGTLLTVNGS
TKKGSMBPESLSTGGRYSDTKNTASKSFSLRISDLRVEDSGTYHCEAMVVPYDWGAIGMIEGGGTTVTVKGS
TKKGLDERWSLSTGGRYSDTKNTASKSFSLRISDLRVEDSGTYHCEAMVVPYDWGAIGMIEGGGTTLTVNGS
```

Figure 29 Alignment of amino acid sequences of CDR1 (a), HV2 (b) and HV2-CDR1 (c) matured HTRA1 cd-mono3 binding vNAR molecules isolated by FACS. Clone name, selection round, randomized region and occurrence are designated for each clone. Framework mutations are indicated in red, CDR1 is indicated in dim grey, HV2 in grey and CDR3 in black.

Sequences for CDR1 matured clones are shown in figure 29b. All of the KH clones were identical in their CDR3 sharing the sequence of K07 from enrichment previous to maturation as observed in three of four clones in HV2 maturation. KH01 and KH02 share the framework besides the naturally occurring framework reconstituted in CDR1, while KH03 and KH04 showed differences in their framework compared with KH01 and KH02 revealing that they are not derived from the same CDR3 clone as assumed for molecules from HV2 maturation. Moreover these clones have totally different residues at all five positions of HV2 resulting in no conserved position of any functionality delivered by **the amino acid side chains. Nevertheless motif "HW" found in KC02 in position 1**-2 is present in KH05 in position 3-**4. The motif "GNW" of KH03 using framework residue together with positio**n 1-2 of

CDR1 is also found in position 2-4 in KC05. Additionally motif "RH" in position 2-3 of KH02 was also found in position1-2 of CDR3 of clone KC03.

Unique clones were subjected to an affinity titration. Results are presented after the subsequent affinity maturation of HV2 matured clones in section 5.4.4.

5.4.3. Second Affinity Maturation of HV2 Matured Clones by CDR1 Randomization

In theory a binding resulting from three independent regions could be stronger than one mediated by two regions. This strategy is performed by nature in a single domain of an antibody due to the larger surface that could be covered. While for a mixture of vNAR clones matured in CDR1 it is technically difficult to mature a region between both CDR's by keeping the sequence both of CDR3 and of HV2, it is easily possible to apply the *in vitro* affinity maturation of CDR1 to the clones previously matured in CDR3 and HV2.

As initial population of clones for CDR1 maturation, cells isolated from round one of the HV2 maturation were used. Transformation of yeast cells resulted in a library size of 10^7 independent CDR1 matured clones. Four rounds of enrichment were performed. Yeast cells for the first round were labeled with relatively high concentration of 100 nM HTRA1 cd-mono3 aimed at isolating all clones binding target irrespective of their affinity. Histograms of sorting rounds are shown in figure 28c. In the first round 1.1 % of cells were sorted out followed by a resort confirming the efficiency with 15.1 % of cells being in the sorting window. In the next round concentration was dropped to 10 nM target concentration resulting in 5.4 % sorted cells and 39.4 % cells in the resort. Cells in the third round were labeled again with 10 nM HTRA1 cd-mono3. 8.4 % cells were isolated while 14.4 % were confirmed in the resort. In the fourth round target concentration was additionally dropped to 1 nM. 3.2 % of cells were enriched and 14.1 % were confirmed in a resort.

After the fourth round of enrichment twelve single clones were analyzed for HTRA1 cd-mono3 binding. Clones KHC01-08 and KHC11-12 were positive in HTRA1 cd-mono3 binding when labeled with 100 nM target, as well as in presentation of carboxyl-terminal myc-tag. DNA sequencing revealed nine unique clones while clone KHC04 appeared twice, as it was identical with KHC05. Sequences are shown in figure 29c. Interestingly, all analyzed clones shared the same CDR3 of clone K07 from enrichment previous to maturation. Clones KHC04, 06 and 07 contained identical HV2, but are unrelated with respect to their CDR1 sequence. Nevertheless these three clones show different framework mutations at the carboxyl-terminus making it conceivable that they did not derive from the same parental HV2 clone. Further, no examined clone contained a HV2 region that was observed after HV2 maturation.

With respect to the CDR1 sequence, the nine unique clones are all unique. Clone KHC01 has on position 3 and 4 identical residues as KC01, namely glutamine and lysine. KHC01 has in position 2 and 3 of CDR1 a tryptophan and a glutamine. These residues were found on the same positions at KH03 in HV2. KHC08 shows the motif NXQS in position 1-4 in CDR1. The same motif was found at the same positions in HV2 of KH03.

Conspicuously five clones carry a tyrosine on position 5 in CDR1 and six clones carry a glutamine on position 5 of HV2. These framework-flanking positions may have an impact on folding and stability for the whole vNAR molecule.

Due to the large sequence diversity of CDR1 and HV2 after 4 rounds despite the decrease of target concentration to 1 nM an additional round was performed. In this round a k_{off} screening was executed with incubation of yeast cells for 8 hours after labeling with 10 nM fluorescently labeled target in presence of 10 µM unlabeled target. The presented molecules releasing the labeled target in this time period will statistically bind an unlabeled target molecule next. This approach should result in the isolation of molecules with a low dissociation rate. 5.1 % cells were isolated and 13.9 % were confirmed in a resort (Results not shown). The ten clones analyzed were positive for target binding and DNA sequence analysis revealed that they were all identical clones, in detail KHC01 from previous round.

The unique clones of round 4 were subjected to an affinity titration. Results are described in following section 5.4.4.

5.4.4. Affinity Titration

For determination of the binding quality of different enriched vNAR molecules unique single clones were analyzed by affinity titration. Additionally it was investigated, whether the maturation procedure delivered higher affine vNAR molecules compared to isolated initial molecules. Therefore, single clones were labeled with decreasing concentrations of fluorescently labeled HTRA1-mono3 as described previously (4.2.5). After analysis fluorescence intensities were related to target concentration for determination of K_D, using a fitting procedure applied on sigma plot software[306]. Plots with acquired data and corresponding fitted curves for vNAR affinity titrations are shown in Appendix A.

vNAR molecules randomized in CDR3 after the fourth sorting round showed K_D values in the micromolar range. The highest K_D was observed from variant K07 with 24.5 µM while the best was observed from variant K03 and K13 with 1.3 µM each. The results are summed up in table 1.

Table 1 Summary of K_D values of isolated HTRA cd-mono3 binding molecules determined by affinity titration. For vNAR molecules parental clones for successive rounds of affinity maturation are indicated. Clone KHC04 is identical to KHC05.

scaffold	engineered region	clone	K_D [nM]	CDR3 clone	HV2 clone	occurrence
VHH	immunized repertoire	KV01	117 ± 52			6/10
		KV07	505 ± 302			4/10
McoTI-II	loop1, flanking regions, loop4	KS01	650 ± 206			10/10
vNAR	CDR3	K03	1,250 ± 158	-	-	2/13
		K07	24,476 ± 10,088	-	-	2/13
		K09	6,151 ± 5,619	-	-	2/13
		K10	8,292 ± 2,513	-	-	5/13
		K13	1,328 ± 187	-	-	1/13
		K14	n.d.	-	-	1/13
	CDR3 + HV2	KH01	469 ± 108	K07	-	1/4
		KH02	1,396 ± 501	K07	-	1/4
		KH03	1,757 ± 1,108	K07	-	1/4
		KH05	2,801 ± 1,170	K07	-	1/4
	CDR3 + CDR1	KC01	3,218 ± 889	K07	-	1/4
		KC02	550 ± 258	K07	-	1/4
		KC03	452 ± 241	K14	-	1/4
		KC05	290 ± 179	K07	-	1/4
	CDR3 + HV2 + CDR1	KHC01	53 ± 32	K07	new	1/10
		KHC02	n.d.	K07	new	1/10
		KHC03	65 ± 40	K07	new	1/10
		KHC04	34 ± 24	K07	new	2/10 (KHC05)
		KHC05	90 ± 64	K07	new	2/10 (KHC04)
		KHC06	47 ± 37	K07	new	1/10
		KHC07	n.d.	K07	new	1/10
		KHC08	65 ± 56	K07	new	1/10
		KHC11	55 ± 60	K07	new	1/10
		KHC12	60 ± 56	K07	new	1/10

After maturation of HV2 the variant KH01 displayed a K_D of 470 nM while the three further analyzed variants remain in the low single digit micromolar range. Considering that parental molecule of all four analyzed molecules is K07 with K_D of 24.5 µM all clones were successfully matured or enhanced in their affinity against HTRA1 cd-mono3, respectively.

For CDR3 clones matured in CDR1 the highest K_D was observed for variant KC01 with a value of 3.2 µM. The three further analyzed variants revealed K_D values in the triple digit nanomolar range with

the lowest K_D of 290 nM represented by KC05. Besides KC03, which is a derivative of K14, all other clones were derived again from clone K07.

In the maturation screening of double matured clones nine unique clones were titrated. Additionally KHC05, which is identical with KHC04, was titrated for controlling deviation of the method by two individual clones presenting the same vNAR molecule. Unfortunately clones KHC02 and KHC07 showed irregularities in concentration dependent binding or insufficient surface presentation for accurate K_D determination. The seven other clones revealed K_D values in the double digit nanomolar range. The lowest K_D was observed for clone KHC04 to be 34 nM. Nevertheless its twin clone KHC05 revealed slightly higher K_D of 90 nM. The last remaining clone after final k_{off} screening in round five was KHC01 with a K_D of 53 nM.

5.5. Expression and Characterization of HTRA1 Binding Molecules

For more detailed analysis of isolated HTRA1 binding molecules soluble expression was performed. To this end, DNA sequences of binding molecules were amplified by PCR from screening vector pCT using oligonucleotides that introduce target vector specific cloning sites. Due to experience from literature expression hosts were chosen specifically for the different classes of molecules. Isolated vNAR variants were expressed as maltose-binding protein (MBP) fusion in *E. coli*, while the McoTI-II derived molecule was expressed fused to Fc part of IgG in human embryonic kidney cells (HEK293). VHH variants were also cloned as Fc fusion protein because expression as MBP fusion was unsuccessful. Expression and purification is described in in detail in the following section 5.5.1.

5.5.1. Expression of vNAR Molecules in *E. coli*

For recombinant expression of vNAR molecules, sequences were amplified from screening vector using oligonucleotides introducing recognition sites for restriction enzymes *Acc*65I at 5' end and *Xba*I at 3' end for ligation into pMX vector as carboxyl-terminal fusion to MBP. Additionally a Tobacco-Edge-Virus (TEV) cleavage-site was introduced between both molecules as well as six histidine residues (His-Tag) at the carboxyl-terminus for purification using immobilized metal ion affinity chromatography (IMAC). Clones carrying correct insert were verified after ligation and transformation by sequencing. Isolated vector was transformed into strain BMH 71-18 for protein production in 1 L scale. Since fusion proteins are directed to the periplasm by an amino-terminal signal sequence, outer membrane of *E. coli* was enzymatically destructed by lysozyme. After isolation via IMAC the fusion proteins were cleaved with TEV protease and separated with size-exclusion chromatography (SEC). Plots of SEC are shown in figure 30. Only clones K07, K10, K13, K14 and KHC01 resulted in sufficient yields for further analysis under applied fermentation conditions (figure 30). The first elution peak corresponds to MBP and the second peak to vNAR. Only for K07 small amounts of uncleaved protein remained. Expression of K07, K10 and K14 resulted in high yields as indicated by absorption intensity above 200 mAU at 220 nm, while K13 showed only low amount with absorption intensity about 30 mAU. Extremely low amounts were isolated from KHC01.

Eluted fractions of each vNAR were pooled and concentrated by ultra-filtration to a final concentration of about 30-50 µM. Yields of purified vNARs were calculated by their OD_{280} in respect of their specific molar extinction coefficients. The yield for K07 was 12 mg, for K10 it was 7 mg, for K14 it was 4.5 mg and for K13 it was 1 mg. The yield for KHC01, with the lowest yield, was determined on 200 µg.
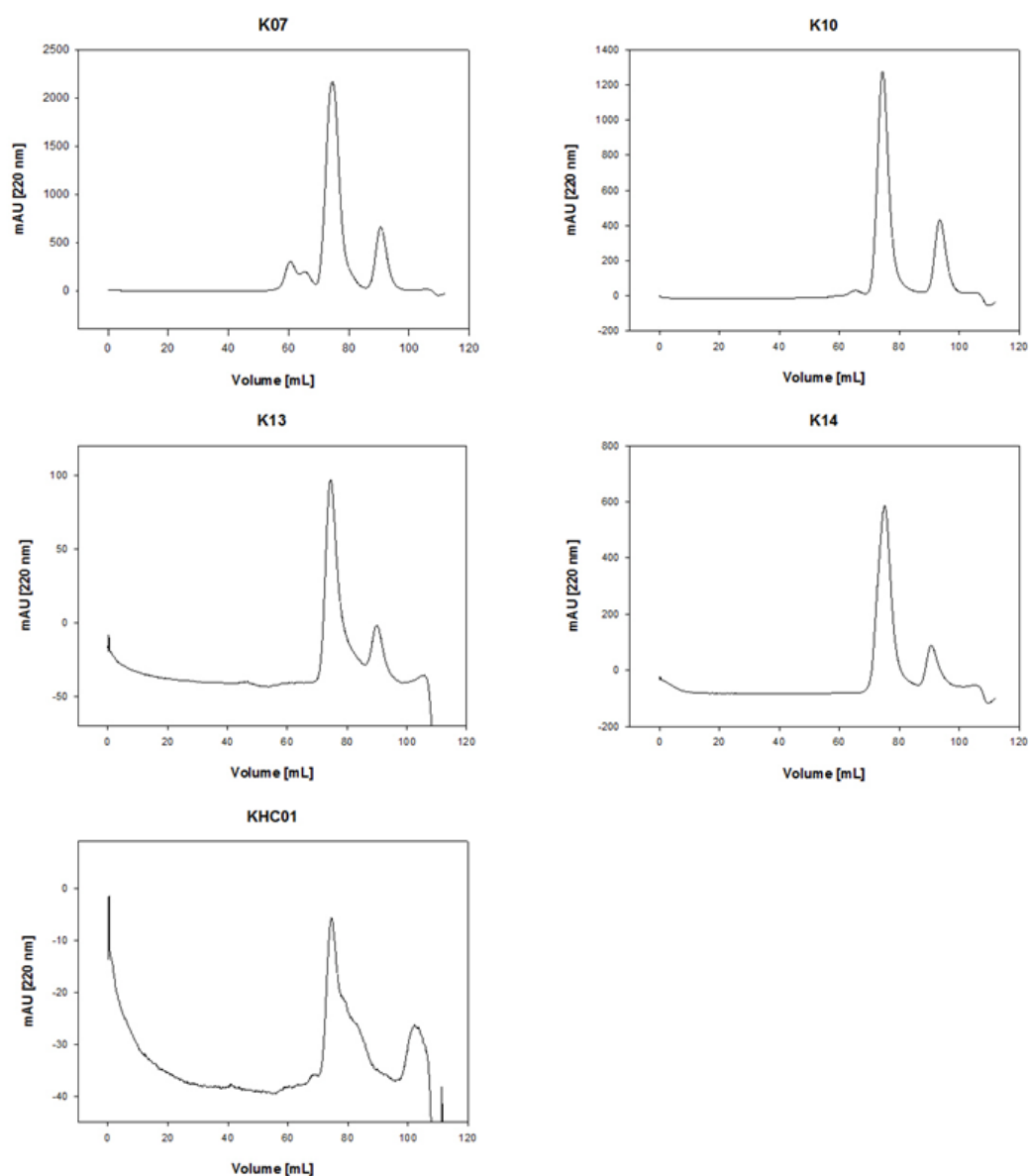
Figure 30 Plots of size-exclusion chromatography of successfully recombinant expressed vNAR-MBP fusion proteins after TEV cleavage on Superdex 75 16/60 column. First elution peak is MBP. Second elution peak is particular vNAR. Detection was at 220 nm wavelength.

5.5.2. Expression of VHH and McoTI-II Molecules in HEK Cells

For recombinant expression of VHH and McoTI-II based molecules, sequences were amplified from screening vector using oligonucleotides introducing recognition sites for restriction enzymes *Nhe*I at 5' end and *Apa*I at 3' end for ligation into pEXPR vector as amino-terminal fusion to Fc part of an IgG antibody. Clones carrying correct insert were verified after ligation and transformation by sequencing. HEK cells were transfected with high concentration of purified vector for protein production in Freestyle™ 293 media for 5 days. Fusion proteins were purified from cell culture supernatant using Protein A affinity chromatography.

For Fc part, KV07-Fc and McoTI-II wildtype sequence high yields were observed in purification by Protein A affinity column (figure 31). For McoTI-II-derived molecule KS01-Fc yield was significantly lower, but still sufficient for further analysis of influence on activity. Eluted fractions of each Fc fusion protein were pooled and concentrated by ultra-filtration until concentration of about 30-50 µM. Yields of purified Fc fusion proteins were calculated by their OD_{280} in respect of their specific molar extinction

coefficients. The yield for Fc-KV07 and Fc-McoTI were 6 mg each and for single Fc it was 2.5 mg. The yield for KS01-Fc, molecule with lowest yield, was determined to be 300 µg.
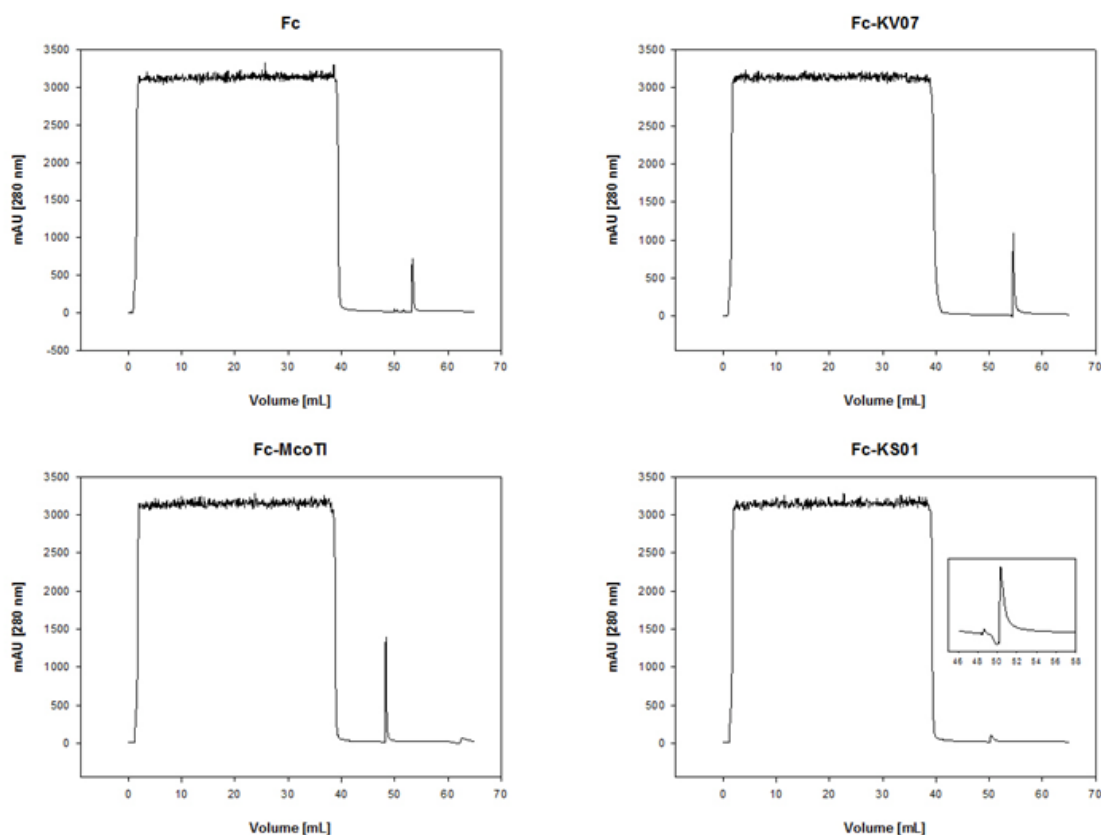
Figure 31 Plots of Protein A affinity chromatography of successfully recombinant expressed Fc and Fc fusion proteins of VHH and McoTI-II derived molecules. 0-40 ml is cell culture supernatant applied to column followed by elution with citric acid. Elution peak of KS01-Fc is additionally shown zoomed in (inside the plot). Detection was at 280 nm wavelength.

5.5.3. Melting Curves of Binding Molecules

For determination of thermal stability of recombinant expressed vNAR and Fc fusion proteins melting curve analysis was performed (4.1.2). Melting curves are shown in figure 32. The fusion protein KV07-Fc denatured at 59 °C and displayed higher stability compared to K07 lacking Fc (51.5 °C).

The thermal stability of vNAR molecules covers a broad range. Thus, K07 and K13 melted around 51 °C, while K10 and KHC01 revealed a melting temperature above 60 °C. Variant K14 displayed a melting temperature of 74.5 °C, although background noise is relatively high for this sample.

Nevertheless all molecules displayed thermal stability clearly above physiological temperature of humans of 36 °C. Additionally all molecules showed signal occurring through binding of SYPRO-Orange to hydrophobic patches. That means hydrophobic patches were exposed to solvent by increasing temperature, indicating that these were previously buried in a protein fold.
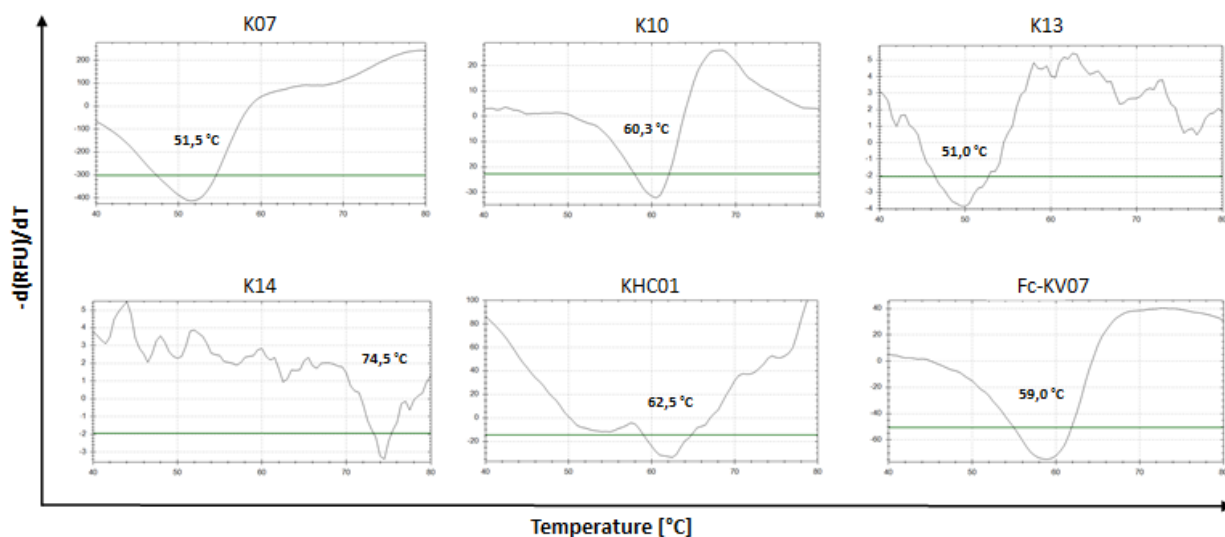
Figure 32 Melting curve analysis of recombinant expressed vNAR molecules and KV07-Fc using SYPRO-Orange. Melting temperatures were measured in duplicates and melting point values are indicated in the plots.

5.5.4. Influence on Activity of Soluble HTRA1 Binding vNAR Molecules

For the investigation, whether isolated vNAR molecules binding to HTRA1 cd-mono3 monomeric fraction modulate activity of HTRA1 variants, an activity measurement in presence of isolated molecules was carried out. To this end, activity of HTRA1 cd-mono3 monomeric fraction and HTRA1 cd (trimeric fraction) was measured in presence of vNAR molecules. As negative control an unrelated vNAR molecule isolated for binding target EpCAM[272] was used. Conditions were the same as for determination of activity of HTRA1 variants described in section 5.1.5 of this work (0.625 µM protease; 12.6 µM substrate). Concentration of vNAR molecules was 14 µM.

The plots of activity measurement for vNAR molecules are shown in figure 33. No influence on activity of HTRA1 cd (trimeric fraction) was observed in presence of K10, K13 and negative control (EpCAM vNAR) compared to absence of vNAR. For K14 a slight acceleration in substrate conversion was observed compared to controls. For K07, the clone with highest K_D of 24.5 µM of all isolated vNAR variants, acceleration of substrate conversion was significantly higher compared to EpCAM vNAR. Interestingly KHC01 with a K_D of 53 nM that shares CDR3 with K07 showed most enhanced acceleration of H2Opt-K conversion. The 500-fold lower K_D of KHC01 seems to correlate with stronger effect on protease activity.
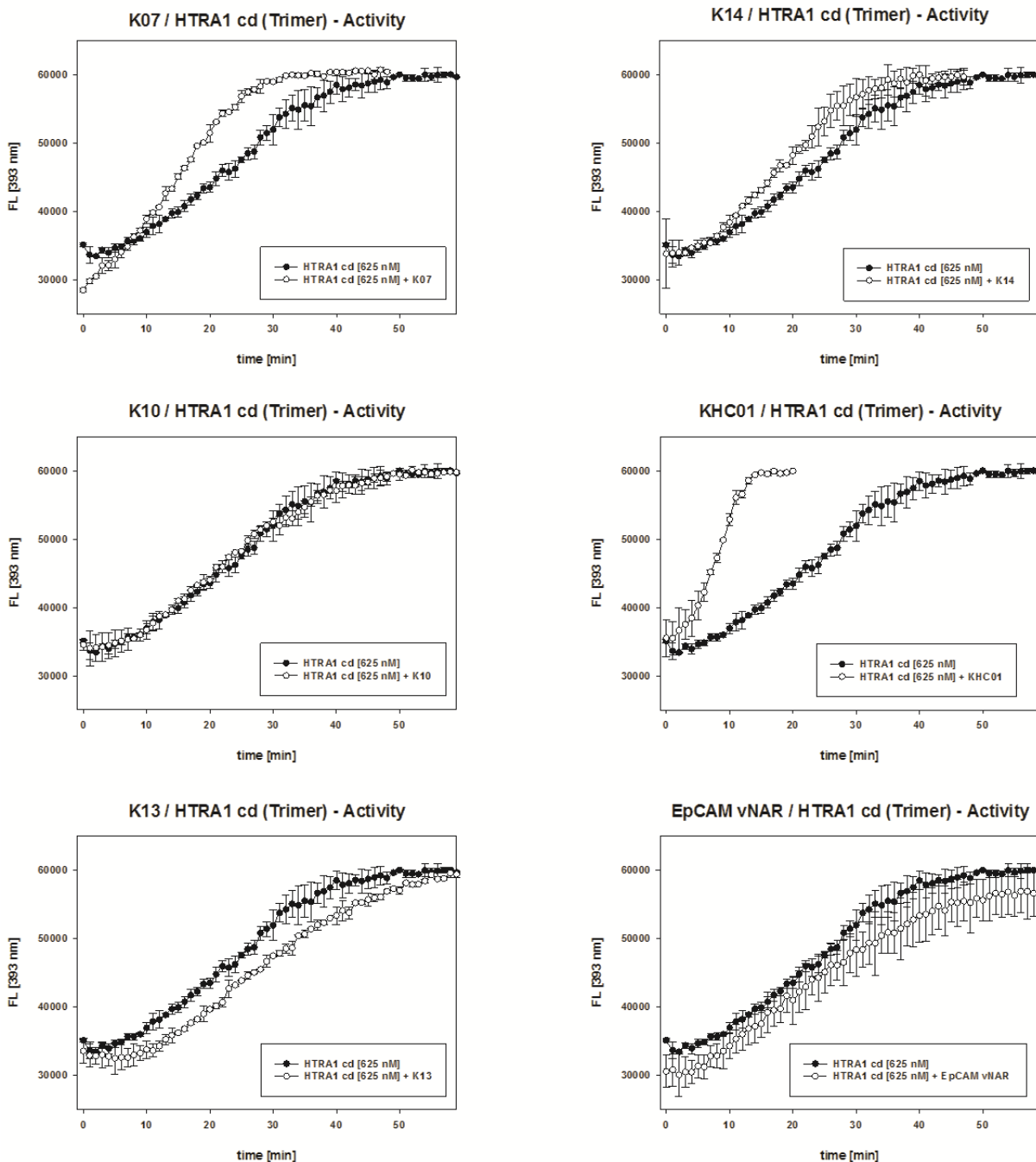
Figure 33 Activity measurement of HTRA1 cd (Trimer) in addition with HTRA1 cd-mono3 binding vNAR variants. Concentration of vNAR variants was adjusted to 14 µM. Cleavage of fluorescence quenched substrate H2Opt-K over time in duplicates.

For HTRA1 cd-mono3 (monomeric fraction) no influence on activity of vNAR variants was observed (results not shown). As for determination of activity of different HTRA1 variants and their gel filtration fractions no activity modulation of H2Opt-K cleavage was measured. Thus the activating effect of K07, K14 and KHC01 observed on HTRA1 cd trimeric fraction was not observed for the less active variant HTRA1 cd-mono3 (monomeric fraction).

For better comparison of activating or inhibiting effects all isolated and recombinantly expressed molecules were analyzed for initial velocity (v_0) of substrate cleavage. Initial velocity was calculated from slope of linear increase of substrate conversion by HTRA1 cd (trimeric fraction) in presence of different molecules as well as in absence. Measurement was in duplicates and standard deviation is indicated by bars. Value of HTRA1 cd trimeric fraction was set to 100 percent. The bar graph summarizing the initial velocities is shown in figure 34.
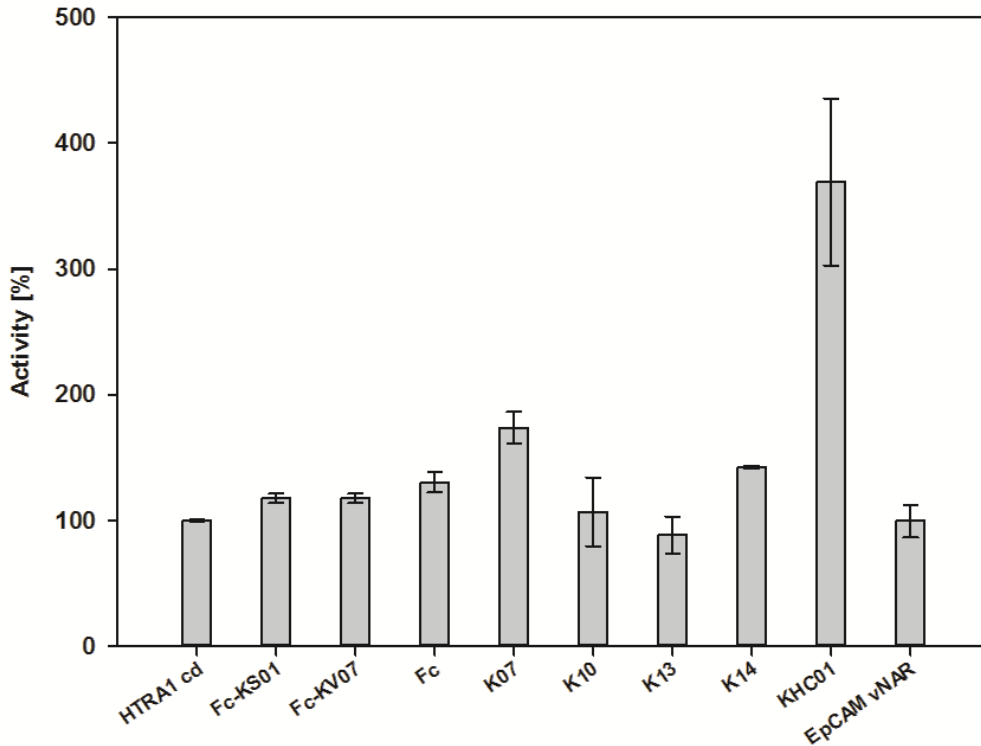
Figure 34 Activity of HTRA1 cd (Trimer) in presence of recombinant vNAR and Fc Fusion proteins of isolated vNAR, VHH and ocMcoTI-II derived molecules. V_0 was measured in double determination by cleavage of fluorescence quenched substrate H2Opt-K over time.

The results underline observations from activity measurements described above. K10 and K13 showed no shift in v_0 compared to HTRA1 cd or the presence of EpCAM vNAR. Values are comparable by considering standard deviation. K14 showed slightly enhanced v_0 (150 %). Likewise, observations for KHC01 and its parental molecule K07 were confirmed. K07 has almost double v_0 compared to negative control with an acceptable standard deviation. KHC01 has a v_0 of nearly 400 %. Although error is not small data underline clearly that KHC01 has strongest activating effect of all isolated and recombinantly expressed molecules.

Additionally VHH and McoTI-II based molecules were compared with respect to their initial velocity. KV07-Fc and KS01-Fc seem to show slight activation compared with HTRA1 cd without addition of a molecule. Although showing only small standard deviation the negative control which was only Fc part is in the same range of v_0. In conclusion no activation is mediated by isolated molecules KV07-Fc and KS01-Fc.

6. Discussion

6.1. Expression and Characterization of Different HTRA1 Variants

To reach the goal of isolating HTRA1 modulators/inhibitors, several characteristics of the protease have to be taken into consideration when performing evolutionary protein design. In a search for HTRA1 binders, the multi domain organization of HTRA1 enhances the likeliness for isolating molecules that do not bind the catalytic site but bind somewhere else. Additionally, multiple domains are more difficult in expression and handling. Fortunately a published method exists for expression of the HTRA1 catalytic domain and the catalytic domain in combination with a PDZ domain[31]. Moreover, presence of proteolytic activity could have an adverse effect, for example by auto-degradation or degradation of the effector peptidic molecule.

Further problems could be caused by the unpredictable oligomeric states of the protease, as it appeared as a major problem when starting this work. This lead to the concept of designing the target molecule in a more suitable format for the subsequent screening for binders and modulators of enzyme function. To this end, the human HTRA1 catalytic domain with and without addition of PDZ domain was expressed. The combination of both domains was chosen because it was shown that the PDZ domain has an influence on length of the proteolytic cleavage product while having no effect on activity[57]. Nevertheless this domain seems to be involved in substrate processing. Additionally it remains unclear whether the PDZ domain of HTRA1 is involved in higher oligomer formation as it is assumed for the *E. coli* homologue DegP[23, 314]. It was shown that HTRA1 activity can be deleted by mutating the active-site serine of the catalytic triad into an alanine[31, 315]. Nevertheless, the catalytic triad of all expressed variants in this work was kept intact. This was done since one initial objective of this work was the isolation of molecules that reduce or fully block enzyme activity. If residues were exchanged in the active-site of HTRA1, the chance to find competitive inhibitors would be reduced drastically.

The HTRA proteases are known to exist in various conformational states that relate to different enzyme activities. The residues of the catalytic triad of HTRA proteases are flexible in their orientation, resulting from localization on loops in the protease scaffold which have a high structural flexibility. There are four loops of HTRA1 that have been shown to change conformation when switching from the inactive into the active state. Thus, there are many epitopes conceivable that would have an effect on orientation of the catalytic triad with the consequence of retaining the active or inactive protease conformation[31].

Another unsolved problem for the experimental design was the presence of different oligomeric states of human HTRA1. A mixture of oligomeric states of various size, assembly and activity would lead to an unpredictable molar ratio of target to modulator, but more severe is the unpredictable accessibility for designed binding molecules to potential epitopes that may be surface exposed or not, depending on the oligomeric state.

Although no data is available on how higher oligomeric states are assembled, the crystal structures of HTRA1 provided clues that three key amino acid residues located in the catalytic domain are responsible for trimer formation[31]. This lead to the idea of generating a HTRA1 catalytic domain mutant, that does not assemble into trimers and possibly also not into higher oligomers. Two different variants were generated in this work by site-directed mutagenesis. For the first variant, HTRA1 cd-mono2, only two of the three key residues were replaced by alanine (Y169A, F171A), while the second variant HTRA1 cd-mono3 carried a third substitution (F278A).

All wild-type derived and the two generated HTRA1 variants showed good expression levels in *E. coli*. In the second purification step by SEC, different oligomeric states were observed and the corresponding protein fractions were collected separately. Fractions containing HTRA1 variants were verified by SDS-PAGE. Oligomeric states were derived from the molecular weight (MW) that correlates with the elution volume of the fractioned molecules and the calibration proteins. For the two variants with native catalytic domain only trimeric and higher oligomeric states were detected. According to the

calibrator proteins, the higher oligomers displayed a molecular weight above 600,000. For the two genetically engineered variants a third fraction was isolated by SEC. This additional fraction eluted at a volume corresponding to the size of a monomer with a molecular weight of 25,000. This fraction made up the largest amount for both mutated variants.

Although the monomeric state was successfully induced by mutations, trimeric and higher oligomeric states were still present. Thus, the introduced mutations did not completely prevent trimer formation, but shifted the equilibrium of monomeric versus oligomeric states towards the monomeric state. Monomeric HTRA1 was neither present in a preparation of the native HTRA1 catalytic domain, nor in a construct carrying the catalytic domain and the PDZ domain. Additionally, the ratio of monomeric state compared to oligomeric states was enhanced by the third mutation introduced in HTRA1 cd-mono3, which emphasizes the role of the three selected residues for trimer formation. Nevertheless, the monomeric variants still assemble to some extent into a higher oligomer, while trimeric states are almost but not completely absent for both variants. Thereby the ratio of higher oligomer and monomer is comparable to the ratio of higher oligomer and trimer of the non-engineered variants. Thus, the loss of trimerization by introduction of mutations has no influence on higher oligomer formation. Unfortunately, due to the residual presence of trimers it remains unclear, whether high molecular oligomers assemble from HTRA1 trimers or monomers.

Moreover, the collected data from size-exclusion chromatography provide no clue, whether the higher oligomeric state consists of a single ordered form of an oligomeric assembly or of a mixture of various oligomers differing in a number of monomers and assembly. It is unlikely that the truncated HTRA1 version used in this work forms cage-like structures as observed for *E. coli* DegP, since these are formed by PDZ domain contacts, which are absent in all examined variants except one[57, 316].

Another point that is crucial for engineering HTRA1 variants as target for isolation of modulators of HTRA1 activity is the stability and inter-convertability of isolated monomeric/oligomeric states, particularly of the monomeric fraction that should serve as target for screening. Because oligomers are associated non-covalently, different fractions of the mutant variants associated with different oligomeric states could inter-convert due to thermodynamic equilibration. In this work, it was found that the equilibrium was shifted to the monomeric state by introduction of mutations to HTRA1 cd-mono2 and cd-mono3. To investigate whether oligomers are stable or inter-convert, the single fractions were kept at 8 °C for 7 days. The low temperature was chosen to prevent auto-degradation. Afterwards the fractions were applied to an analytical SEC. Results showed that for all four variants the higher oligomeric state is stable under the mentioned conditions. No formation of trimeric or monomeric state was observed. Likewise, the monomers showed no equilibration towards oligomer formation. Only trimers of mutated variants showed a slight equilibration into monomeric, but not into a higher oligomeric state. This can be explained by the exchange of the residues playing a key role in trimerization.

For trimeric states of protease variants HTRA1 cd and HTRA1 cd + PDZ a tail after the elution peak in analytical SEC for evaluation of stability of oligomeric states was detected. Since it was not a distinct peak and therefore did not correspond to a molecule of distinct molecular weight, which was also supported by PAGE (results not shown), it probably indicates auto-degradation products. This is further supported by the absence of this tail after the elution peak in the analytical SEC of both trimeric fractions of monomeric variants that have been shown to be substantial less active in proteolytic cleavage of a fluorescent substrate. Impurities as source of the observed tail after the elution peak can be excluded, because the trimeric fractions were previously isolated by preparative SEC and showed no impurities in the PAGE. Thus, the smaller fractions in analytical SEC should be proteolytic products that have been cleaved by the purified trimeric protease upon 7 days storage at 8 °C with itself as the only present substrate. Intrestingly, only the trimeric fractions of variants with native protease sequence display autoproteolytic activity. Although higher oligomers also showed proteolytic activity in general, our findings indicate resistance to auto-cleavage which is either caused by altered substrate specificity of both oligomeric states or by altered accessibility of recognition sites for cleavage of higher oligomeric states.

Another interesting observation was made for trimeric fraction of HTRA1 cd-mono2 and HTRA1 cd-mono3. Both variants showed in analytical SEC equilibration of the trimeric state with the monomeric state, but not *vice versa*. Moreover, the higher oligomeric states revealed no inter-conversion with the trimeric state or the monomeric state of both mutant variants. Presently, there is no data availaible, whether in its natural environment the trimeric or higher oligomeric state of HTRA1 is predominant, or whether an altered equilibrium between both oligomeric states is a mechanism for tuning the proteolytic activity of HTRA1 under physiological conditions.

Thermal stability measured by evaluation of melting points of expressed variants and their isolated fractions showed that all expressed variants are most likely folded having thermal transition upon heat denaturation that is typical for folded proteins. For detailed comparison of isolated fractions of HTRA1 cd-mono3 that were separated by SEC, it is obvious that trimeric and higher oligomeric fractions share a melting point (T_m) above 60 °C. In contrast, the T_m of the monomeric fraction is reduced to 54.5 °C. This is confirmed by the T_m of HTRA1 cd-mono2 monomeric fraction with a value of 51.5 °C. The melting points of HTRA1 cd and of HTRA1 cd+PDZ trimeric fractions are in the same range as the trimeric and higher oligomeric fractions of HTRA1 cd-mono3 with values around 60 °C. These data indicate clearly a loss of stability in monomers, but not in trimers and higher oligomers by substitution of residues that are important for HTRA1 trimer formation. Possibly the effect of amino acid exchanges on the fold of the catalytic domain is compensated by stabilizing effects of higher oligomerization. Finally no multiple melting peaks were detected for all variants that were caused by stepwise conversion of higher oligomers into trimers or from trimers into monomers.

Substrate recognition for the family of HTRA proteases is not well understood, besides that the mechanism is much more complicated compared to proteases like trypsin, where a single amino acid functional group is sufficient for cleavage behind this residue. For HTRA proteases plenty of natural and artificial peptidic and protein substrates are described, but no consensus recognition sequence could be deduced[44, 46-52, 317]. Comparison of peptide sequences that are cleaved by HTRA1 provided no indication of a prefered recognition motif and cleavage site[31]. It was investigated in this work whether isolated fractions of all variants display proteolytic activity towards fluorescence quenched peptide substrate H2Opt-K. Interestingly, for higher oligomeric fractions activity was detected, but for trimeric fractions only the variants with native protease sequence revealed activity under comparable substrate and protease concentrations. In contrast, the trimeric fraction of HTRA1 cd-mono3 was only active compared to trimeric variants with the native protease domain when substrate concentration was increased 5-fold. This tendency was consequently observed for the monomeric fractions which were only found for mutant variants. For these fractions the protease concentration had to be increased additionally to substrate concentration by 15-fold for comparable substrate conversion.

There is a clear tendency for the three different states, that the higher the oligomeric state, the higher the activity. This was demonstrated for all variants. Moreover, it was published that activity as well as the formation of higher oligomers increased 2.8-fold when HTRA1 was incubated with citrate-synthase[31]. A chromogenic substrate (DPMFKLV-pNA) was deduced for DegP from a peptide derived from citrate-synthase[318] that is also cleaved by human HTRA1, but is less sensitive for activity measurements compared to H2Opt-K (data not shown). Truebestein *et al.* concluded that citrate synthase causes protease activation of human HTRA1 by stabilizing a higher oligomeric state[31], but it is uncertain whether it acts only as ligand or also as substrate.

It was shown that a monomeric variant that was generated by a single mutation of the HTRA family member HTRA2 is proteolytic inactive[319]. This finding correlates with our results of strongly reduced activity for mutant variants and their monomeric fractions, respectively. Even the decreased proteolytic activity of trimers fits to this observation, in consideration that analytical SEC of trimeric fractions of mutant variants revealed a shift from trimeric into monomeric state. Taken together, these findings provide clues for the generation of modulators of HTRA1 activity, for example by preventing or enhancing higher oligomerization, as well as triggering the disassembly of trimers or hampering the assembly of monomers by interfering with regions involved in oligomeric interactions. This would introduce additional modes of modulation compared to inhibitors targeting the active site, or allosteric

activators and inhibitors addressing the orientation of the active-site of a monomer, as described previously.

A reversible activation mechanism of HTRA1 protease is currently discussed in the literature based on substrate induced-fit or conformational selection of protease towards the substrate[30, 31]. While in the induced-fit model[320, 321] the substrate is part of the mechanism that switches an enzyme into the active conformation, in the conformational selection model[320, 321] the enzyme just equilibrates between the active or inactive conformation, whereas the substrate is only bound and processed by the active conformation. As a consequence in the induced-fit model mainly the substrate is the driving force for switching human HTRA1 in the active conformation, depending on how efficient it re-orientates the active-site. In contrast, the conformational selection model depends strongly on the equilibrium of the enzyme's conformational states, because only the active conformation will process a substrate to a product upon binding. Nevertheless, both models depend on the environmental conditions as well as on the affinity towards a specific substrate.

Interestingly, for the induced-fit mechanism suggested by Truebestein *et al.* an allosteric activation is suggested to be absent, because the formation of a proteolytic active conformation of the activation domain is directly induced by substrate binding in the active site[31]. This is different compared to the well examined HTRA1 family members DegP and DegS, which were shown to be activated by a variety of allosteric ligands[26, 58, 322, 323]. Thus a totally new mode of activation of catalytic triad in human HTRA1 is supposed by Truebestein *et al.*, although they expect additional regulatory mechanisms. The induced-fit mechanism cannot explain the observation of allosteric HTRA1 activation by protoporphyrins[324] as well as the irreversible inhibition by diisopropyl fluorophosphate[30], which only attacks a serine of a catalytic triad in the active orientation. These findings and additional structural observations by Eigenbrodt *et al.* suggested a conformational selection mechanism with one or more inactive conformations which equilibrate with an active conformation, separated by an energy barrier[30]. The assumption of a conformational selection mechanism correlates with our result that the trimeric fraction of HTRA1 cd-mono3 shows increased activity compared to the monomeric fraction. Moreover, the higher oligomeric fraction displays further increased activity compared to the trimeric fraction of HTRA1 cd-mono3. This is also the case for HTRA1 cd and corroborated by findings made by Truebestein *et al.*[31]. Thus, it could be supposed that the higher an oligomeric state of HTRA1, the lower is the conformational flexibility, because the oligomers that are connected by the protease domain may reduce the range of different structural orientations. This assumption supports a conformational selection model with one active and various inactive conformations and correlates well with the general model that higher oligmerization of trimeric HTRA1 is a physiological activation mechanism of proteolytic activity[31, 324]. This regulation mechanism by altered oligomerization was first described for DegP the *E. coli* homologue of HTRA1[58, 325, 326]. However, there are striking differences between DegP and HTRA1 in oligomer formation since in contrast to DegP for HTRA1 the PDZ domain is not required for higher oligomer formation[31, 55, 57, 323, 325, 326]. Nevertheless, mechanisms that are a mixture of induced-fit and conformational selection models are in general conceivable[320].

For the *E. coli* homologue of HTRA1 DegP, additionally a cooperative effect in catalysis is suggested [23, 55]. Herein, when one subunit binds a substrate, it triggers a structural change in the neighboring subunit that switches it into the active conformation. If this is also applicable to human HTRA1, its activation mechanism fits better to the conformational selection than to the induced-fit model, because the protease neighboring catalytic domain is turned to an active state without presence of substrate at its active-site. Furthermore, presence of a cooperative effect in human HTRA1 would be an explanation for the observation of Truebestein[31], as well as of our results, that the activity of native protease domain is increased by formation of higher oligomers compared to trimers. Additionally, the strongly reduced activity of the monomeric fraction of the monomeric variant support a cooperative effect, due to the missing activation of the neighboring catalytic domains present in a trimer or higher oligomer.

In summary, the important outcome for the further work of the generation of mutant variants and their characterizations is that the successfully expressed and purified monomeric fraction of the monomeric variants is stable as individual molecule species without being arranged in a trimer. This

was shown by the successful expression with passing the quality control mechanisms of the expression host, the continuous stability of the particular oligomeric states, the thermal stability and the residual activity, that was measured at high substrate and protease concentrations. Moreover, the monomeric and both oligomeric states of all analyzed variants are mostly stable and do not equilibrate into another. Interestingly, the purified monomeric and trimeric states of HTRA1 cd-mono2 and HTRA1 cd-mono3 showed significantly decreased activity compared to the purified trimeric fractions and oligomeric states of HTRA1 cd and HTRA1 cd+PDZ. The previously discussed results of this work and other groups outline four potential modes of HTRA1 activity modulation by engineered molecules that bind monomeric HTRA1, such as preventing or enhancing higher oligomerization, dissociation of oligomers into monomers, inhibitors targeting the active site, as well as allosteric activators and inhibitors addressing the orientation of the active-site of a single HTRA1 monomer.

However it remains unclear how human HTRA1 monomers are arranged in higher oligomeric states, how formation of different oligomeric states is triggered and how the different oligomeric states contribute to regulation of protease activity.

6.2. Isolation and Characterization of HTRA1 Binding Molecules from a VHH Library

Besides the classical scaffolds used for selection of binding molecules that were derived from the mammal immune system such as IgG antibodies or more recent camelid single chain antibodies, there is large interest for finding alternative scaffolds for therapeutics and diagnostic applications. Along that line, vNAR molecules derived from shark single chain antibodies together with the open chain variant of squash trypsin inhibitor McoTI-II were used as scaffold for the design and screening of combinatorial libraries[129, 272, 311].

The best understood scaffold molecule employed in this work was the camelid-derived binding unit of a single chain antibody, the so called VHH molecule that was engineered in a classical way by immunization of a llama[193, 211]. The library constructed for yeast surface display technology cloned from the B-cell repertoire after immunization with catalytic domain of HTRA1 delivered no VHHs binding HTRA1 cd (data not shown). Problems were accredited to the target molecule because ELISA of serum that also contains classical antibodies against HTRA1 cd showed successful immunization. Additionally it was shown that VHHs against other targets that were combined for the immunization of a single animal were successfully isolated from the same library [309]. Therefore isolation of VHH molecules was repeated by changing the target to the monomeric state of the engineered variant HTRA1 cd-mono3. This delivered two independent clones after five rounds of enrichment. Occurrence of both clones was four and six, respectively, out of ten sequenced clones. KV01 that was found six times revealed a longer CDR3 with 12 residues compared with KV07 that has only seven residues. However CDR1 and CDR2 had the same length. Furthermore, many different framework mutations are present that demonstrate the distant lineage of both clones which underlines the complexity of the library. Nevertheless, only two different molecules were isolated. The immunization with the native protease domain could be one reason for the low variety of clones, because screening was performed with HTRA1 cd-mono3 with three substituted residues. But also library generation and immunization with multiple targets could influence the content and quality of HTRA1 binding molecules in the library, as well as stringency of HTRA1 binding during screening.

The ELISA of Fc-fused KV07 revealed only binding to HTRA1 cd-mono3, but not to the variant used for immunization. Evaluation of the post-immune serum towards HTRA1 cd-mono3 would give interesting insights in the distribution of the library of matured VHH candidates binding native or mutant variant. Eventually the peptides generated by the immune system for maturation of KV07 VHH *in vivo* represent epitopes that are buried in an HTRA1 oligomer.

KV07 had no effect on HTRA1 cd activity. Additionally no activating effect was observed on HTRA1 cd-mono3 under applied conditions. Nevertheless measurement with elevated substrate and protease concentrations for HTRA1 cd-mono3 were not performed. Unfortunately, KV01 was not expressed in sufficient amounts to investigate, whether this molecule is binding both targets or has an effect on the protease with native or mutant sequence, respectively. Furthermore KV01 has a 5-fold lower K_D

towards HTRA1 cd-mono3 compared with KV07. This and its different CDR sequences indicate that KV01 and KV07 address different epitopes of HTRA1. Hence, it might be worth to further optimize conditions for expression of KV01 to obtain sufficient protein amounts for further evaluation

6.3. Isolation and Characterization of HTRA1 Binding Molecules from McoTI-II Library

The squash trypsin inhibitor library based on open chain variant of McoTI-II delivered only one single binding molecule against HTRA1 cd-mono3, KS01. This scaffold was chosen due to its natural function which is protruding into the active-site of serine proteases such as trypsin or matriptase-1[129]. Variants binding and inhibiting other serine proteases were generated either by rational or evolutionary design methods[129, 327]. However these variants share common sequence features not observed in KS01. Furthermore loop 1 of KS01 that is mainly involved in inhibition of serine proteases has a totally different sequence compared with reported variants. Here large aromatic amino acids are predominant, in detail four of six. Interestingly the position 1 is changed from proline to phenylalanine although this position is suggested to be important for formation of the canonical inhibitor loop conformation[21, 22].

The isolated variant KS01 revealed a K_D value of 650 nM by affinity titration on the yeast surface. The 100-fold lower K_Ds reported for McoTI-II derived protease inhibitors are due to the specific mechanism of competitive inhibition. Interestingly monoclonal antibodies with six much longer CDRs that are mediating target binding have comparable K_D values[328, 329]. Especially the later discussed results of the affinity maturation of a vNAR library demonstrate the power of the selected McoTI-II derived molecule, because vNARs prior to maturation show at least 10-fold higher K_Ds against HTRA1 cd-mono3. Even if antibodies mediate their binding by up to six independent segments there are examples where single domains or even single loops are powerful enough for affinities in the low nanomolar range[129, 272, 330-332].

Miniprotein KS01 was synthesized by solid-phase peptide synthesis. Establishing the three disulfides in this short sequence is difficult to apply[300]. Nevertheless after *in vitro* folding it was shown that three cystines were formed (data not shown), while having no information whether the disulfide bond connectivity 1-4, 2-5 and 3-6 prevails. Unfortunately solubility was very poor for further evaluation which made the recombinant expression as Fc fusion protein necessary. Analysis of the Fc fusion of KS01 showed specific binding of HTRA1 cd-mono3, but no binding of HTRA1 cd, similar as it was observed for VHH candidate KV07. This result was confirmed by yeast cells presenting KS01 on their surface when being labeled with the different HTRA1 variants. Only labeling with HTRA1 cd-mono3 displayed an increase in fluorescence intensity compared to the unlabeled cells. Furthermore, no effect was measured on HTRA1 cd activity and HTRA1 cd-mono3, respectively. These findings are comparable with those for VHH molecule KV07. Similar to the VHH library, isolation of miniproteins binding HTRA1 cd trimeric fraction remained unsuccessful. Nevertheless the finding that no McoTI-II variants were obtained that bound the native protease domain is not as surprising as for VHH library which was immunized with HTRA1 cd. Despite the fact that the difference of both targets is only comprised by three amino acid residues the chance for selection of molecules binding both should be equally high.

A major problem of addressing HTRA1 is that a substrate, as well as various allosteric ligands could turn the trimeric oligomeric state into a higher oligomeric state, as discussed in section 6.1. Thus, a majority of epitopes that could be targeted by the library in the monomeric fraction of HTRA1 cd-mono3 could be inaccessible in a higher oligomer of unknown composition. But even in a trimer epitopes are buried that were accessible in a monomer. Nevertheless, the major competence of a miniprotein binding molecule is the extremely small size which allows protruding into niches and small pores of proteins and therefore may be advanatageous over the VHH scaffold to access recessed epitopes.

It will be worth repeating the screening of the library, because it is technically difficult to sample the complete set of variants of the library, due to its large size and the limitations of fluorescence activated cell sorting (FACS). Here switching the target from monomeric to trimeric fraction from round to

round could result in molecules binding both variants. Furthermore candidates could be isolated that have an influence on HTRA1 activity.

6.4. Isolation and Characterization of HTRA1 Binding Molecules from vNAR Library and the Matured Sub-Libraries

The library derived from a shark santibody domain named vNAR combined two features. It carries the naïve repertoire of a cohort of three bamboo sharks and a synthetically randomized CDR3. This has the benefit of different framework mutations residing in the scaffold that may contribute to scaffold stabilizing effects in combination with rational biased randomization of a special binding region (CDR3). Although the large library size covers not the whole theoretical sequence variety, multiple binding molecules against HTRA1 cd-mono3 were isolated. After four rounds of enrichment thirteen of fifteen clones showed HTRA1 cd-mono3 binding, while six individual clones were obtained. In contrast to the isolated clones of VHH and McoTI-II based library screening, five analyzed clones displayed binding of HTRA1 cd and HTRA1 cd+PDZ with native protease domain, as well as an additional PDZ domain. This result could raise the expectation that also native HTRA1 is addressed by these molecules.

One clone was found five times, three clones twice and two clones only one times. Interestingly, K10 that was found five times did not show the lowest K_D but the second highest with 8 µM. The isolated clones in general have a K_D value in the micromolar range, ranging from 1.25 µM for K03 up to 24.4 µM for K07. The K_D values determined by affinity titration in general suit well with the K_D values determined for the identical soluble molecules as reported by Wittrup *et al*[333, 334]. Furthermore CDR3 sequences of the analyzed molecules revealed no consensus sequence suggesting that they all address different epitopes. This fueled expectations that at least one candidate should have an effect on HTRA1 activity. Moreover sequences of HV2 were identical in all clones and CDR1 only contains slight variations from third to fifth position. The isolated clones also revealed differences in the framework on eight positions. Combining the results of similar sequences of binding segments with the naïve framework variety it is conceivable that CDR1 and HV2 are only recruited by the affinity maturation **process of the shark's immune system when confronted with antigen. Thus initial occurring single** domain antibodies seem to mediate binding only by CDR3. This observation matches with the sequence analyses of non-immunized bamboo shark which was done before library construction[272, 311]. The eight positions with observed framework variations reveal the desired variety of pooled starting material for construction of the library that reflects the naïve repertoire of framework variations of the bamboo shark. It is still uncertain whether these mutations are necessary for maintaining the vNAR-fold in combination with different HV and CDR sequences or whether they just appeared in the directed evolution experiment by coincidence.

The affinity maturation of isolated CDR3 clones by recruiting HV2 or CDR1, respectively, delivered five different HV2 as well as five different CDR1 clones of five analyzed clones each. Four clones of each matured sub-library showed HTRA1 cd-mono3 binding. Interestingly all clones of HV2 maturation and three clones of CDR1 maturation share CDR3 of K07 which showed the highest K_D value with 24.5 µM in the initial enrichment approach. Under consideration that target concentration in the first round of maturation was 100 nM it is distinctly obvious that the additional binding region contributes to affinity. It is very unlikely that binding is only mediated by the newly recruited binding segment HV2 or CDR1 because libraries were quite small, only two rounds for selection were performed and only five residues were involved in randomization. Further it is currently unclear why the other CDR3 sequences mediating higher affinities to HTRA1 did not give rise to variants with enhanced affinity upon maturation. Several reasons such as biased amplification by PCR for sub-library construction, clone dependent differences in cell doubling times upon growth or instabilities in folding for example could account for this finding. The sequences of HV2 revealed no conserved positions in view of functionality of the amino acid side chains although they may face a related epitope due to the same CDR3 sequence. A similar observation is made for CDR1 sequences. Structure analysis revealed that CDR1 is facing in most vNAR isoforms in the same direction as CDR3, while HV2 is facing more in an angle of 90° to the side[311]. A vNAR with bi-functionality introduced through HV2 emphasizes this

feature[311]. Interestingly, K_D values of affinity improved variants from the HV2 sublibrary are comparable with clones matured in CDR1.

The K_D values determined by affinity titration on the yeast surface ranged from 0.47 μM to 2.80 μM for HV2 matured clones and from 0.29 μM to 3.22 μM for CDR1 matured clones. Compared with parental K07 the affinity was increased about 10 to 100-fold. This result demonstrates the effect on affinity by recruiting an extra region that mediates interactions with the target. The K_D determined for KC03 that has K14 as origin is in the triple-digit nanomolar range between that of KC02 and KC05. Unfortunately there was no K_D determined for parental K14. Only one of the HV2 matured clones, but three of the CDR1 matured clones showed K_D values in the nanomolar range, while the others showed K_D values in the micromolar range. This result confirm the notion of the structure analysis described above, that CDR1 is facing more in direction of the target compared to HV2 and therefore may be better suited to support CD3-mediated target binding. Here again evaluation of more clones would lead to a statistically better understanding of this assumption.

To bring matters to a head, clones that were previously matured in HV2 were followed by maturation of CDR1. Implementation of this was easy by using the same strategy as for CDR1 maturation of initial isolated CDR3 clones. The library constructed from mixture of clones enriched in the first round of HV2 maturation was used as starting point for receiving high diversity despite the small size of the HV2 sub-library. Size of generated vNAR CDR1-HV2-CDR3 library was 200-fold larger with 10^7 independent clones compared with the HV2 sub-librariy of the first maturation step. Ten of twelve analyzed clones showed HTRA1 cd-mono3 binding and shared CDR3 sequence with K07. This is not surprising due to the fact that almost 90 % of clones from first maturation attempts contained this sequence. Only two clones appeared twice, namely KHC04 and KHC05, while the other eight clones were individual at least in CDR1. Different from the first maturation approach conserved positions in CDR1 emerged. A tyrosine on position five appeared in five clones and large aliphatic amino acids in two clones of the nine individual sequences. In position four also large aliphatic sidechains are prominent in five clones and aromatic side chains in three clones. For positions one to three no preference for side chains could be detected.

In HV2 of isolated double matured clones no sequences of the initial affinity maturation attempt of HV2 were detected. HV2 sequence of clones KHC04, KHC06, and KHC07 were identical and contained a glutamine in position one and five, while CDR1 sequences of these clones were independent. Interestingly, also clone KH01 from the previous HV2 maturation carried a glutamine in position one and five in HV2. This clone showed the lowest K_D value in HV2 maturation with 469 nM, while the other clones of this maturation attempt showed K_D values in the micromolar range. According to this finding, these residues seem to be important in HTRA1 cd-mono3 binding in combination with CDR3 of K07. Besides the HV2 sequences of KHC04, KHC06, and KHC07, the remaining isolated clones were individual. In the HV2 sequences of clones KHC01, KHC02, and KHC08 also a glutamine was present in position five, additionally emphasizing the importance of a glutamine in this position. In position four, a proline emerged in the four independent clones KHC01, KHC02, KHC03, and KHC11. Thus, positions one, four and five seem to be involved in target binding in combination with CDR3 of parental clone K07. The absence of HV2 sequences found upon HV2 affinity maturation in the clones obtained by the following maturation by CDR1 variation could have several reasons. An explanation could be cooperative effects of HV2 and CDR1 in the tertiary structure of the folded vNAR, whereby one segment is involved in binding while the other segment is responsible for the orientation of the residues of the first one. Thus, not all three designed regions have to be involved directly in increased affinity, but could also act indirectly by improving molecular interactions between epitope and paratope.

It is important to note that the engineered regions of the isolated molecules share no motifs with the recognition sequences of known native or synthetic substrate[335, 336]. The presence of HTRA1 substrate recognition sequences in the isolated molecules would raise expectations for candidates that directly interact with the active site, like canonical inhibitors[337]. If these sequences were recognized, but not

proteolytically degraded, they could competitive block the active site as shown for cystine knot miniproteins for example[338].

The seven unique isolated clones of the second maturation attempt that were titrated revealed K_D values in the double digit nanomolar range. Here again an additional increase in affinity of the factor 10-100 was measured compared to the K_D values of analyzed clones after initial maturation of HV2 or CDR1. In general molecules isolated from synthetic or naïve libraries are often in the micromolar range[339, 340]. The engineering of affinity by the applied method enables transformation of candidates fulfilling a biological task into molecules with affinities being in the low nanomolar range that would be required for therapeutic applications[103].

Interestingly, the high occurence of a tyrosine in position five found in the initial affinity maturation step of CDR1 was not confirmed upon CDR1 maturation of the CDR3-HV2 binders. Hence, it is not totally clear after the second maturation attempt, whether binding is mediated by an additional region resulting in interactions of all three recruited regions or just by CDR3 and CDR1. Even other combinations of segments involved in binding such as CDR3 and HV2, HV2 and CDR1 or only CDR1 are theoretically possible that might have emerged upon screening for high affinity binders. To clarify this point grafting of nonbinding segments, an alanine scanning[341], saturation transfer difference (STD) NMR[342] or a co-crystal structure of an interesting candidate in combination with HTRA1 could be considered. The stepwise increase in affinity upon stepwise affinity maturation not necessarily indicates that an enhanced affinity is mediated by the interaction of a target epitope by three instead of two loops. For example, the increase in affinity could also be related to the larger library size used for the second maturation and additional rounds of enrichment compared to the first one. Likewise, the enhanced affinity could also be the result of avidity effects that may arise upon target interaction with two independent binding units addressing two distinct epitopes[343]. If one binding unit, for example that mediated by CDR3/CDR1 binding dissociates from the target the other one, e.g. mediated by HV2 might remain bound to another epitope prior to complete diffusion from the target. Nevertheless, it could be shown that each step of affinity maturation individually contributed to increased affinity.

Zielonka *et al.* demonstrated that it is possible to generate bispecific vNAR molecules by screening a CDR1 matured single clone against EpCAM by an additional screening of randomized HV2 towards CD3ε and human Fcγ[311, 312]. Thus, HV2 could be used for different purposes such as increasing affinity as shown in this work, or for binding an additional target.

Double determination of K_D values as it was performed for the clones KHC04 and KHC05 which were identical clones reveals that affinity titration suits well for basic assertion of affinity, but not for a detailed ranking of isolated clones with similar affinities. For a more detailed comparison analysis of soluble molecules by surface plasmon resonance or bio-layer interferometry should provide more reliable data.

Due to the high number of different sequences observed in CDR1 and HV2 after four screening rounds, an extra competitive k_{off} screening was performed. By additional incubation with excess of unlabeled target after labeling with 10 nM fluorescently labeled HTRA1, clone KHC02 emerged as the only clone upon analysis of ten sequences. Unfortunately KHC02 showed low yeast surface presentation resulting in an unacceptable error in affinity titration. It should be emphasized that a low dissociation rate constant does not necessarily indicate a low K_D since the association rate constant may also be compromised. Here again more detailed binding kinetics especially for k_{on} and k_{off} rates should be evaluated by surface plasmon resonance or bio-layer interferometry[328].

Comparison of clones isolated in this work with clones from the same library isolated against EpCAM or EphA2 showed that compared to the target HTRA1 initial CDR3 clones against EpCAM and EphA2 revealed 10-fold lower K_D values each[272]. Nevertheless screening towards interleukin-8 delivered a vNAR in the same range as vNARs against HTRA1 cd-mono3. Additionally the affinity maturation of CDR1 delivered 100-fold lower K_D values in only two rounds for EpCAM, but only less than 10-fold for interleukin-8. These results demonstrate the impact of different targets when isolating vNARs from a

master library. Nevertheless, the K_D values of HTRA1 cd-mono3 binding vNARs decreased with the first step of affinity maturation affecting HV2 or CDR1 and the second step affecting CDR1 at least 10-fold for each approach.

For HTRA1 the unpredictable oligomeric states were challenging and resulted in no enrichment of binding molecules over several initial attempts. Similar problems were reported by Ciferri *et al.* who tried isolation of HTRA1 inhibitors by phage display from a human Fab library against human full-length HTRA1[335]. They overcame the problems by using a murine variant composed only of the catalytic domain comparable to HTRA1 cd used in this work. Unfortunately they did not specify whether they separated fractions of different oligomeric states and if yes, which one they used for screening. In this work the problem was overcome through engineering the target prior to screening binding molecules. By reviewing all selection experiments it becomes apparent that not the alternating change of labeling as it was performed for VHH library screening but the engineering of the target made the difference in successful isolation of binding molecules since screening for VHH or McoTI-II based binders against native protease was unsuccessful. Despite all these difficulties multiple binding molecules of different classes were isolated against monomeric variant of HTRA1. At least an effect on activity of native catalytic domain of HTRA1 was demonstrated for various vNAR molecules. Thus, engineering the oligomeric state of a target protein prior to screening for binding molecules could be a general strategy for difficult to address oligomeric targets.

Although there was an anti HTRA1 antibody against the catalytic domain isolated by phage display[335], the generation of HTRA1 monomer in our opinion was crucial for isolating binding molecules by yeast surface display. Using large oligomers as target protein bears a high risk of isolating low affinity binders due to avidity effects. Additionally in our first screening attempts HTRA1 oligomers were that large that they were detectable in FACS and it was nearly impossible to distinguish between yeast cells and protein particles by side-scatter analysis. Unfortunately it was technically impossible to involve the forward-scatter of the FACS in the sorting decision, which might help to detect and sort out only particles of the distinct characteristic of yeast cell.

The most interesting question for binding molecules interacting with enzymes is whether they have an influence on enzyme activity. It was desirable in this project that the isolated molecules were not only able to bind native HTRA1, which was shown for multiple molecules, but also to affect the protease activity. To investigate, whether the isolated binders also act as modulators of enzyme activity several proteins were produced recombinantly. For vNAR molecules K07, K10, K13 and K14 sufficient proteins amounts were obtained after purification for further studies as for double matured clone KHC01. For the missing initial clones and the missing double matured clones expression conditions have to be optimized or they have to be formatted differently, for example as Fc-fusion proteins as previously described for VHH and McoTI-II derived molecules. The clones only matured in CDR1 or HV2, respectively, were not included in the functional examination because they share the CDR3 of initial clones or were less affine than double matured clones.

Successfully expressed molecules showed thermal stability between 51°C and 75°C which is in the range of antibodies and adequate for application in mammals[344]. Clones K10 and K13 had no effect on HTRA1 activity, as well as the control vNAR that binds EpCAM. This led to the conclusion that both vNARs recognize epitopes not involved in substrate processing, substrate recognition or structural changes during switching from active to inactive conformation. Clone K14 had a slight activating effect on the trimeric protease by increasing activity by around 150 % compared to control vNAR. Moreover, activity was almost doubled in presence of clone K07, despite the fact that it showed the highest K_D of all isolated molecules. The most prominent effect was observed in presence of KHC01 with around 4-fold enhancement of activity compared with EpCAM binding vNAR serving as a control. This result was not unexpected, because K07 and KHC01 share the same CDR3 sequence so they most probably address the same epitope. Furthermore, the much higher affinity of KHC01 most likely leads to a higher activation due to its significantly enhanced affinity compared to K07. It will be interesting to investigate, whether the other single and double matured molecules containing CDR3 of K07 have a comparable effect on HTRA1. A more detailed evaluation of soluble expressed KC03, an affinity

matured derivative of the K14, a binder that was found to slightly enhance HTRA1 activity would also be of great interest.

Currently, only a few molecules are reportedly HTRA1 activators. A number of protoporphyrins was shown to increase HTRA1 activity by triggering higher oligomerization[324]. The same mechanism for HTRA1 activation was reported for citrate synthase that additionally acted as a substrate[31]. Furthermore it was shown that activity of *E. coli* homologue DegP was enhanced in presence of different peptides[26]. Only for human HTRA1 family member HTRA3 a classical monoclonal antibody 6G6 was published, that activated proteolytic activity[336]. It was shown that the antibody simultaneously binds to the PDZ domain and catalytic domain. The epitope recognized in the catalytic domain is supposedly located in the substrate sensor loop L3. Thus, a reorientation of PDZ domain was suggested to be the mechanism for activation. The PDZ domain is suggested to be bended to the opposite site of the catalytic domain of the disc shaped HTRA3 trimer. This observation is interesting because HTRA3 activity is independent of the PDZ domain, as it is for HTRA1[336]. The antibody 6G6 increased relative activity of HTRA3 by about 130 % when 4 µg and by 140 % when 20 µg were applied. The isolated vNAR molecules in this work mediated an increase of relative activity of HTRA1 in the range of 150 % to 400 % in a comparable concentration range. In this respect the isolated vNAR molecules K07, K14 and KHC01 are the first specifically isolated activators of HTRA1 activity that exclusively address the catalytic domain. Moreover, molecules K07 and KHC01 that most probably address the same epitope showed an affinity-dependent potency to act as activators.

Activators of HTRA1 could be interesting candidates as therapeutics in cancers because it was shown that HTRA1 is downregulated in many different types of cancer[18, 43, 46, 48, 49, 56, 59, 61, 62]. Especially the combination of HTRA1 enhancers with chemotherapy could be attractive due to the fact that chemo-therapeutic success is highly reduced if HTRA1 is downregulated[61]. Such type of activators could become valuable tools to study the general involvement of the protease in formation and progression of cancers in cell culture or animal models. It will be interesting to investigate, whether the vNAR-derived activators generated in this work are active in a rat or mouse model since rodent HTRA1 catalytic domains are highly homolog to human HTRA1 with only a few amino acid exchanges. For therapeutic applications, the potential immunogenicity of the non-human vNAR domain would have to be taken into consideration. Nevertheless, methods for humanizing non-human derived candidates have been reported[197]. Moreover, computer-assisted prediction for vNAR molecules suggest low tendency for immunogenicity of vNARs in general[266, 345].

Another interesting field of application of HTRA1 activators would be in the context of treatment of Alzheimer's disease via enhancing the HTRA1-mediated cleavage of tau-protein[77]. Likewise, activation of HTRA1 could be used to study and better understand the influence and the involvement of HTRA1 in other diseases like osteoarthritis (OA) or age-related macular degeneration (AMD) where it was shown that HTRA1 expression levels are elevated[48, 56, 60]. In animal disease models these activators could become useful compounds to elucidate, how the multimeric protease is involved in disease progression. This would also open new avenues for the investigation, whether HTRA1 contributes by its proteolytic activity or by other domains to the progression in these diseases, when a catalytic domain selective activator is used. In current animal models such as rat or dog, OA is often induced by surgical intervention, which is an unselective trigger[346]. Activation of HTRA1 that is suggested to be a potential elicitor of OA could provide a more native scenario for disease induction in an animal model.

Interestingly only binders were found in this work that enhanced proteolytic activity, but unexpectedly no molecules that reduced HTRA1 activity were isolated. It is possible that such candidates exist in the vNAR library since only a relatively small subset of clones was evaluated for activity modulation. Their identification would require a high-throughput expression, purification and functional screening of hundreds of candidates, which was beyond the scope and possibilities of this project. An inhibitory Fab fragment (Fab94) was recently reported by Genentech[335]. For the isolation of Fab94 from a phage display library that was additionally formatted as IgG94 antibody, the murine catalytic domain was used as a target which shares 96 % homology with the catalytic domain of human HTRA1, because screening with human HTRA1 failed. This is in accordance with the problems in isolating molecules

against human HTRA1 cd in this work. The K_D value of Fab94 was 48.1 nM against human HTRA1, while the IC_{50} value of Fab94 was 17.7 nM and of IgG94 1.58 nM for human HTRA1 catalytic domain. No significant difference in binding affinity and inhibition was observed between the catalytic domain and full-length HTRA1, indicating that molecules isolated towards the active site of HTRA1 maintain their effect also in the physiologically relevant oligomeric state. The authors proposed a competitive inhibition mechanism, where Fab94 blocks substrate entrance to the active site. Analysis of negative-staining EM of IgG94 in complex with HTRA1 catalytic domain revealed an interesting mode of action. Three IgG molecules address two HTRA1 trimers which resulted in formation of a distinct macromolecular inhibition complex. One Fab of each IgG binds one active site of the same HTRA1 trimer and the same is done for the other trimer by the remaining antigen binding fragments. The linkage of both trimers to a cage-like structure is mediated by the Fc-parts via the Fab arms. This mechanism solved the problem of steric hindrance due to the close proximity of the active sites in a trimer. Incubation of the catalytic domain of HTRA1 with IgG94 at different molar ratios always resulted in the same single complex with a 2:3 ratio of HTRA1 trimers to IgG molecules. Thus, no free Fab arms for building larger aggregates with additional HTRA1 trimers remained. This mechanism circumvents the problem for inhibition of all active sites of a trimer by large molecules, but it also demonstrates the need for smaller vNAR, VHH or McoTI-II derived binders that could address all active sites simultaneously without steric hindrance.

In addition to the phage display derived HTRA1 inhibiting IgG94, the monoclonal antibody 10H10 was reported, that inhibited the human HTRA1 family member HTRA3[336]. As for IgG94, the inhibitory mechanism of 10H10 was suggested to be a competitive blocking of the active site by addressing the sensor loop L3. This was confirmed among other data by the observation that activity of HTRA3 was not recovered by allosteric activating antibody 6G6 when being previously incubated with 10H10.

Beyond VHHs, vNARs or knottins, other scaffolds could be considered as starting point for engineering HTRA1 activators or inhibitors. For example alpha-1-antitrypsin could be an interesting basis for engineering highly potent inhibitors against HTRA1, because it is already reported that it inhibits the protease[19, 30, 44, 56]. Moreover it is a protein that consists of 400 amino acids which makes it accessible for rational or evolutionary design. Further, the mechanism of alpha-1-antitrypsin for inhibition in the active site is well described and structural data is available[348]. As reported for cystine-knot miniproteins selectivity and affinity could be enhanced towards HTRA1 by changing residues that interact with the active site[129]. However, it was published recently that alpha-1-antitrypsin is degraded by HTRA1 resulting in loss of inhibitor function which is contradictory to previous reports[349].

Both up- and downregulation of HTRA1 is connected to different diseases, a finding that renders it questionable whether HTRA1 can be considered as a therapeutic target. Nevertheless different compartments of the human body are involved in the diseases mentioned above. Thus fusion of activators or inhibitors to binding molecules addressing unique structures for these compartments could lead to a specific localization thereby reducing unwanted side effects. For example activators could be fused to antibodies against tumor cell specific markers for localization in a tissue, where HTRA1 is downregulated, aimed at enhancing the anti-carcinogenic effect of HTRA1.

As previously mentioned, the studies of Truebestein[31] and Jo[324], as well as our results, emphasize the correlation between HTRA1 higher oligomeric states and an increase in activity. Thus it would be interesting to investgate, whether our isolated activators have an impact on oligomerization. Size-exclusion chromatography would reveal the influence of isolated molecules when being incubated with the different protease variants aimed at addressing the question whether activators act in a way that they shift the equilibrium to higher oligomers.

Additionally it would be interesting to investigate, whether HTRA1 substrates induce higher oligomer formation in general and if this only enhances or initiates activity. In the *E. coli* homologue DegP for example it is suggested that the oligomer size depends on the substrate size. Moreover it was shown that hexameric DegP is proteolytic inactive, because two trimers are inhibiting each other by a special loop that is not present in human HTRA1[58, 314]. If active protease does not result from higher oligomerization, but is enhanced by this process, the isolated molecules showing no effect on trimeric

activity could act as inhibitors of higher oligomer formation and thus reduce activity for substrates inducing higher oligomer formation.

Deeper insight into the addressed epitopes of isolated vNAR molecules and the differences of VHH and McoTI-II derived molecules that bound HTRA1 cd-mono3 but not HTRA1 cd could be obtained by structural analysis. Accordingly, the assumption that isolated VHH and McoTI-II derived molecules bound epitopes that are buried in trimeric HTRA1 could be confirmed and epitopes responsible for the increase in activity by isolated vNAR molecules could be identified. There are already structural elements that were described to be involved in HTRA1 activation such as the sensor loop L3[31]. In the diploma theses of Bert Luck polyclonal antibodies against a hapten with chemically synthesized loop L3 were developed by immunization of a rabbit. However, corresponding antibodies purified by affinity chromatography of L3 showed specific binding towards HTRA1, but had no effect on activity, a finding that once more underlines the highly complicated mode of action of this enzyme[347].

7. References

1.   Kassell, B. & Kay, J. Zymogens of proteolytic enzymes. Science 180(4090), 1022-7 (1973).
2.   Neurath, H. Mechanisms of Zymogen Activation. Fed Proc. 23, 1-7 (1964).
3.   Kitano, H. Systems biology: a brief overview. Science 295, 1662-4 (2002).
4.   Khorana, H. G. et al. Polynucleotide synthesis and the genetic code. Cold Spring Harb. Symp. Quant Biol. 31, 39-49 (1966).
5.   Martin, R. B. Free energies and equilibria of peptide bond hydrolysis and formation. Biopolymers 45, 351-35 (1998).
6.   Rawlings, N. D. & Barrett, A. J. Evolutionary families of peptidases. Biochem J 290, 205-218 (1993).
7.   Rawlings, N. D., Barrett, A. J. & Bateman, A. MEROPS: the peptidase database. Nucleic Acids Res. 38, 227-233 (2010).
8.   Rawlings, N. D., O'Brien, E. & Barrett, A. J. MEROPS: the protease database. Nucleic Acids Res 30, 343-6 (2002).
9.   Rawlings, N. D., Tolle, D. P. & Barrett, A. J. MEROPS: the peptidase database. Nucleic Acids Res 32, D160-4 (2004).
10.   Rawlings, N. D., Barrett, A. J. & Bateman, A. Asparagine Peptide Lyases: A Seventh Catalytic Type of Proteolytic Enzymes. J Biol Chem 286(44), 38321-8 (2011).
11.   Rawlings, N. D. & Barrett, A. J. Families of serine peptidases. Methods Enzymol 244, 19-61 (1994).
12.   Bode, W. & Huber, R. Structural basis of the endoproteinase-protein inhibitor interaction. Biochim Biophys Acta 1477, 241-52 (2000).
13.   Ye, S. & Goldsmith, E. J. Serpins and other covalent protease inhibitors. Curr Opin Struct Biol 11, 740-5 (2001).
14.   Huang, X. et al. Modulation of recombinant human prostate-specific antigen: activation by Hofmeister salts and inhibition by azapeptides. Appendix: thermodynamic interpretation of the activation by concentrated salts. Biochemistry 40, 11734-41 (2001).
15.   Spiess, C., Beil, A. & Ehrmann, M. A temperature-dependent switch from chaperone to protease in a widely conserved heat shock protein. Cell 97, 339-47 (1999).
16.   Chien, J., Campioni, M., Shridhar, V. & Baldi, A. HtrA serine proteases as potential therapeutic targets in cancer. Curr Cancer Drug Targets 9, 451-68 (2009).
17.   Coleman, H. R., Chan, C. C., Ferris, F. L., 3rd & Chew, E. Y. Age-related macular degeneration. Lancet 372, 1835-45 (2008).
18.   Grau, S. et al. Implications of the serine protease HtrA1 in amyloid precursor protein processing. Proc Natl Acad Sci U S A 102, 6021-6 (2005).
19.   Hara, K. et al. Association of HTRA1 mutations and familial ischemic cerebral small-vessel disease. N Engl J Med 360, 1729-39 (2009).
20.   Milner, J. M., Patel, A. & Rowan, A. D. Emerging roles of serine proteinases in tissue turnover in arthritis. Arthritis Rheum 58, 3644-56 (2008).
21.   Avrutina, O. et al. Trypsin inhibition by macrocyclic and open-chain variants of the squash inhibitor MCoTI-II. Biol Chem 386, 1301-6 (2005).
22.   Heitz, A. et al. Knottin cyclization: impact on structure and dynamics. BMC Struct Biol 8, 54 (2008).
23.   Weber, N. & Kolmar, H. in Handbook of Proteolytic Enzymes (ed. Barrett, R., Woessner) 2567-2571 (Elsevier, 2013).
24.   Lipinska, B., Sharma, S. & Georgopoulos, C. Sequence analysis and regulation of the htrA gene of Escherichia coli: a sigma 32-independent mechanism of heat-inducible transcription. Nucleic Acids Res 16, 10053-67 (1988).
25.   Danese, P. N., Snyder, W. B., Cosma, C. L., Davis, L. J. & Silhavy, T. J. The Cpx two-component signal transduction pathway of Escherichia coli regulates transcription of the gene specifying the stress-inducible periplasmic protease, DegP. Genes Dev 9, 387-98 (1995).

26. Meltzer, M. et al. Allosteric activation of HtrA protease DegP by stress signals during bacterial protein quality control. Angew Chem Int Ed Engl 47(7), 1332-4 (2008).

27. Meltzer, M. et al. Structure, function and regulation of the conserved serine proteases DegP and DegS of Escherichia coli. Res Microbiol 160, 660-6 (2009).

28. Supanji, Shimomachi, M., Hasan, M. Z., Kawaichi, M. & Oka, C. HtrA1 is induced by oxidative stress and enhances cell senescence through p38 MAPK pathway. Exp Eye Res 112, 79-92 (2013).

29. Clausen, T., Southan, C. & Ehrmann, M. The HtrA Family of Proteases: Implication for Protein Composition and Cell Fate. Molecular Cell 10, 443-455 (2002).

30. Eigenbrot, C. et al. Structural and functional analysis of HtrA1 and its subdomains. Structure 20, 1040-50 (2012).

31. Truebestein, L. et al. Substrate-induced remodeling of the active site regulates human HTRA1 activity. Nat Struct Mol Biol 18, 386-8 (2011).

32. Risor, M. W. et al. The autolysis of human HtrA1 is governed by the redox state of its N-terminal domain. Biochemistry 53, 3851-7 (2014).

33. Khan, A. R. & James, M. N. Molecular mechanisms for the conversion of zymogens to active proteolytic enzymes. Protein Sci 7, 815-36 (1998).

34. Boehr, D. D., Nussinov, R. & Wright, P. E. The role of dynamic conformational ensembles in biomolecular recognition. Nat Chem Biol 5, 789-96 (2009).

35. Subrini, O. & Betton, J. M. Assemblies of DegP underlie its dual chaperone and protease function. FEMS Microbiol Lett 296, 143-148 (2009).

36. Maurizi, M. R. Love it or cleave it: Tough choices in protein quality control. nat Struct Biol 9, 410-412 (2002).

37. Chien, J., He, X. & Shridhar, V. Identification of tubulins as substrates of serine protease HtrA1 by mixture-based oriented peptide library screening. J Cell Biochem 107, 253-63 (2009).

38. Mauney, J., Olsen, B. R. & Volloch, V. Matrix remodeling stem cell recruitment: A novel in vitro model for homing of human bone marrow stromla cells to the site of injury shows crucial role of extracellular collagen matrix. Matrix Biology 29, 657-663 (2010).

39. Lorenzi, T. et al. Expreesion Patterns of Two Serine Protease HTRA1 Forms in Human Placentas Complicated by Preeclampsia with and without Intrauterine Growth Restriction. Placenta 30, 35-40 (2009).

40. Zurawa-Janicka, D., Skorko-Glonek, J. & Lipinska, B. HtrA proteins as targets in therapy of cancer and other diseases. Expert Opin Ther Targets 14(7), 665-679 (2010).

41. Chien, J. et al. Serine protease HtrA1 associates with microtubules and inhibits cell migration. Mol Cell Biol 29, 4177-87 (2009).

42. Altobelli, E., Marzioni, D., Lattanzi, A. & Angeletti, P. M. HtrA1: Its future potential as a novel biomarker for cancer. Oncology Reports 34, 555-566 (2015).

43. Baldi, A. et al. The HtrA1 serine protease is down-regulated during human melanoma progression and represses growth of metastatic melanoma cells. Oncogene 21, 6684-8 (2002).

44. Hou, J., Clemmons, D. R. & Smeekens, S. Expression and characterization of a serine protease that preferentially cleaves insulin-like growth factor binding protein-5. J Cell Biochem 94, 470-84 (2005).

45. Launay, S. et al. HtrA1-dependent proteolysis of TGF-beta controls both neuronal maturation and developmental survival. Cell Death Differ 15, 1408-16 (2008).

46. Oka, C. et al. HtrA1 serine protease inhibits signaling mediated by Tgfbeta family proteins. Development 131, 1041-53 (2004).

47. Campioni, M. et al. The serine protease HtrA1 specifically interacts and degrades the tuberous sclerosis complex 2 protein. Mol Cancer Res 8, 1248-60 (2010).

48. Grau, S. et al. The role of human HtrA1 in arthritic disease. J Biol Chem 281, 6124-9 (2006).

49. Tsuchiya, A. et al. Expression of mouse HtrA1 serine protease in normal bone and cartilage and its upregulation in joint cartilage damaged by experimental arthritis. Bone 37, 323-36 (2005).

50. An, E., Sen, S., Park, S. K., Gordish-Dressman, H. & Hathout, Y. Identification of novel substrates for the serine protease HTRA1 in the human RPE secretome. Invest Ophthalmol Vis Sci 51, 3379-86 (2010).
51. Lipinska, B., Zylicz, M. & Georgopoulos, C. The HtrA (DegP) protein, essential for Escherichia coli survival at high temperatures, is an endopeptidase. J Bacteriol 172, 1791-7 (1990).
52. Swamy, K. H., Chung, C. H. & Goldberg, A. L. Isolation and characterization of protease do from Escherichia coli, a large serine protease containing multiple subunits. Arch Biochem Biophys 224, 543-54 (1983).
53. Martins, L. M. et al. Binding specificity and regulation of the serine protease and PDZ domains of HtrA2/Omi. J Biol Chem 278, 49417-27 (2003).
54. Skorko-Glonek, J., Wawrzynow, A., Krzewski, K., Kurpierz, K. & Lipinska, B. Site-directed mutagenesis of the HtrA (DegP) serine protease, whose proteolytic activity is indispensable for Escherichia coli survival at elevated temperatures. Gene 163, 47-52 (1995).
55. Clausen, T., Kaiser, M., Huber, R. & Ehrmann, M. HTRA proteases: regulated proteolysis in protein quality control. Nat Rev Mol Cell Biol 12, 152-62 (2011).
56. Hu, S. I. et al. Human HtrA, an evolutionarily conserved serine protease identified as a differentially expressed gene product in osteoarthritic cartilage. J Biol Chem 273, 34406-12 (1998).
57. Krojer, T. et al. Interplay of PDZ and protease domain of DegP ensures efficient elimination of misfolded proteins. Proc Natl Acad Sci U S A 105, 7702-7 (2008).
58. Krojer, T. et al. Structural basis for the regulated protease and chaperone function of DegP. Nature 453, 885-90 (2008).
59. Ajayi, F. et al. Elevated expression of serine protease HtrA1 in preeclampsia and its role in trophoblast cell migration and invasion. Am J Obstet Gynecol 199, 557 e1-10 (2008).
60. Dewan, A. et al. HTRA1 promoter polymorphism in wet age-related macular degeneration. Science 314, 989-92 (2006).
61. Chien, J. et al. Serine protease HtrA1 modulates chemotherapy-induced cytotoxicity. J Clin Invest 116, 1994-2004 (2006).
62. Chien, J. et al. A candidate tumor suppressor HtrA1 is downregulated in ovarian cancer. Oncogene 23, 1636-44 (2004).
63. Mullany, S. A. et al. Expression and functional significance of HtrA1 loss in endometrial cancer. Clin Cancer Res 17, 427-36 (2011).
64. Bowden, M. A., Di Nezza-Cossens, L. A., Jobling, T., Salamonsen, L. A. & Nie, G. Serine proteases HTRA1 and HTRA3 are down-regulated with increasing grades of human endometrial cancer. Gynecol Oncol 103, 253-60 (2006).
65. Wang, N. et al. Down-regulation of HtrA1 activates the epithelial-mesenchymal transition and ATM DNA damage response pathways. PLoS One 7, e39446 (2012).
66. Baldi, A. et al. The serine protease HtrA1 is a novel prognostic factor for human mesothelioma. Pharmacogenomics 9, 1069-77 (2008).
67. Zhu, F. et al. Serine protease HtrA1 expression in human hepatocellular carcinoma. Hepatobiliary Pancreat Dis Int 9, 508-12 (2010).
68. Catalano, V. et al. HtrA1, a potential predictor of response to cisplatin-based combination chemotherapy in gastric cancer. Histopathology 58, 669-78 (2011).
69. He, X. et al. Downregulation of HtrA1 promotes resistance to anoikis and peritoneal dissemination of ovarian cancer cells. Cancer Res 70, 3109-18 (2010).
70. Rosenthal, A., Gohr, C. M., Ninomiya, J. & Wakim, B. T. Proteomic Analysis of Articular Cartilage Vesicles From Normal and Osteoarthritic Cartilage. Arthritis Rheum 63, 401-411 (2011).
71. Chamberland, A. et al. Identification of a Novel HtrA1-susceptible Cleavage Site in Human Aggrecan. J Biol Chem 284, 27352–27359 (2009).
72. Poole, C. A., Ayad, S. & Schofield, J. R. Chondrons from articular cartilage: I. Immunolocalization of type VI collagen in the pericellular capsule of isolated canine tibial chondrons. J Cell Sci 90 (Pt 4), 635-43 (1988).

73. Poole, C. A. Articular cartilage chondrons: form, function and failure. J Anat 191 (Pt 1), 1-13 (1997).
74. Wu, J. et al. Comparative proteomic characterization of articular cartilage tissue from normal donors and patients with osteoarthritis. Arthritis Rheum 56, 3675-84 (2007).
75. Polur, I., Lee, P. L., Servais, J. M., Xu, L. & Li, Y. Role of HTRA1, a serine protease, in the progression of articular cartilage degeneration. Histol Histopathol 25, 599-608 (2010).
76. Skorko-Glonek, J. et al. HtrA protease family as therapeutic targets. Curr Pharm Des 19, 977-1009 (2013).
77. Tennstaedt, A. et al. Human high temperature requirement serine protease A1 (HTRA1) degrades tau protein aggregates. J Biol Chem 287, 20931-41 (2012).
78. Human insulin receives FDA approval. FDA Drug Bull 12, 18-9 (1982).
79. Goeddel, D. V. et al. Expression in Escherichia coli of chemically synthesized genes for human insulin. Proc Natl Acad Sci U S A 76, 106-10 (1979).
80. Kohler, G. & Milstein, C. Continuous cultures of fused cells secreting antibody of predefined specificity. Nature 256, 495-7 (1975).
81. Beck, A., Wurch, T., Bailly, C. & Corvaia, N. Strategies and challenges for the next generation of therapeutic antibodies. Nat Rev Immunol 10, 345-52 (2010).
82. Kellner, C., Derer, S., Valerius, T. & Peipp, M. Boosting ADCC and CDC activity by Fc engineering and evaluation of antibody effector functions. Methods 65, 105-13 (2014).
83. Scott, A. M., Wolchok, J. D. & Old, L. J. Antibody therapy of cancer. Nat Rev Cancer 12, 278-287 (2012).
84. Bradbury, A. R. M., Sidhu, S., Dübel, S. & McCafferty, J. Beyond natural antibodies: the power of in vitro display technologies Nat Biotechnol 29, 245-254 (2011).
85. Presta, L. G. Selection, design, and engineering of therapeutic antibodies. J Allergy Clin Immunol 116, 731-6 (2005).
86. Carter, P. J., Hazuda, D. & Wells, J. A. Next generation therapeutics. Curr Opin Chem Biol 17, 317-9 (2013).
87. Chan, A. C. & Carter, P. J. Therapeutic antibodies for autoimmunity and inflammation. Nat Rev Immunol 10, 301-16 (2010).
88. Kolmar, H. Natural and engineered cystine knot miniproteins for diagnostic and therapeutic applications. Curr Pharm Des 17, 4329-36 (2011).
89. Pillay, V., Gan, H. K. & Scott, A. M. Antibodies in oncology. Nat Biotechnol 28, 518-29 (2011).
90. Wurch, T., Pierré, A. & Depil, S. Novel protein scaffolds as emerging therapeutic proteins from discovery to clinical proof-of-concept. Trends Biotechnol 30, 575-82 (2012).
91. Saerens, D., Ghassabeh, G. H. & Muyldermans, S. Single-domain antibodies as building blocks for novel therapeutics. Curr Opin Pharmacol 8, 600-8 (2008).
92. Grandjenette, C., Dicato, M. & Diederich, M. Bispecific antibodies: an innovative arsenal to hunt, grab and destroy cancer cells. Curr Pharm Biotechnol 16, 670-83 (2015).
93. Skerra, A. Engineered protein scaffolds for molecular recognition. J Mol Recognit 13, 167-87 (2000).
94. Schroeder, H. W., Jr. & Cavacini, L. Structure and function of immunoglobulins. J Allergy Clin Immunol 125, S41-52 (2010).
95. Gilbreth, R. N. & Koide, S. Structural insights for engineering binding proteins based on non-antibody scaffolds. Curr Opin Struct Biol 22, 413-20 (2012).
96. Löfblom, J., Frejd, F. Y. & Stahl, S. Non-immunoglobulin based protein scaffolds. Curr Opin Biotechnol 22, 843-8 (2011).
97. Richter, A., Eggenstein, E. & Skerra, A. Anticalins: exploiting a non-Ig scaffold with hypervariable loops for the engineering of binding proteins. FEBS Lett 588, 213-8 (2014).
98. Hey, T., Fiedler, E., Rudolph, R. & Fiedler, M. Artificial, non-antibody binding proteins for pharmaceutical and industrial applications. Trends Biotechnol 23, 514-22 (2005).
99. Smith, G. P. Filamentous fusion phage: novel expression vectors that display cloned antigens on the virion surface. Science 228, 1315-7 (1985).

100. Sanger, F. et al. Nucleotide sequence of bacteriophage phi X174 DNA. Nature 265, 687-95 (1977).
101. Pande, J., Szewczyk, M. M. & Grover, A. K. Phage display: Concept, innovations, applications and future. Biotechnol Adv 28, 849-58 (2010).
102. Lipovsek, D. & Pluckthun, A. In-vitro protein evolution by ribosome display and mRNA display. J Immunol Methods 290, 51-67 (2004).
103. Boder, E. T., Raeeszadeh-Sarmazdeh, M. & Price, J. V. Engineering antibodies by yeast display. Arch Biochem Biophys 526, 99-106 (2012).
104. Getz, J. A., Schoep, T. D. & Daugherty, P. S. Peptide Discovery Using Bacterial Display and Flow Cytometry. Methods Enzymol 503, 75-97 (2012).
105. Boder, E. T. & Wittrup, K. D. Yeast surface display for screening combinatorial polypeptide libraries. Nat Biotechnol 15, 553-7 (1997).
106. Traxlmayr, M. W. & Obinger, C. Directed evolution of proteins for increased stability and expression using yeast display. Arch Biochem Biophys 526, 174-80 (2012).
107. Richman, S. A., Kranz, D. M. & Stone, J. D. Biosensor detection systems: engineering stable, high-affinity bioreceptors by yeast surface display. Methods Mol Biol 504, 323-50 (2009).
108. Raymond, C. K., Pownder, T. A. & Sexson, S. L. General method for plasmid construction using homologous recombination. Biotechniques 26, 134-8, 140-1 (1999).
109. Rakestraw, J. A., Aird, D., Aha, P. M., Baynes, B. M. & Lipovsek, D. Secretion-and-capture cell-surface display for selection of target-binding proteins. Protein Eng Des Sel 24, 525-30 (2011).
110. Benatuil, L., Perez, J. M., Belk, J. & Hsieh, C. M. An improved yeast transformation method for the generation of very large human antibody libraries. Protein Eng Des Sel 23, 155-9 (2010).
111. VanAntwerp, J. J. & Wittrup, K. D. Fine affinity discrimination by yeast surface display and flow cytometry. Biotechnol Prog 16, 31-7 (2000).
112. Boder, E. T., Midelfort, K. S. & Wittrup, K. D. Directed evolution of antibody fragments with monovalent femtomolar antigen-binding affinity. Proc Natl Acad Sci U S A 97, 10701-5 (2000).
113. Kieke, M. C., Cho, B. K., Boder, E. T., Kranz, D. M. & Wittrup, K. D. Isolation of anti-T cell receptor scFv mutants by yeast surface display. Protein Eng 10, 1303-10 (1997).
114. Meusser, B., Hirsch, C., Jarosch, E. & Sommer, T. ERAD: the long road to destruction. Nat Cell Biol 7, 766-72 (2005).
115. Bowley, D. R., Labrijn, A. F., Zwick, M. B. & Burton, D. R. Antigen selection from an HIV-1 immune antibody library displayed on yeast yields many novel antibodies compared to selection from the same library displayed on phage. Protein Eng Des Sel 20, 81-90 (2007).
116. Blaise, L. et al. Construction and diversification of yeast cell surface displayed libraries by yeast mating: application to the affinity maturation of Fab antibody fragments. Gene 342, 211-8 (2004).
117. Weaver-Feldhaus, J. M. et al. Yeast mating for combinatorial Fab library generation and surface display. FEBS Lett 564, 24-34 (2004).
118. Walker, L. M., Bowley, D. R. & Burton, D. R. Efficient recovery of high-affinity antibodies from a single-chain Fab yeast display library. J Mol Biol 389, 365-75 (2009).
119. Wozniak-Knopp, G. et al. Introducing antigen-binding sites in structural loops of immunoglobulin constant domains: Fc fragments with engineered HER2/neu-binding sites and antibody properties. Protein Eng Des Sel 23, 289-97 (2010).
120. Dong, J. et al. A single-domain llama antibody potently inhibits the enzymatic activity of botulinum neurotoxin by binding to the non-catalytic alpha-exosite binding region. J Mol Biol 397, 1106-18 (2010).
121. Ryckaert, S., Pardon, E., Steyaert, J. & Callewaert, N. Isolation of antigen-binding camelid heavy chain antibody fragments (nanobodies) from an immune library displayed on the surface of Pichia pastoris. J Biotechnol 145, 93-8 (2010).
122. Graff, C. P., Chester, K., Begent, R. & Wittrup, K. D. Directed evolution of an anti-carcinoembryonic antigen scFv with a 4-day monovalent dissociation half-time at 37 degrees C. Protein Eng Des Sel 17, 293-304 (2004).

123. Orcutt, K. D. et al. Engineering an antibody with picomolar affinity to DOTA chelates of multiple radionuclides for pretargeted radioimmunotherapy and imaging. Nucl Med Biol 38, 223-33 (2011).
124. Hu, X., Kang, S., Lefort, C., Kim, M. & Jin, M. M. Combinatorial libraries against libraries for selecting neoepitope activation-specific antibodies. Proc Natl Acad Sci U S A 107, 6252-7 (2010).
125. Papo, N., Silverman, A. P., Lahti, J. L. & Cochran, J. R. Antagonistic VEGF variants engineered to simultaneously bind to and inhibit VEGFR2 and alphavbeta3 integrin. Proc Natl Acad Sci U S A 108, 14067-72 (2011).
126. Jones, D. S., 2nd, Tsai, P. C. & Cochran, J. R. Engineering hepatocyte growth factor fragments with high stability and activity as Met receptor agonists and antagonists. Proc Natl Acad Sci U S A 108, 13035-40 (2011).
127. Lahti, J. L. et al. Engineered epidermal growth factor mutants with faster binding on-rates correlate with enhanced receptor activation. FEBS Lett 585, 1135-9 (2011).
128. Shpilman, M. et al. Development and characterization of high affinity leptins and leptin antagonists. J Biol Chem 286, 4429-42 (2011).
129. Glotzbach, B. et al. Combinatorial optimization of cystine-knot peptides towards high-affinity inhibitors of human matriptase-1. PLoS One 8, e76956 (2013).
130. Moore, S. J. & Cochran, J. R. Engineering knottins as novel binding agents. Methods Enzymol 503, 223-51 (2012).
131. Silverman, A. P., Levin, A. M., Lahti, J. L. & Cochran, J. R. Engineered cystine-knot peptides that bind alpha(v)beta(3) integrin with antibody-like affinities. J Mol Biol 385, 1064-75 (2009).
132. Kimura, R. H. et al. Functional mutation of multiple solvent-exposed loops in the Ecballium elaterium trypsin inhibitor-II cystine knot miniprotein. PLoS One 6, e16112 (2011).
133. Koide, S., Koide, A. & Lipovsek, D. Target-binding proteins based on the 10th human fibronectin type III domain ((1)(0)Fn3). Methods Enzymol 503, 135-56 (2012).
134. Hackel, B. J., Kapila, A. & Wittrup, K. D. Picomolar affinity fibronectin domains engineered utilizing loop length diversity, recursive mutagenesis, and loop shuffling. J Mol Biol 381, 1238-52 (2008).
135. Gera, N., Hussain, M., Wright, R. C. & Rao, B. M. Highly stable binding proteins derived from the hyperthermophilic Sso7d scaffold. J Mol Biol 409, 601-16 (2011).
136. Chen, I., Dorr, B. M. & Liu, D. R. A general strategy for the evolution of bond-forming enzymes using yeast display. Proc Natl Acad Sci U S A 108, 11399-404 (2011).
137. Han, S. Y., Zhang, J. H., Han, Z. L., Zheng, S. P. & Lin, Y. Combination of site-directed mutagenesis and yeast surface display enhances Rhizomucor miehei lipase esterification activity in organic solvent. Biotechnol Lett 33, 2431-8 (2011).
138. Lee, G. Y. et al. Isomaltulose production via yeast surface display of sucrose isomerase from Enterobacter sp. FMB-1 on Saccharomyces cerevisiae. Bioresour Technol 102, 9179-84 (2011).
139. Parthasarathy, R., Bajaj, J. & Boder, E. T. An immobilized biotin ligase: surface display of Escherichia coli BirA on Saccharomyces cerevisiae. Biotechnol Prog 21, 1627-31 (2005).
140. Wen, F., Sun, J. & Zhao, H. Yeast surface display of trifunctional minicellulosomes for simultaneous saccharification and fermentation of cellulose to ethanol. Appl Environ Microbiol 76, 1251-60 (2010).
141. Colby, D. W. et al. Engineering antibody affinity by yeast surface display. Methods Enzymol 388, 348-58 (2004).
142. Wang, X. X. et al. Affinity maturation of human CD4 by yeast surface display and crystal structure of a CD4-HLA-DR1 complex. Proc Natl Acad Sci U S A 108, 15960-5 (2011).
143. Wen, F., Sethi, D. K., Wucherpfennig, K. W. & Zhao, H. Cell surface display of functional human MHC class II proteins: yeast display versus insect cell display. Protein Eng Des Sel 24, 701-9 (2011).

144. Boersma, Y. L., Chao, G., Steiner, D., Wittrup, K. D. & Pluckthun, A. Bispecific designed ankyrin repeat proteins (DARPins) targeting epidermal growth factor receptor inhibit A431 cell proliferation and receptor recycling. J Biol Chem 286, 41273-85 (2011).
145. Bidlingmaier, S. & Liu, B. Construction of yeast surface-displayed cDNA libraries. Methods Mol Biol 729, 199-210 (2011).
146. Schuijt, T. J. et al. Identification and characterization of Ixodes scapularis antigens that elicit tick immunity using yeast surface display. PLoS One 6, e15926 (2011).
147. Kantha, S. S. A centennial review; the 1890 tetanus antitoxin paper of von Behring and Kitasato and the related developments. Keio J Med 40, 35-9 (1991).
148. Tiselius, A. & Kabat, E. A. An Electrophoretic Study of Immune Sera and Purified Antibody Preparations. J Exp Med 69, 119-31 (1939).
149. Chaplin, D. D. Overview of the immune response. J Allergy Clin Immunol 125, 3-23 (2010).
150. Thomas, L. R., Cobb, R. M. & Oltz, E. M. Dynamic regulation of antigen receptor gene assembly. Adv Exp Med Biol 650, 103-15 (2009).
151. Huston, D. P. The biology of the immune system. Jama 278, 1804-14 (1997).
152. Bonilla, F. A. & Oettgen, H. C. Adaptive immunity. J Allergy Clin Immunol 125, S33-40 (2010).
153. Williams, A. F. & Barclay, A. N. The immunoglobulin superfamily--domains for cell surface recognition. Annu Rev Immunol 6, 381-405 (1988).
154. Terry, W. D. & Fahey, J. L. Subclasses of Human Gamma-2-Globulin Based on Differences in the Heavy Polypeptide Chains. Science 146, 400-1 (1964).
155. Smith, K. A. et al. Demystified...recombinant antibodies. J Clin Pathol 57, 912-7 (2004).
156. Leder, P. The genetics of antibody diversity. Sci Am 246, 102-15 (1982).
157. Tonegawa, S. Somatic generation of antibody diversity. Nature 302, 575-81 (1983).
158. Normansell, D. E. Human immunoglobulin subclasses. Diagn Clin Immunol 5, 115-28 (1987).
159. Torres, M. & Casadevall, A. The immunoglobulin constant region contributes to affinity and specificity. Trends Immunol 29, 91-7 (2008).
160. Nimmerjahn, F. & Ravetch, J. V. Antibodies, Fc receptors and cancer. Curr Opin Immunol 19, 239-45 (2007).
161. Ravetch, J. V. & Bolland, S. IgG Fc receptors. Annu Rev Immunol 19, 275-90 (2001).
162. Arnold, J. N., Wormald, M. R., Sim, R. B., Rudd, P. M. & Dwek, R. A. The impact of glycosylation on the biological function and structure of human immunoglobulins. Annu Rev Immunol 25, 21-50 (2007).
163. Liu, H., Bulseco, G. G. & Sun, J. Effect of posttranslational modifications on the thermal stability of a recombinant monoclonal antibody. Immunol Lett 106, 144-53 (2006).
164. Siberil, S. et al. Selection of a human anti-RhD monoclonal antibody for therapeutic use: impact of IgG glycosylation on activating and inhibitory Fc gamma R functions. Clin Immunol 118, 170-9 (2006).
165. Kanda, Y. et al. Comparison of biological activity among nonfucosylated therapeutic IgG1 antibodies with three different N-linked Fc oligosaccharides: the high-mannose, hybrid, and complex types. Glycobiology 17, 104-18 (2007).
166. Natsume, A. et al. Fucose removal from complex-type oligosaccharide enhances the antibody-dependent cellular cytotoxicity of single-gene-encoded antibody comprising a single-chain antibody linked the antibody constant region. J Immunol Methods 306, 93-103 (2005).
167. Raju, T. S. Terminal sugars of Fc glycans influence antibody effector functions of IgGs. Curr Opin Immunol 20, 471-8 (2008).
168. Khan, W. N. B cell receptor and BAFF receptor signaling regulation of B cell homeostasis. J Immunol 183, 3561-7 (2009).
169. Kurosaki, T. & Hikida, M. Tyrosine kinases and their substrates in B lymphocytes. Immunol Rev 228, 132-48 (2009).
170. Malisan, F. et al. Interleukin-10 induces immunoglobulin G isotype switch recombination in human CD40-activated naive B lymphocytes. J Exp Med 183, 937-47 (1996).
171. Chaudhuri, J. et al. Evolution of the immunoglobulin heavy chain class switch recombination mechanism. Adv Immunol 94, 157-214 (2007).

172. Schmidlin, H., Diehl, S. A. & Blom, B. New insights into the regulation of human B-cell differentiation. Trends Immunol 30, 277-85 (2009).

173. Burnet, F. M. The immunological significance of the thymus: an extension of the clonal selection theory of immunity. Australas Ann Med 11, 79-91 (1962).

174. Dorner, T., Foster, S. J., Farner, N. L. & Lipsky, P. E. Somatic hypermutation of human immunoglobulin heavy chain genes: targeting of RGYW motifs on both DNA strands. Eur J Immunol 28, 3384-96 (1998).

175. Rada, C., Ehrenstein, M. R., Neuberger, M. S. & Milstein, C. Hot spot focusing of somatic hypermutation in MSH2-deficient mice suggests two stages of mutational targeting. Immunity 9, 135-41 (1998).

176. Tangye, S. G. & Tarlinton, D. M. Memory B cells: effectors of long-lived immune responses. Eur J Immunol 39, 2065-75 (2009).

177. Hamers-Casterman, C. et al. Naturally occurring antibodies devoid of light chains. Nature 363, 446-8 (1993).

178. Blanc, M. R. et al. A one-step exclusion-binding procedure for the purification of functional heavy-chain and mammalian-type gamma-globulins from camelid sera. Biotechnol Appl Biochem 54, 207-12 (2009).

179. Alexander, A. et al. gamma Heavy chain disease in man: cDNA sequence supports partial gene deletion model. Proc Natl Acad Sci U S A 79, 3260-4 (1982).

180. Cogne, M., Preud'homme, J. L. & Guglielmi, P. Immunoglobulin gene alterations in human heavy chain diseases. Res Immunol 140, 487-502 (1989).

181. Decanniere, K., Muyldermans, S. & Wyns, L. Canonical antigen-binding loop structures in immunoglobulins: more structures, more canonical classes? J Mol Biol 300, 83-91 (2000).

182. Nguyen, V. K., Hamers, R., Wyns, L. & Muyldermans, S. Camel heavy-chain antibodies: diverse germline V(H)H and specific mechanisms enlarge the antigen-binding repertoire. Embo J 19, 921-30 (2000).

183. Harmsen, M. M. et al. Llama heavy-chain V regions consist of at least four distinct subfamilies revealing novel sequence features. Mol Immunol 37, 579-90 (2000).

184. Muyldermans, S., Atarhouch, T., Saldanha, J., Barbosa, J. A. & Hamers, R. Sequence and structure of VH domain from naturally occurring camel heavy chain immunoglobulins lacking light chains. Protein Eng 7, 1129-35 (1994).

185. Vu, K. B., Ghahroudi, M. A., Wyns, L. & Muyldermans, S. Comparison of llama VH sequences from conventional and heavy chain antibodies. Mol Immunol 34, 1121-31 (1997).

186. Chothia, C., Novotny, J., Bruccoleri, R. & Karplus, M. Domain association in immunoglobulin molecules. The packing of variable domains. J Mol Biol 186, 651-63 (1985).

187. Muyldermans, S., Cambillau, C. & Wyns, L. Recognition of antigens by single-domain antibody fragments: the superfluous luxury of paired domains. Trends Biochem Sci 26, 230-5 (2001).

188. Nguyen, V. K., Hamers, R., Wyns, L. & Muyldermans, S. Loss of splice consensus signal is responsible for the removal of the entire C(H)1 domain of the functional camel IGG2A heavy-chain antibodies. Mol Immunol 36, 515-24 (1999).

189. Woolven, B. P., Frenken, L. G., van der Logt, P. & Nicholls, P. J. The structure of the llama heavy chain constant genes reveals a mechanism for heavy-chain antibody formation. Immunogenetics 50, 98-101 (1999).

190. Maass, D. R., Sepulveda, J., Pernthaner, A. & Shoemaker, C. B. Alpaca (Lama pacos) as a convenient source of recombinant camelid heavy chain antibodies (VHHs). J Immunol Methods 324, 13-25 (2007).

191. van der Linden, R. H. et al. Comparison of physical chemical properties of llama VHH antibody fragments and mouse monoclonal antibodies. Biochim Biophys Acta 1431, 37-46 (1999).

192. Dumoulin, M. et al. Single-domain antibody fragments with high conformational stability. Protein Sci 11, 500-15 (2002).

193. Arbabi Ghahroudi, M., Desmyter, A., Wyns, L., Hamers, R. & Muyldermans, S. Selection and identification of single domain antibody fragments from camel heavy-chain antibodies. FEBS Lett 414, 521-6 (1997).

194. Saerens, D. et al. Single domain antibodies derived from dromedary lymph node and peripheral blood lymphocytes sensing conformational variants of prostate-specific antigen. J Biol Chem 279, 51965-72 (2004).

195. Coppieters, K. et al. Formatted anti-tumor necrosis factor alpha VHH proteins derived from camelids show superior potency and targeting to inflamed joints in a murine model of collagen-induced arthritis. Arthritis Rheum 54, 1856-66 (2006).

196. Baral, T. N. et al. Experimental therapy of African trypanosomiasis with a nanobody-conjugated human trypanolytic factor. Nat Med 12, 580-4 (2006).

197. Vincke, C. et al. General strategy to humanize a camelid single-domain antibody and identification of a universal humanized nanobody scaffold. J Biol Chem 284, 3273-84 (2009).

198. Barlow, J. N., Conrath, K. & Steyaert, J. Substrate-dependent modulation of enzyme activity by allosteric effector antibodies. Biochim Biophys Acta 1794, 1259-68 (2009).

199. Oyen, D., Srinivasan, V., Steyaert, J. & Barlow, J. N. Constraining enzyme conformational change by an antibody leads to hyperbolic inhibition. J Mol Biol 407, 138-48 (2011).

200. Conrath, K. E. et al. Beta-lactamase inhibitors derived from single-domain antibody fragments elicited in the camelidae. Antimicrob Agents Chemother 45, 2807-12 (2001).

201. Hendrickx, M. L. et al. TAFIa inhibiting nanobodies as profibrinolytic tools and discovery of a new TAFIa conformation. J Thromb Haemost 9, 2268-77 (2011).

202. Transue, T. R., De Genst, E., Ghahroudi, M. A., Wyns, L. & Muyldermans, S. Camel single-domain antibody inhibits enzyme by mimicking carbohydrate substrate. Proteins 32, 515-22 (1998).

203. Lauwereys, M. et al. Potent enzyme inhibitors derived from dromedary heavy-chain antibodies. Embo J 17, 3512-20 (1998).

204. Ledeboer, A. M. et al. Preventing phage lysis of Lactococcus lactis in cheese production using a neutralizing heavy-chain antibody fragment from llama. J Dairy Sci 85, 1376-82 (2002).

205. Stijlemans, B. et al. Efficient targeting of conserved cryptic epitopes of infectious agents by single domain antibodies. African trypanosomes as paradigm. J Biol Chem 279, 1256-61 (2004).

206. Cortez-Retamozo, V. et al. Efficient cancer therapy with a nanobody-based conjugate. Cancer Res 64, 2853-7 (2004).

207. Ismaili, A. et al. Production and characterization of anti-(mucin MUC1) single-domain antibody in tobacco (Nicotiana tabacum cultivar Xanthi). Biotechnol Appl Biochem 47, 11-9 (2007).

208. Frenken, L. G., Hessing, J. G., Van den Hondel, C. A. & Verrips, C. T. Recent advances in the large-scale production of antibody fragments using lower eukaryotic microorganisms. Res Immunol 149, 589-99 (1998).

209. Frenken, L. G. et al. Isolation of antigen specific llama VHH antibody fragments and their high level secretion by Saccharomyces cerevisiae. J Biotechnol 78, 11-21 (2000).

210. Arbabi-Ghahroudi, M., Tanha, J. & MacKenzie, R. Prokaryotic expression of antibodies. Cancer Metastasis Rev 24, 501-19 (2005).

211. van der Linden, R. et al. Induction of immune responses and molecular cloning of the heavy chain antibody repertoire of Lama glama. J Immunol Methods 240, 185-95 (2000).

212. Davies, J. & Riechmann, L. Antibody VH domains as small recognition units. Biotechnology (N Y) 13, 475-9 (1995).

213. Tanha, J. et al. Optimal design features of camelized human single-domain antibody libraries. J Biol Chem 276, 24774-80 (2001).

214. Chames, P. & Baty, D. Bispecific antibodies for cancer therapy. Curr Opin Drug Discov Devel 12, 276-83 (2009).

215. Emmerson, C. D. et al. Enhancement of polymeric immunoglobulin receptor transcytosis by biparatopic VHH. PLoS One 6, e26299 (2011).

216. Hmila, I. et al. VHH, bivalent domains and chimeric Heavy chain-only antibodies with high neutralizing efficacy for scorpion toxin AahI'. Mol Immunol 45, 3847-56 (2008).

217. Bell, A. et al. Differential tumor-targeting abilities of three single-domain antibody formats. Cancer Lett 289, 81-90 (2010).

218. de Marco, A. Biotechnological applications of recombinant single-domain antibody fragments. Microb Cell Fact 10, 44 (2011).

219. Wesolowski, J. et al. Single domain antibodies: promising experimental and therapeutic tools in infection and immunity. Med Microbiol Immunol 198, 157-74 (2009).

220. Harmsen, M. M. & De Haard, H. J. Properties, production, and applications of camelid single-domain antibody fragments. Appl Microbiol Biotechnol 77, 13-22 (2007).

221. Perez-Martinez, D., Tanaka, T. & Rabbitts, T. H. Intracellular antibodies and cancer: new technologies offer therapeutic opportunities. Bioessays 32, 589-98 (2010).

222. Tanaka, T., Sewell, H., Waters, S., Phillips, S. E. & Rabbitts, T. H. Single domain intracellular antibodies from diverse libraries: emphasizing dual functions of LMO2 protein interactions using a single VH domain. J Biol Chem 286, 3707-16 (2011).

223. Rothbauer, U. et al. A versatile nanotrap for biochemical and functional studies with fluorescent fusion proteins. Mol Cell Proteomics 7, 282-9 (2008).

224. Schmidthals, K., Helma, J., Zolghadr, K., Rothbauer, U. & Leonhardt, H. Novel antibody derivatives for proteome and high-content analysis. Anal Bioanal Chem 397, 3203-8 (2010).

225. Romer, T., Leonhardt, H. & Rothbauer, U. Engineering antibodies and proteins for molecular in vivo imaging. Curr Opin Biotechnol 22, 882-7 (2011).

226. Koide, S. Engineering of recombinant crystallization chaperones. Curr Opin Struct Biol 19, 449-57 (2009).

227. Kirchhofer, A. et al. Modulation of protein properties in living cells using nanobodies. Nat Struct Mol Biol 17, 133-8 (2010).

228. Broisat, A. et al. Nanobodies targeting mouse/human VCAM1 for the nuclear imaging of atherosclerotic lesions. Circ Res 110, 927-37 (2012).

229. Vaneycken, I. et al. Preclinical screening of anti-HER2 nanobodies for molecular imaging of breast cancer. Faseb J 25, 2433-46 (2011).

230. Vosjan, M. J. et al. Facile labelling of an anti-epidermal growth factor receptor Nanobody with 68Ga via a novel bifunctional desferal chelate for immuno-PET. Eur J Nucl Med Mol Imaging 38, 753-63 (2011).

231. Vaneycken, I. et al. Immuno-imaging using nanobodies. Curr Opin Biotechnol 22, 877-81 (2011).

232. Kontermann, R. E. Strategies for extended serum half-life of protein therapeutics. Curr Opin Biotechnol 22, 868-76 (2011).

233. Iqbal, U. et al. Kinetic analysis of novel mono- and multivalent VHH-fragments and their application for molecular imaging of brain tumours. Br J Pharmacol 160, 1016-28 (2010).

234. Perruchini, C. et al. Llama VHH antibody fragments against GFAP: better diffusion in fixed tissues than classical monoclonal antibodies. Acta Neuropathol 118, 685-95 (2009).

235. Li, T. et al. Cell-penetrating anti-GFAP VHH and corresponding fluorescent fusion protein VHH-GFP spontaneously cross the blood-brain barrier and specifically recognize astrocytes: application to brain imaging. Faseb J 26, 3969-79 (2012).

236. Holz, J. B. The TITAN trial--assessing the efficacy and safety of an anti-von Willebrand factor Nanobody in patients with acquired thrombotic thrombocytopenic purpura. Transfus Apher Sci 46, 343-6 (2012).

237. Flajnik, M. F. & Rumfelt, L. L. The immune system of cartilaginous fish. Curr Top Microbiol Immunol 248, 249-70 (2000).

238. Dooley, H. & Flajnik, M. F. Antibody repertoire development in cartilaginous fish. Dev Comp Immunol 30, 43-56 (2006).

239. Clem, I. W., De Boutaud, F. & Sigel, M. M. Phylogeny of immunoglobulin structure and function. II. Immunoglobulins of the nurse shark. J Immunol 99, 1226-35 (1967).

240. Greenberg, A. S. et al. A new antigen receptor gene family that undergoes rearrangement and extensive somatic diversification in sharks. Nature 374, 168-73 (1995).

241. Barelle, C., Gill, D. S. & Charlton, K. Shark novel antigen receptors--the next generation of biologic therapeutics? Adv Exp Med Biol 655, 49-62 (2009).

242. Rumfelt, L. L., Diaz, M., Lohr, R. L., Mochon, E. & Flajnik, M. F. Unprecedented multiplicity of Ig transmembrane and secretory mRNA forms in the cartilaginous fish. J Immunol 173, 1129-39 (2004).

243. Diaz, M., Greenberg, A. S. & Flajnik, M. F. Somatic hypermutation of the new antigen receptor gene (NAR) in the nurse shark does not generate the repertoire: possible role in antigen-driven reactions in the absence of germinal centers. Proc Natl Acad Sci U S A 95, 14343-8 (1998).

244. Streltsov, V. A. et al. Structural evidence for evolution of shark Ig new antigen receptor variable domain antibodies from a cell-surface receptor. Proc Natl Acad Sci U S A 101, 12444-9 (2004).

245. Diaz, M., Velez, J., Singh, M., Cerny, J. & Flajnik, M. F. Mutational pattern of the nurse shark antigen receptor gene (NAR) is similar to that of mammalian Ig genes and to spontaneous mutations in evolution: the translesion synthesis model of somatic hypermutation. Int Immunol 11, 825-33 (1999).

246. Du Pasquier, L., Wilson, M., Greenberg, A. S. & Flajnik, M. F. Somatic mutation in ectothermic vertebrates: musings on selection and origins. Curr Top Microbiol Immunol 229, 199-216 (1998).

247. Roux, K. H. et al. Structural analysis of the nurse shark (new) antigen receptor (NAR): molecular convergence of NAR and unusual mammalian immunoglobulins. Proc Natl Acad Sci U S A 95, 11804-9 (1998).

248. Stanfield, R. L., Dooley, H., Flajnik, M. F. & Wilson, I. A. Crystal structure of a shark single-domain antibody V region in complex with lysozyme. Science 305, 1770-3 (2004).

249. Diaz, M., Stanfield, R. L., Greenberg, A. S. & Flajnik, M. F. Structural analysis, selection, and ontogeny of the shark new antigen receptor (IgNAR): identification of a new locus preferentially expressed in early development. Immunogenetics 54, 501-12 (2002).

250. Criscitiello, M. F. & Flajnik, M. F. Four primordial immunoglobulin light chain isotypes, including lambda and kappa, identified in the most primitive living jawed vertebrates. Eur J Immunol 37, 2683-94 (2007).

251. Hinds, K. R. & Litman, G. W. Major reorganization of immunoglobulin VH segmental elements during vertebrate evolution. Nature 320, 546-9 (1986).

252. Lee, V. et al. The evolution of multiple isotypic IgM heavy chain genes in the shark. J Immunol 180, 7461-70 (2008).

253. Kokubu, F., Litman, R., Shamblott, M. J., Hinds, K. & Litman, G. W. Diverse organization of immunoglobulin VH gene loci in a primitive vertebrate. Embo J 7, 3413-22 (1988).

254. Lee, S. S., Fitch, D., Flajnik, M. F. & Hsu, E. Rearrangement of immunoglobulin genes in shark germ cells. J Exp Med 191, 1637-48 (2000).

255. Lee, S. S., Greenberg, A. & Hsu, E. Evolution and somatic diversification of immunoglobulin light chains. Curr Top Microbiol Immunol 248, 285-300 (2000).

256. Rumfelt, L. L. et al. A shark antibody heavy chain encoded by a nonsomatically rearranged VDJ is preferentially expressed in early development and is convergent with mammalian IgG. Proc Natl Acad Sci U S A 98, 1775-80 (2001).

257. Malecek, K. et al. Somatic hypermutation and junctional diversification at Ig heavy chain loci in the nurse shark. J Immunol 175, 8105-15 (2005).

258. Bartl, S. et al. Terminal deoxynucleotidyl transferases from elasmobranchs reveal structural conservation within vertebrates. Immunogenetics 55, 594-604 (2003).

259. Marchalonis, J. & Edelman, G. M. Phylogenetic origins of antibody structure. I. Multichain structure of immunoglobulins in the smooth dogfish (Mustelus canis). J Exp Med 122, 601-18 (1965).

260. Marchalonis, J. & Edelman, G. M. Polypeptide chains of immunoglobulins from the smooth dogfish (Mustelus canis). Science 154, 1567-8 (1966).

261. Clem, L. W. & Small, P. A., Jr. Phylogeny of immunoglobulin structure and function. I. Immunoglobulins of the lemon shark. J Exp Med 125, 893-920 (1967).

262. Dooley, H. & Flajnik, M. F. Shark immunity bites back: affinity maturation and memory response in the nurse shark, Ginglymostoma cirratum. Eur J Immunol 35, 936-45 (2005).

263. Fange, R. & Pulsford, A. Structural studies on lymphomyeloid tissues of the dogfish, Scyliorhinus canicula L. Cell Tissue Res 230, 337-51 (1983).
264. Rumfelt, L. L., McKinney, E. C., Taylor, E. & Flajnik, M. F. The development of primary and secondary lymphoid tissues in the nurse shark Ginglymostoma cirratum: B-cell zones precede dendritic cell immigration and T-cell zone formation during ontogeny of the spleen. Scand J Immunol 56, 130-48 (2002).
265. Liu, J. L. et al. Selection of cholera toxin specific IgNAR single-domain antibodies from a naive shark library. Mol Immunol 44, 1775-83 (2007).
266. Dooley, H., Flajnik, M. F. & Porter, A. J. Selection and characterization of naturally occurring single-domain (IgNAR) antibody fragments from immunized sharks by phage display. Mol Immunol 40, 25-33 (2003).
267. Shao, C. Y., Secombes, C. J. & Porter, A. J. Rapid isolation of IgNAR variable single-domain antibody fragments from a shark synthetic library. Mol Immunol 44, 656-65 (2007).
268. Malecek, K. et al. Immunoglobulin heavy chain exclusion in the shark. PLoS Biol 6, e157 (2008).
269. Nuttall, S. D. et al. A naturally occurring NAR variable domain binds the Kgp protease from Porphyromonas gingivalis. FEBS Lett 516, 80-6 (2002).
270. Nuttall, S. D. et al. Isolation and characterization of an IgNAR variable domain specific for the human mitochondrial translocase receptor Tom70. Eur J Biochem 270, 3543-54 (2003).
271. Nuttall, S. D. et al. Selection and affinity maturation of IgNAR variable domains targeting Plasmodium falciparum AMA1. Proteins 55, 187-97 (2004).
272. Zielonka, S. et al. Shark Attack: high affinity binding proteins derived from shark vNAR domains by stepwise in vitro affinity maturation. J Biotechnol 191, 236-45 (2014).
273. Nuttall, S. D. et al. Isolation of the new antigen receptor from wobbegong sharks, and use as a scaffold for the display of protein loop libraries. Mol Immunol 38, 313-26 (2001).
274. Simmons, D. P. et al. Dimerisation strategies for shark IgNAR single domain antibody fragments. J Immunol Methods 315, 171-84 (2006).
275. Chiche, L. et al. Squash inhibitors: from structural motifs to macrocyclic knottins. Curr Protein Pept Sci 5, 341-349 (2004).
276. Gracy, J. et al. KNOTTIN: the knottin or inhibitor cystine knot scaffold in 2007. Nucleic Acids Res 36, D314-9 (2008).
277. Reinwarth, M., Nasu, D., Kolmar, H. & Avrutina, O. Chemical synthesis, backbone cyclization and oxidative folding of cystine-knot peptides: promising scaffolds for applications in drug design. Molecules 17, 12533-52 (2012).
278. Gelly, J. C. et al. The KNOTTIN website and database: a new information system dedicated to the knottin scaffold. Nucleic Acids Res 32, D156-9 (2004).
279. Werle, M., Kafedjiiski, K., Kolmar, H. & Bernkop-Schnurch, A. Evaluation and improvement of the properties of the novel cystine-knot microprotein McoEeTI for oral administration. Int J Pharm 332, 72-9 (2007).
280. Werle, M., Kolmar, H., Albrecht, R. & Bernkop-Schnurch, A. Characterisation of the barrier caused by luminally secreted gastro-intestinal proteolytic enzymes for two novel cystine-knot microproteins. Amino Acids 35, 195-200 (2008).
281. Werle, M. et al. The potential of cystine-knot microproteins as novel pharmacophoric scaffolds in oral peptide drug delivery. J Drug Target 14, 137-46 (2006).
282. Puttamadappa, S. S., Jagadish, K., Shekhtman, A. & Camarero, J. A. Backbone dynamics of cyclotide MCoTI-I free and complexed with trypsin. Angew Chem Int Ed Engl 49, 7030-4 (2010).
283. Craik, D. J. Discovery and applications of the plant cyclotides. Toxicon 56, 1092-102 (2010).
284. Craik, D. J., Cemazar, M. & Daly, N. L. The cyclotides and related macrocyclic peptides as scaffolds in drug design. Curr Opin Drug Discov Devel 9, 251-60 (2006).
285. Craik, D. J., Cemazar, M. & Daly, N. L. The chemistry and biology of cyclotides. Curr Opin Drug Discov Devel 10, 176-84 (2007).

286. Daly, N. L. & Craik, D. J. Bioactive cystine knot proteins. Curr Opin Chem Biol 15, 362-8 (2011).

287. Hernandez, J. F. et al. Squash trypsin inhibitors from Momordica cochinchinensis exhibit an atypical macrocyclic structure. Biochemistry 39, 5722-30 (2000).

288. Daly, N. L., Love, S., Alewood, P. F. & Craik, D. J. Chemical synthesis and folding pathways of large cyclic polypeptides: studies of the cystine knot polypeptide kalata B1. Biochemistry 38, 10606-14 (1999).

289. Tam, J. P., Lu, Y. A., Yang, J. L. & Chiu, K. W. An unusual structural motif of antimicrobial peptides containing end-to-end macrocycle and cystine-knot disulfides. Proc Natl Acad Sci U S A 96, 8913-8 (1999).

290. Jennings, C., West, J., Waine, C., Craik, D. & Anderson, M. Biosynthesis and insecticidal properties of plant cyclotides: the cyclic knotted proteins from Oldenlandia affinis. Proc Natl Acad Sci U S A 98, 10614-9 (2001).

291. Favel, A. et al. Protease inhibitors from Ecballium elaterium seeds. Int J Pept Protein Res 33, 202-8 (1989).

292. Felizmenio-Quimio, M. E., Daly, N. L. & Craik, D. J. Circular proteins in plants: solution structure of a novel macrocyclic trypsin inhibitor from Momordica cochinchinensis. J Biol Chem 276, 22875-82 (2001).

293. Bode, W., Greyling, H. J., Huber, R., Otlewski, J. & Wilusz, T. The refined 2.0 A X-ray crystal structure of the complex formed between bovine beta-trypsin and CMTI-I, a trypsin inhibitor from squash seeds (Cucurbita maxima). Topological similarity of the squash seed inhibitors with the carboxypeptidase A inhibitor from potatoes. FEBS Lett 242, 285-92 (1989).

294. Kimura, R. H., Cheng, Z., Gambhir, S. S. & Cochran, J. R. Engineered knottin peptides: a new class of agents for imaging integrin expression in living subjects. Cancer Res 69, 2435-42 (2009).

295. Sommerhoff, C. P. et al. Engineered cystine knot miniproteins as potent inhibitors of human mast cell tryptase beta. J Mol Biol 395, 167-75 (2010).

296. Christmann, A., Walter, K., Wentzel, A., Kratzner, R. & Kolmar, H. The cystine knot of a squash-type protease inhibitor as a structural scaffold for Escherichia coli cell surface display of conformationally constrained peptides. Protein Eng 12, 797-806 (1999).

297. Avrutina, O. et al. Head-to-tail cyclized cystine-knot peptides by a combined recombinant and chemical route of synthesis. Chembiochem 9, 33-7 (2008).

298. Stricher, F. et al. Combinatorial optimization of a CD4-mimetic miniprotein and cocrystal structures with HIV-1 gp120 envelope glycoprotein. J Mol Biol 382, 510-24 (2008).

299. Jiang, L. et al. 111In-labeled cystine-knot peptides based on the Agouti-related protein for targeting tumor angiogenesis. J Biomed Biotechnol 2012, 368075 (2012).

300. Reinwarth, M. et al. Oxidative folding of peptides with cystine-knot architectures: kinetic studies and optimization of folding conditions. Chembiochem 14, 137-46 (2013).

301. Sun, X., Goh, P. E., Wong, K. T., Mori, T. & Yap, M. G. Enhancement of transient gene expression by fed-batch culture of HEK 293 EBNA1 cells in suspension. Biotechnol Lett 28, 843-8 (2006).

302. Hermanson, G. T. Bioconjugate Techniques (Elsevier, 2008).

303. Hermanson, G. T. Bioconjugate Techniques (Elsevier, 2008).

304. Mojsov, S. & Merrifield, R. B. An improved synthesis of crystalline mammalian glucagon. Eur J Biochem 145, 601-5 (1984).

305. Knight, C. G., Willenbrock, F. & Murphy, G. A novel coumarin-labelled peptide for sensitive continuous assays of the matrix metalloproteinases. FEBS Lett 296, 263-6 (1992).

306. Chao, G. et al. Isolating and engineering human antibodies using yeast surface display. Nat Protoc 1, 755-68 (2006).

307. Dickgießer, S. in Chemie (TU Darmstadt, Darmstadt, 2016).

308. Pace, C. N., Vajdos, F., Fee, L., Grimsley, G. & Gray, T. How to measure and predict the molecular absorption coefficient of a protein. Protein Sci 4, 4211-23 (1995).

309. Steinmann, B. in Clemens-Schöpf-Institut (TU-Darmstadt, Darmstadt, 2015).

310. Maass, F. et al. Cystine-knot peptides targeting cancer-relevant human cytotoxic T lymphocyte-associated antigen 4 (CTLA-4). J Pept Sci 21, 651-60 (2015).
311. Zielonka, S. in Chemistry (TU-Darmstadt, Darmstadt, 2015).
312. Zielonka, S. et al. The Shark Strikes Twice: Hypervariable Loop 2 of Shark IgNAR Antibody Varaible Domains and Its Potential to Function as an Autonomous Paratope. Mar Biotechnol 17, 386-92 (2015).
313. Könning, D. et al. Camelid and shark single domain antibodies: structural feautures and therapeutic potetial. Curr Opin Struct Biol 45, 10-16 (2016).
314. Sawa, J., Heuck, A., Ehrmann, M. & Clausen, T. Molecular transformers in the cell: lessons learned from the DegP protease-chaperone. Curr Opin Struct Biol 20, 253-8 (2010).
315. Krojer, T., Garrido-Franco, M., Huber, R., Ehrmann, M. & Clausen, T. Crystal structure of DegP (HtrA) reveals a new protease-chaperone machine. Nature 416, 455-9 (2002).
316. Jiang, J. et al. Activation of DegP chaperone-protease via formation of large cage-like oligomers upon binding to substrate proteins. Proc Natl Acad Sci U S A 105, 11939-44 (2008).
317. Tocharus, J. et al. Developmentally regulated expression of mouse HtrA3 and its role as an inhibitor of TGF-beta signaling. Dev Growth Differ 46, 257-74 (2004).
318. Hauske, P. et al. Selectivity profiling of DegP substrates and inhibitors. Bioorg & Med Chem 17, 2920-24 (2009).
319. Nam, M. K. et al. The homotrimeric structure of HtrA2 is indispensable for executing its serine protease activity. Exp Mol Med 38, 36-43 (2006).
320. Boehr, D. D. & Wright, P. E. How Do Proteins Interact? Science 320, 1429-30 (2008).
321. Changeux, J. P. & Edelstein, S. Conformational selection or induced fit? 50 years of debate resolved. F1000 Biol Rep 3, 19 (2011).
322. Hasselblatt, H. et al. Regulation of the sigmaE stress response by DegS: how the PDZ domain keeps the protease inactive in the resting state and allows integration of different OMP-derived stress signals upon folding stress. Genes Dev 21, 2659-70 (2007).
323. Wilken, C., Kitzing, K., Kurzbauer, R., Ehrmann, M. & Clausen, T. Crystal structure of the DegS stress sensor: How a PDZ domain recognizes misfolded protein and activates a protease. Cell 117, 483-94 (2004).
324. Jo, H., Patterson, V., Stoessel, S., Kuan, C. Y. & Hoh, J. Protoporphyrins enhance oligomerization and enzymatic activity of HtrA1 serine protease. PLoS One 9, e115362 (2014).
325. Krojer, T., Sawa, J., Huber, R. & Clausen, T. HtrA proteases have a conserved activation mechanism that can be triggered by distinct molecular cues. Nat Struct Mol Biol 7, 844-52 (2010).
326. Merdanovic, M. et al. Determinants of structural and functional plasticity of a widely conserved protease chaperone complex. Nat Struct Mol Biol 7, 837-43 (2010).
327. Sommerhoff, C. P. et al. Engineered cystine knot miniproteins as potent inhibitors of human mast cell tryptase beta. J Mol Biol 395, 167-75 (2009).
328. Ernst, R. E., High, K. N., Glass, T. R. & Zhao, Q. in Therapeutic Monoclonal Antibodies: From Bench to Clinic (ed. An, Z.) (John Wiley & Sons Inc., Hoboken, New Jersey, 2009).
329. Gibson, C. R., andhu, P. & Hanley, W. D. in Therapeutic Monoclonal Antibodies: From Bench to Clinic (ed. An, Z.) (John Wiley & Sons Inc., Hoboken, New Jersey, 2009).
330. Puorger, C. et al. Infinite kinetic stability against dissociation of supramolecular protein complexes through donor strand complementation. Structure 16, 631-42 (2008).
331. Lorey, S. et al. Novel ubiquitin-derived high affinity binding proteins with tumor targeting properties. J Biol Chem 289, 8493-507 (2014).
332. Mahon, C. M. et al. Comprehensive interrogation of a minimalist synthetic CDR-H3 library and its ability to generate antibodies with therapeutic potential. J Mol Biol 425, 1712-30 (2013).
333. Gai, S. A. & Wittrup, K. D. Yeast surface display for protein engineering and characterization. Curr Opin Struct Biol 17, 467-73 (2007).
334. Lipovsek, D. et al. Evolution of an interloop disulfide bond in high-affinity antibody mimics based on fibronectin type III domain and selected by yeast surface display: molecular

convergence with single-domain camelid and shark antibodies. J Mol Biol 368, 1024-41 (2007).

335. Ciferri, C. et al. The trimeric serine protease HtrA1 forms a cage-like inhibition complex with an anti-HtrA1 antibody. Biochem J 472, 169-81 (2015).
336. Singh, H., Nero, T. L., Wang, Y., Parker, M. W. & Nie, G. Activity-modulating monoclonal antibodies to the human serine protease HtrA3 provide novel insights into regulating HtrA proteolytic activities. PLoS One 9, e108235 (2014).
337. Krowarsch, D., Cierpicki, T., Jelen, F. & Otlewski, J. Canonical protein inhibitors of serine proteases. Cell Mol Life Sci 60, 2427-44 (2003).
338. Daly, N. L. et al. Structural insights into the role of the cyclic backbone in a squash trypsin inhibitor. J Biol Chem 288, 36141-8 (2013).
339. Boder, E. T. & Jiang, W. Engineering antibodies for cancer therapy. Annu Rev Chem Biomol Eng 2, 53-75 (2011).
340. Wark, K. L. & Hudson, P. J. Latest technologies for the enhancement of antibody affinity. Adv Drug Deliv Rev 58, 657-70 (2006).
341. Morrison, K. L. & Weiss, G. A. Combinatorial alanine-scanning. Curr Opin Chem Biol 5, 302-7 (2001).
342. Mayer, M. & Meyer, B. Group epitope mapping by saturation transfer difference NMR to identify segments of a ligand in direct contact with a protein receptor. J Am Chem Soc 135, 6108-17 (2001).
343. Wolff, E. A., Schreiber, G. J., Cosand, W. L. & Raff, H. V. Monoclonal antibody homodimers: enhanced antitumor activity in nude mice. Cancer Res 53, 2560-5 (1993).
344. Rahbarizadeh, F., Ahmadvand, D. & Sharifzadeh, Z. Nanobody; an old concept and new vehicle for immunotargeting. Immunol Invest 40, 299-338 (2011).
345. Muller, M. R. et al. Improving the pharmacokinetic properties of biologics by fusion to an anti-HSA shark VNAR domain. MAbs 4, 673-85 (2012).
346. Bendele, A. M. Animal models of osteoarthritis. J Musculoskelet Neuronal Interact 1, 363-76 (2001).
347. Luck, B. in Clemens-Schöpf-Institut (TU Darmstadt, Darmstadt, 2013).
348. Dementiev, A., Dobo, J. & Gettins, P. G. Active site distortion is sufficient for proteinase inhibition by serpins: structure of the covalent complex of alpha1-proteinase inhibitor with porcine pancreatic elastase. J Biol Chem 281, 3452-7 (2006).
349. Frochaux, V., Hildebrand, D., Talke, A., Linscheid, M. W. & Schluter, H. Alpha-1-antitrypsin: a novel human high temperature requirement protease A1 (HTRA1) substrate in human placental tissue. PLoS One 9, e109483 (2014).

8. Appendix

8.1. Appendix A: Fitted data of K_D values of single clones determined by yeast surface display

KH01

KH02

KH03

KH05

KC01

KC02

KC03

KC05

KHC01

KHC03

KHC04

KHC05

KHC06

KHC08

KHC11

KHC12
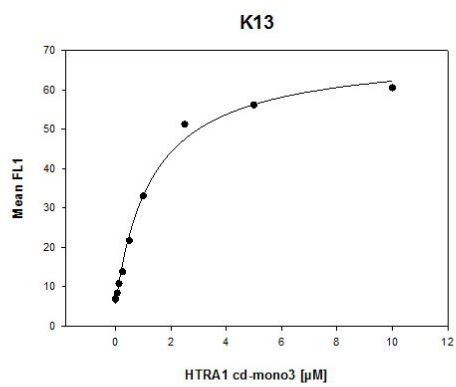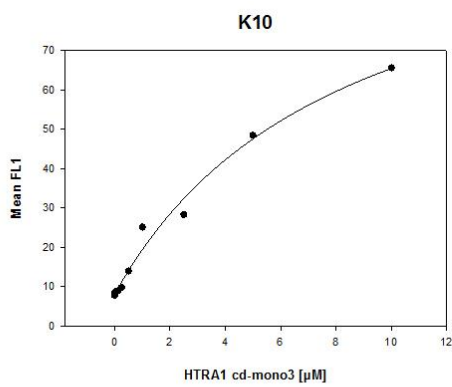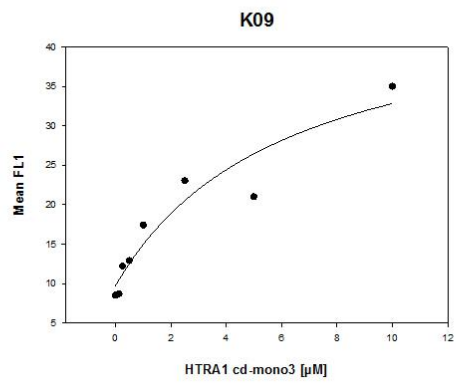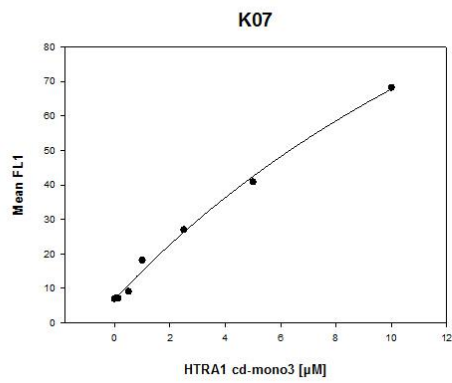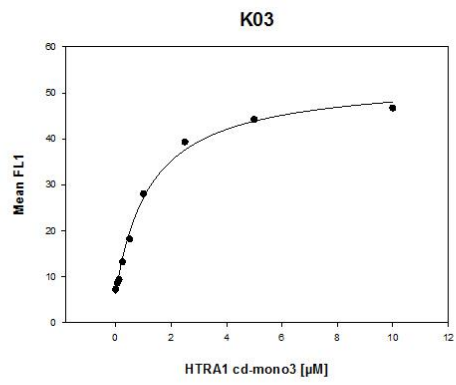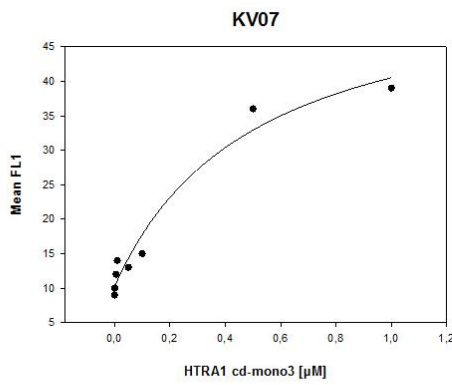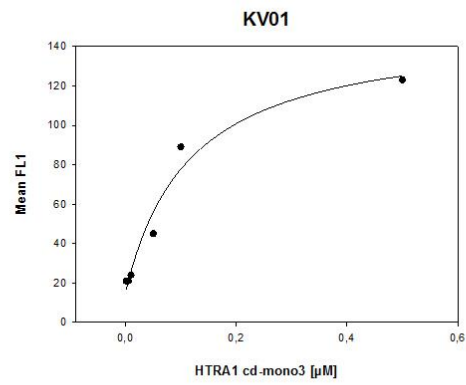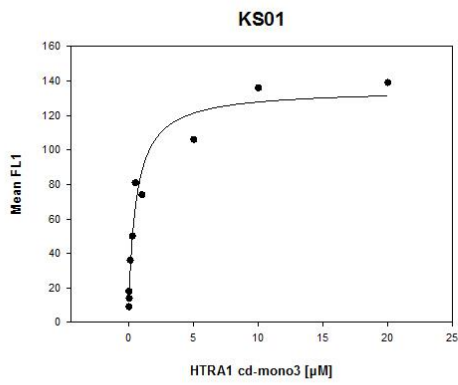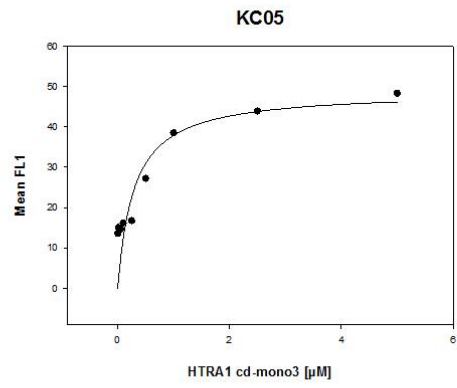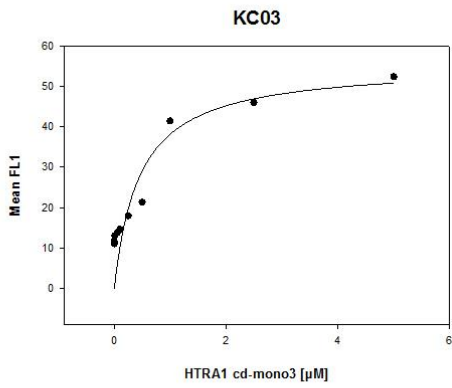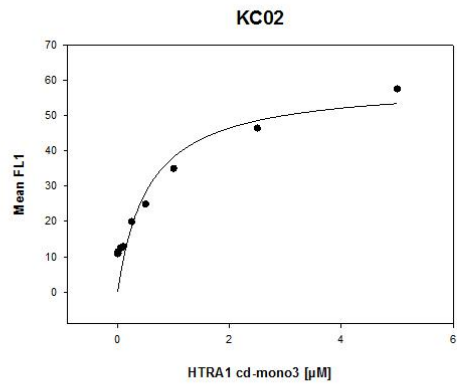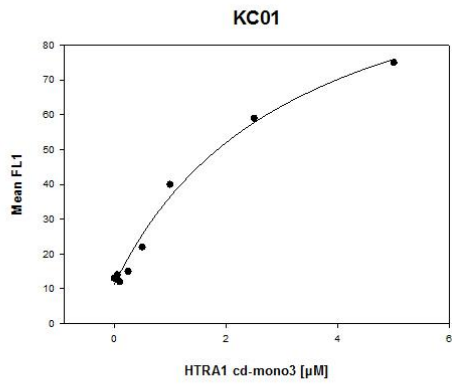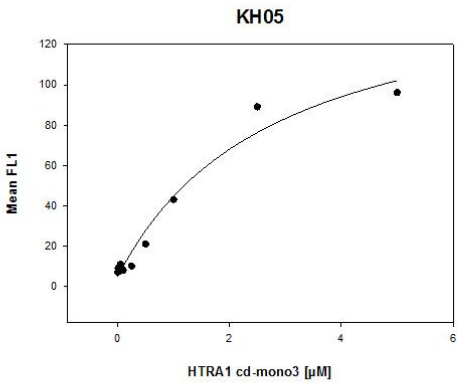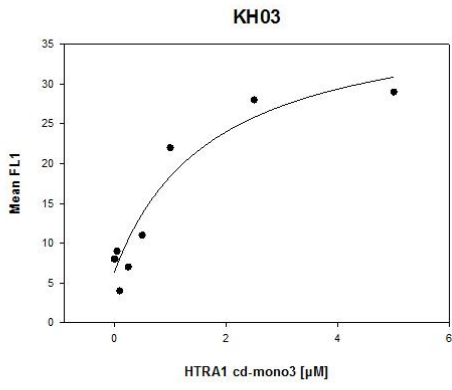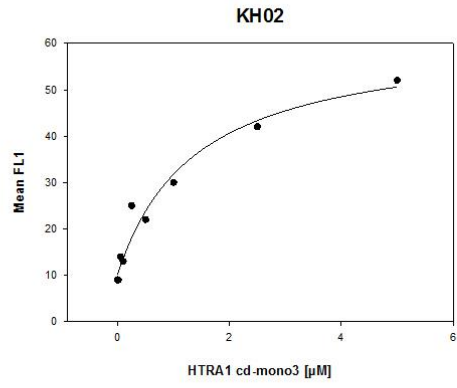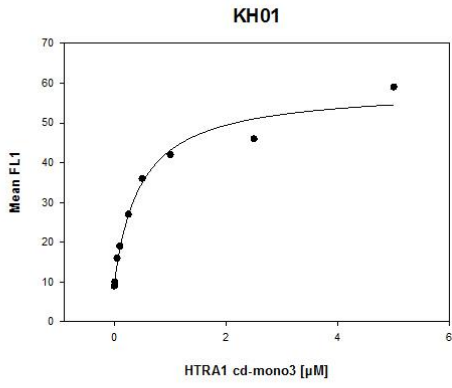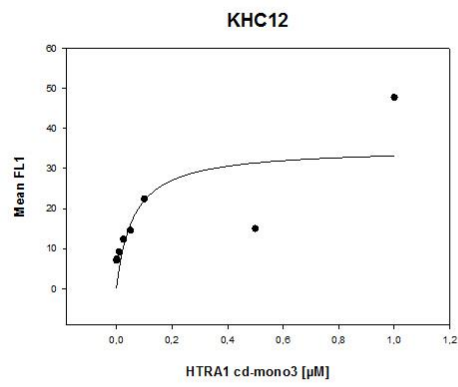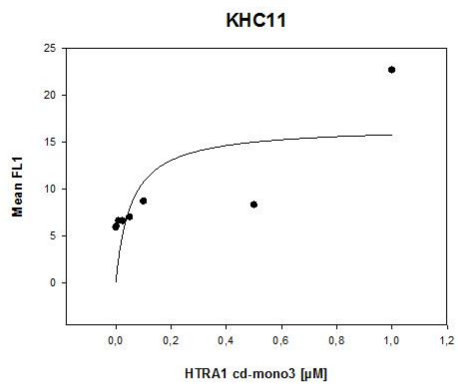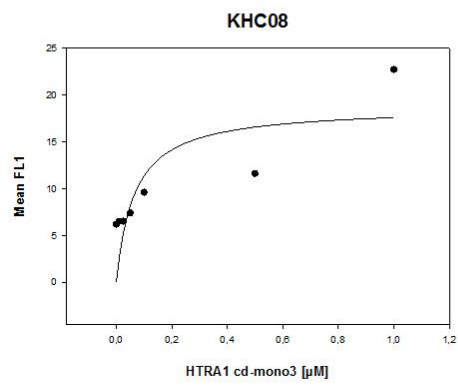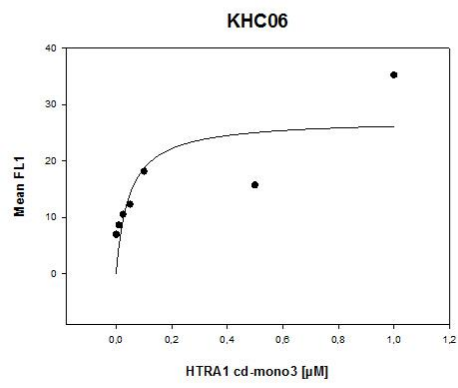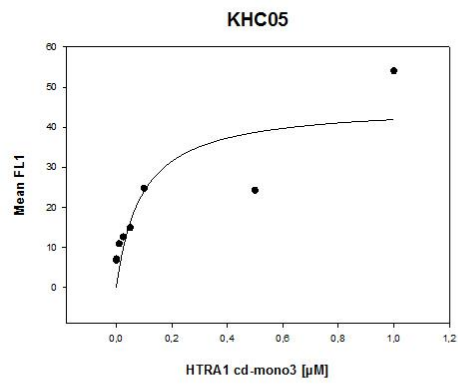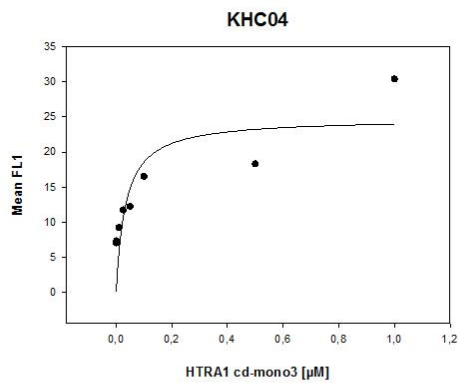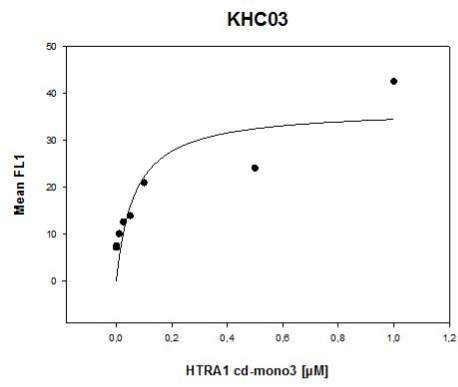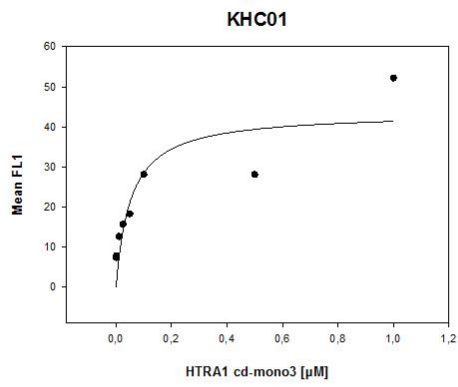
8.2. Appendix B: Abbreviations

A	Adenine
aa	Amino acid(s)
ADCC	Antibody-dependent cellular cytotoxicity
Aga1p	a-agglutinin anchoring subunit 1
Aga2p	a-agglutinin anchoring subunit 2
amp	Ampicillin
APC	Allophycocyanin
APS	Ammonium persulfate
bp	basepairs
BSA	Bovine serum albumin
C	Cytosine
CDC	Complement-dependent cytotoxicity
CDR	Complementarity determining region
CH	Constant domain of the heavy chain
CL	Constant domain of the light chain
Cm	Chloramphenicol
DMF	Dimethylformamide
DMSO	Dimethyl sulfoxide
DNA	Deoxyribonucleic acid
dNTP	Deoxynucleoside triphosphate
DTT	Dithiothreitol
dYT	Double concentrated yeast extract tryptone
E. coli	*Escherichia coli*
ECM	Extracellular matrix
EDTA	Ethylenediaminetetraacetic acid
EpCAM	Epithelial cell adhesion molecule
EphA2	Receptor tyrosine kinase EphA2
Fab	Fragment antigen binding
FACS	Fluorescence-activated cell sorting
Fc	Fragment crytalizable
Fcγ	Fc-part of IgG1
FcRn	Neonatal Fc receptor
FDA	US Food and Drug Administration
FITC	Fluorescein isothiocyanate
FPLC	Fast Protein Liquid Chromatography

Fv	fragment variable
G	Guanine
GFC	Gel filtration chromatography
h	hour
HA	Hemagglutinin
HCAb	Heavy-chain only antibody
HEK	Human embryonic kidney
HPLC	High-performance liquid chromatography
HTRA1	High temperature requirement A1
HV	Hypervariable loop
IGFBP	Insulin-like growth factor binding protein
IgG	Immunoglobulin G
IgNAR	Immunoglobulin New Antigen Receptor
IgNAR V domain	IgNAR variable domain
IMAC	Immobilized Metal Ion Affinity Chromatography
IPTG	Isopropyl β-D-1-thiogalactopyranoside
K_D	Equilibrium dissociation constant
kDa	Kilo Dalton
KI	Kazal-like inhibitor domain
k_{off}	Dissociation rate
l	Liter
LB	Low broth
LCMS	liquid chromatography mass spectroscopy
mAbs	Monoclonal antibodies
MalE	Maltose binding protein
MBP	Maltose binding protein
McoTI-II	Momordica cochinchinensis trypsininhibitor II
MHC	Major Histocompatibility Complex
min	Minute
mM	Milimolar
µM	Micromolar
ml	Mililiter
µl	Microliter
MS	Mass spectrometry
MW	Molecular weight
MWCO	Molecular weight cut off

nM	Nanomolar
nm	Nanometer
OD	Optical density
PAGE	Polyacrylamide gel electrophoresis
PDZ	post synaptic density, discs large, zonula occludentes-1
PBS	Phosphate buffered saline
PCR	Polymerase chain reaction
PE	Phycoerythrin
rel	Relative
rpm	Revolutions per minute
s	Second
S. cerevisiae	*Saccharomyces cerevisiae*
scFv	Single-chain variable fragment
SDS	Sodium dodecyl sulfate
SEC	Size exclusion chromatography
SOE	Splicing by overlap extension
T	Thymine
TCR	T-cell receptor
Temed	Tetramethylethylenediamine
TEV	Tabacco etch virus
TM	Transmembrane domain
T_m	Melting temperature
TNF	Tumor necrosis factor
VDJ	Variable, diversifying, joining
VH	Variable domain of the heavy chain
VHH	Variable domain of a camelid heavy-chain only antibody
VL	Variable domain of the light chain
vNAR	IgNAR variable domain
v/v	Volume per volume
Vol	Volume
wt	Wild type
w/v	Weight per volume
YPD	Yeast extract peptone dextrose
YSD	Yeast surface display

8.3. Appendix C: List of Figures

8.4. Appendix D: List of Tables

8.5. Appendix E: *Curriculum Vitae*

Dipl. Biol.
Niklas Weber

Liebfrauenstr. 70
64289 Darmstadt
Germany
Mail: NiklasFabianWeber@googlemail.com

Personal Data

Birth	October 28th 1983 in Bad Hersfeld (Germany)
Nationality	German
Marital Status	Married

Working

Since June 2017	Assay Developer - R-Biopharm AG, Darmstadt
April 2014-Mai 2017	qPCR Specialist - R-Biopharm AG, Darmstadt

Postgraduate

April 2010-April 2017	Doctorate at Technische Universität Darmstadt
	Clemens-Schöpf Institut für Organische Chemie und Biochemie, TU Darmstadt – Biochemistry Prof. Dr. Harald Kolmar

Graduate Degree

Diploma in Biology, Technische Universität Darmstadt

Thesis: *Entwicklung potenter und affiner Inhibitoren von Serinproteasen mit humanmedizinischer Relevanz durch gerichtete Evolution*

Prof. Dr. Harald Kolmar and Prof. Dr. Gerhard Thiel

Final grade: 1.1

School

2000-2003	Gymnasiale Oberstufe Modellschule Obersberg, Bad Hersfeld
1994-2000	Gymnasium Konrad Duden Schule, Bad Hersfeld
1989-1994	Grundschule Wilhelm Neuhaus Schule, Bad Hersfeld

Dipl. Biol. Niklas Weber

Niklas Weber
Liebfrauenstr. 70
64289 Darmstadt

Eidesstattliche Erklärung

Ich erkläre hiermit, dass ich meine Dissertation selbstständig
und nur mit den angegebenen Hilfsmitteln angefertigt habe.

_____

Dipl. Biol. Niklas Weber

Niklas Weber
Liebfrauenstr. 70
64289 Darmstadt

Erklärung

Ich erkläre hiermit, noch keinen Promotionsversuch unternommen zu haben.

———————————————
Dipl. Biol. Niklas Weber

Danksagung

An dieser Stelle möchte ich meinen besonderen Dank nachstehenden Personen entgegen bringen, ohne deren Mithilfe die Anfertigung dieser Promotionsschrift niemals zustande gekommen wäre:

Zunächst gilt mein Dank meinem Doktorvater, Prof. Dr. Harald Kolmar, für die Betreuung dieser Arbeit, so wie sein Vertrauen und seine Geduld, die er auf Grund ihres Verlaufs mir entgegenbrachte. Er war stets offen für meine Ideen und ließ mir den notwendigen Freiraum um diese Arbeit zu einem erfolgreichen Ende zu bringen. Der konstruktive Austausch mit Harald und seine ehrliche, direkte Art, die man in der freien Wirtschaft oft sehr vermisst, werden mir immer in sehr positiver Erinnerung bleiben.

Prof. Dr. Heribert Warzecha danke ich für die Übernahme des Korreferats dieser Arbeit. Prof. Dr. rer.nat.Dr.med.h.c. Siegfried Neumann und Prof. Dr. Alfred Nordmann danke ich für die Übernahme des ersten, bzw. zweiten Fachprüfers meiner Disputation.

Prof. Dr. Michael Ehrmann danke ich für die Expressionsvektoren seiner HTRA1 Varianten.

Ein weiterer Grundpfeiler dieser Dissertation war meine Familie. Dabei gilt der größte Dank meinen Eltern Jutta und Karl, die mich immer wieder unterstüzt und ermutigt haben diese Arbeit zu einem Abschluss zu bringen. Meiner Schwester Nina danke ich für Ihre Zurückhaltung bezüglich Fragen des Status und für das Korrekturlesen der Arbeit, so wie die ablenkenden Gespräche bei einem Glässchen Wein. Meinen Großeltern Helga und Helmut danke ich für das stete Interesse am Fortschritt dieser Arbeit und Ihre motivierenden Worte. Außerdem möchte ich mich bei meinen Schwiegereltern Anni und Hans-Heinrich für die vielen gemeinsamen ablenkenden Stunden bedanken.

Den größten Beitrag zum Entstehen dieser Arbeit hat meine Frau Stefanie geleistet. Neben viel Geduld während der Hochs und Tiefs der letzten Jahre, die sie aufbrachte, konnt ich mich immer auf sie verlassen. Sie hat immer wieder betont, dass ich diese Arbeit nicht für sie, sondern für mich zu einem Enden bringen soll, was mir sehr viel bedeutet hat. Außerdem hat sie mir das schönste Geschenk gemacht, dass ich je bekommen habe – eine eigene Familie!

Ein weiterer Dank gilt dem AK Kolmar. Insbesondere möchte ich mich bei Andreas Christmann bedanken, der mich seit meinem ersten Praktikum im Arbeitskreis unterstützt hat. Vielen Dank für die intensiven fachlichen Diskussionen und auch die, die darüber hinausgingen. Auch Cecilia Gorus (Cili) möchte ich für ihre Hilfe (die nicht zu unterschätzen ist weiß jeder der dabei war als sie Urlaub hatte), Olga Avrutina für so manches gute Gespräch bei einem Glas Wein (wie lange braucht ein Weißwein bei -80°C für die perfekte Trinktemperatur), Barbara Diestelmann für die nette Art und die ganze Organisation (wie schafft Harald es jetzt nur mit einer halben Barbara?) und Janine Fritz (jetzt Becker) für die tolle Freundschaft (eine der wenigen Frauen, die mit auf einen Männerabend darf).

Außerdem möchte ich allen meinen Mitstreitern während der experimentellen Phase danken: Thomas Hofmeyer aka Hofmeister aka Thomhassan (für die einzigartige Benchbruderschaft, die Zuverlässigkeit der Äkta und weitere Dinge, die erwähnt werden sollten, es aber nicht können), Stefan Zielonka aka Stefhan aka Psycho-Stef (für die fantastische Freundschaft, deine Bib, das Brückenbauen, deine wahre Gesinnung „HEF JW 47", und tausend Dinge mehr), , Julius Grzeschik aka Jewelz (für Sky Go und wichtige Dinge), Sebastian Hörner (für die außerberuflichen Events), Maren Paschke (für deine Art), Heiko Fittler aka Bachi (für Musik, Bier, Fussball und die richtige Einstellung), Simon Krah (du weißt schon wofür), Christina Uth (für die gute Zeit, die immer noch andauert), Michael Reinwarth (für deine unbeschreiblich attraktive Arbeitsweise), Stephan Dickgiesser (für deinen Namen, die Zellkultur, aber auch noch mehr), Bernhard Valldorf (für Bier und Witz), Sebastian Fabritz, Alexander Maass, Franziska Maass, Christian Schröter, Nicolas Rasche, Tim Heiseler, Björn Steinmann (für die Bib), Achim Dörner, Martin Empting, Birgitt Piater, Laura Rhiel, Daichi Nasu (für kulinarische Exzesse), Bernhard Glotzbach (für Bib und Bier) und Carolin Mai (für den gemeinsamen Start). Vielleicht hätte ich es auch ohne euch geschafft, aber dann wäre es nicht die bislang schönste Zeit in meinem Leben gewesen.

Großer Dank gilt auch den von mir betreuten Diplomanden Bert Luck und Young-In Ko, deren Ergebnisse auch zu dieser Arbeit beigetragen haben.

Vielen Dank auch liebes iGem Team 2012. Es war ein super Projekt, das richtig Spaß gemacht hat.

Ich möchte auch allen meinen Freundinnen und Freunden, aus den der Promotion vorangegangenen Episoden, den allergrößten Dank aussprechen. Die wichtigsten davon sind Florian Stiel aka Capu/Kappu („ich komm mit harten Arabern und Schwabengelaber", ich bin mir sicher, da wo du jetzt bist gibt es eine Flatrate für alles, nicht nur für Jungfrauen – da chillen wir irgenwann wieder gemeinsam), Stefan Hamann (eine Legende), Sascha Peters aka Muckel (selten, aber immer gut und heftig), Tom Bär (Sag mal Würste), Boris Brückmann (wenn alles schief geht, dann gemeinsam WG über dem Orkan gründen) und Christian Kromm (Mein HEF Last Man Standing), so wie die gesamte Hersi-Gang.

Danke auch allen Leuten mit denen ich boarden war (auch wenn ihr Skifahrer seid).

Vielen Dank auch an die noch nicht genannten Mitglieder der Männertagscrew. Lieber Reiner Hessler, lieber Jojo Lamp, lieber Max Halbritter und lieber Robert Heinz, Städtereisen sind mit euch am schönsten.

Zuletzt möchte ich auch meinen Arbeitskollegen der R-Biopharm AG danken, insbesondere dem FSA Team und dem Allergenlabor. Nicht zu vergessen die Kickergruppe, in der ich die meisten der, an der TU erworbenen, Fähigkeiten einbringen konnte.